공학석사학위 논문

Novel Electron Donating π-Conjugated Organic Materials Based on Indoloindole Unit: Synthesis, Characterization and Optoelectronic Application

인돌로인돌을 기반으로 한 새로운 전자주개 공액 유기 물질: 합성, 특성 분석, 그리고 광전자소자로의 응용에 대한 연구

2014년 2월

서울대학교 대학원

재료공학부

정 혜 연

Novel Electron Donating π-Conjugated Organic Materials Based on Indoloindole Unit: Synthesis, Characterization and Optoelectronic Application

지도교수 박 수 영

이 논문을 공학석사 학위논문으로 제출함
2013 년 12 월

서울대학교 대학원
재료공학부
정 혜 연

정혜연의 석사학위논문을 인준함
2013 년 12 월

위 원 장 _____ (인)

부 위 원 장 _____ (인)

위 원 _____ (인)

Novel Electron Donating π-Conjugated Organic Materials Based on Indoloindole Unit: Synthesis, Characterization and Optoelectronic Application

A THESIS SUBMITTED IN PARTIAL FULFILLMENT OF
THE REQUESTMENTS FOR THE DEGREE OF MASTER
IN ENGINEERING AT THE GRADUATE SCHOOL OF
SEOUL NATIONAL UNIVERSITY

February 2014

By

Hae Yeon Chung

Supervisor

Prof. Soo Young Park

Abstract

Novel Electron Donating π-Conjugated Organic Materials Based on Indoloindole Unit: Synthesis, Characterization and Optoelectronic Application

Hae Yeon Chung

Department of Materials Science and Engineering

The Graduate School

Seoul National University

Heteroacene-containing fused aromatic system has been extensively investigated in the area of fundamental study of molecular property and application to organic devices based on unique photophysical and electronic properties. Recently, heteroacenes have been emerged as a promising backbone unit of organic semiconducting materials due to their remarkable charge carrier mobility, and excellent environmental stability. Among various heteroacens, pyrrole-containing heteroacene backbone exhibits strong electron donating nature originating from the low ionization potential, and possesses planar structure, controllable solubility, and easy functionalization. Based on thier unique properties, indolo[3,2-b]indole, which is one of the pyrrole-containing heteroacene, is suitable for the semiconducting material in optoelectronic system.

Herein, I designed and characterized indolo[3,2-b]indole (IDID) derivatives. By UV/vis spectroscopy and measurement of energy levels, IDID derivatives are clearly confirmed as strong electron donor. To explore electron donating nature of IDID derivatives, I carried out CT complex formation using IDID derivatives as an electron donor, and 2,7-dinitro-9-fluorenone (DNF), and 2,4,7-trinitro-9-fluorenone (TNF), and 7,7,8,8-tetracyanoquinodimethane (TCNQ) as an electron acceptor. Through analyzing the photophysical properties of CT complexes, IDID derivatives were proven to be excellent donor materials for the formation of ground state CT complex with acceptors. Furthermore, using CT co-crystals of IDIDp-TCNQ as the semiconducting active elements, single-crystal OFETs were prepared by solvent vapor annealing (SVA) process, which showed ambipolar p-/n- type field effect mobility up to 1.27×10^{-3} $cm^2V^{-1}s^{-1}$and 3.40×10^{-2} $cm^2V^{-1}s^{-1}$, respectively. On the other hand, IDIDp single-crystal OFETs showed only p-type field effect mobility up to 2.29×10^{-2} $cm^2V^{-1}s^{-1}$.

Secondly, using strong donating nature of IDID core and intramolecular charge transfer (ICT) characteristic of the acceptor-substituted IDID, I designed and synthesized low bandgap A-D-A and D-A-D type triad molecules using IDID as a donor moiety and DPP as an acceptor moiety for high efficiency bulk-heterojunction small molecule organic solar cell (SMOSC). Through comparing optical, electrochemical properties and device performances of A-D-A and D-A-D type IDID-DPP derivatives, A-D-A type triad molecule was found to be an excellent donor molecule in OSCs, where solution processed organic solar cells based on a blend of HD-IDID-EH-DPP as a donor and [6,6]-phenyl-C_{61}-butyric acid methyl

ester ($PC_{61}BM$) as an acceptor exhibited V_{OC} of 0.73 V, J_{SC} of 10.24 $mAcm^{-2}$, FF of 55.6% and PCEs as high as 4.15%. On the other hand, organic solar cells based on a blend of HD-DPP-EH-IDID as a donor and and $PC_{61}BM$ as an acceptor exhibited V_{OC} of 0.64 V, J_{SC} of 4.23 $mAcm^{-2}$, FF of 54.0% and PCEs as high as 1.46%.

Keywords: Indoloindole, Heteroarene-containing Fused Aromatic System, Charge-Transfer complex, Single-Crystal Organic Field-Effect Transistor, Organic Solar Cell

Student Number: 2012-20635

Contents

List of Tables

List of Schemes

List of Figures

Chapter 1. Introduction

1.1 Heteroacene-containing fused aromatic system

Heteroacene is molecular engineered fused aromatic system of acene through incorporating sulphur, nitrogen or selenium atoms instead of carbon atoms of acenes, and exhibits great advantages compared to acenes.[1] These structural modifications lead to increased ambient stability, solubility, functionalizability and enhanced intermolecular interactions resulting in change of packing motif of organic molecules.[2] Based on their unique properties, it is easy for heteroacene derivatives to make feasible energy level tuning, unique molecular arrangement, and supramolecular structures.[2] Furthermore, interaction between adjacent molecules in the crystal state is significantly correlated with the stacking arrangement of molecules, the crystallinity of molecules and morphology of the film in the device.[3] Therefore, heteroacene-fused aromatic system is favorable to effectively control quality of the film and device performance. For these reasons, heteroacene-containing fused aromatic systems have been significantly investigated in the area of fundamental study of chemical structure, photochemical and electrical properties, and application to organic semiconducting materials in organic optoelectronic devices.[4] Benzothieno[3,2-b]benzothiophene (BTBT), dinaphtho[2,3-b:2',3'-f]thieno[3,2-b]thiophene (DATT), benzo[1,2-b:4,5-b']dithiophene (BDT) derivatives and fused thiophene derivatives have already shown high device performances in organic devices, and emerged as a promising candidates for device application.[4]

1.2 Pyrrole-containing fused aromatic system

Among heteroacenes, nitrogen-substituted fused heteroaromatic system has enormous advantages compared to acenes. Especially, pyrrole-containing heteroacene system exhibits increased aromaticity and strong electron donating nature. Furthermore, several substitution sites make various conjugation engineering with N-, 2-, and 3- substitution position in carbazole, and indolocarbazole derivatives. Direct addition of aromatic or aliphatic units to those substitution sites gives chances to control π-conjugation or solubility, and induces feasible band gap tuning. [5] Furthermore, rigid, planar backbone structure induces strong π-π interaction between adjacent molecules, and controls supramolecular structure and crystallinity in solid state, which are critical parameters controlling electronic property of the active elements and the device performance.

Based on benefits of pyrrole-containing fused aromatic system (i.e., carbazole, indolocarbazole), enormous efforts have been focused on exploring electronic property of those materials as an electron donor moiety, and developing the device performance of materials with competitive properties. [6]

1.3 Charge-transfer complex

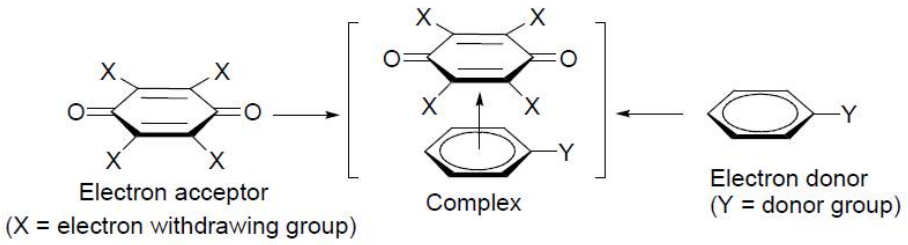

Figure 1.1. Schematic diagram of formation of CT complex.

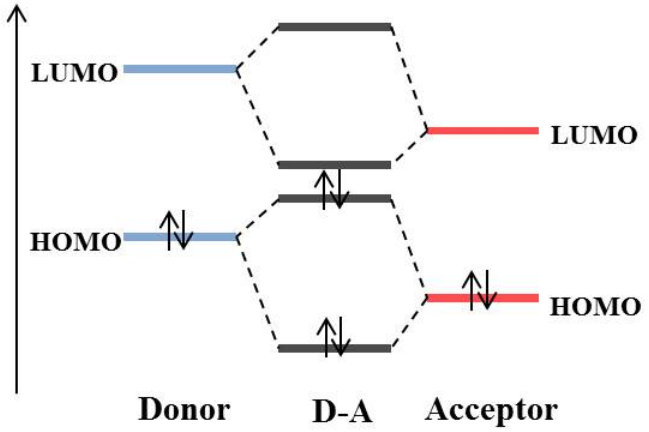

Figure 1.2. Energy levels of donor, acceptor, and CT complex.

Charge transfer complex is an association of organic donor and acceptor molecules. (Figure 1.1) Organic donor is an electron-rich molecule with an electron donating group and organic acceptor is an electron-deficient molecule with an electron withdrawing group in the molecular structure. Attraction, weaker than covalent or ionic bonds, between donor and acceptor molecules makes weak electron resonance system, and forms charge-transfer complex, with the transfer of fraction of electronic charge from donor to acceptor in the ground state providing stabilizing force for the molecular complex. [7]

$$\mathbf{D} + \mathbf{A} \rightarrow \left[\boldsymbol{D}^{+\delta}\right] + \left[\boldsymbol{A}^{-\delta}\right]$$

In the view of the frontier molecular orbital (FMO), charge-transfer complex is formed due to interaction of HOMO of donor and LUMO of acceptor, which is not a stable chemical bond. (Figure 1.2) The difference between ionization potential of donor and electron affinity of acceptor decides the degree of charge transfer (δ) to settle down the partial charges $+\delta$ and $-\delta$ on the donor and acceptor, respectively, and this ionicity of the CT complexes significantly affects the electronic property of them. The overall energy balance (energy gained a spontaneous charge transfer), $\Delta\mathbf{E}$ is defined as follows,

$$\Delta\mathbf{E} = \boldsymbol{E_A} - \boldsymbol{E_I} + \boldsymbol{J}$$

, where $\boldsymbol{E_A}$ is an electron affinity of the acceptor, $\boldsymbol{E_I}$ is an ionization potential of the donor, and $\boldsymbol{J}$ is an electrostatic attraction energy between donor and acceptor in the CT complexes.

Figure 1.3 and Figure 1.4 are conventionally used donor and acceptor molecules in the typical CT complex system, respectively.

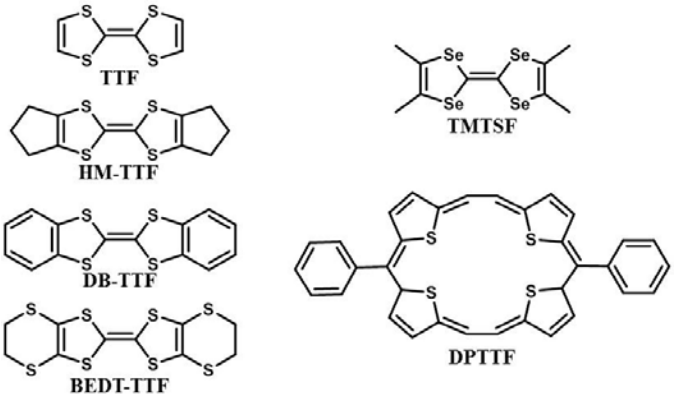

Figure 1.3. Typical TTF-based donor molecules for CT complex. [7(c)]

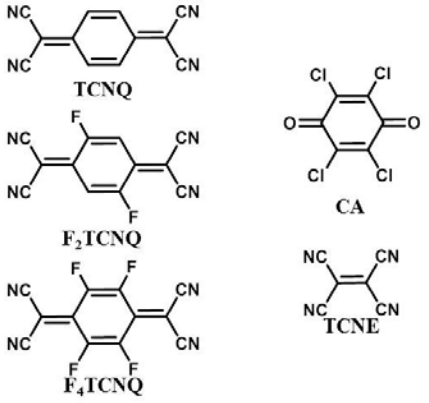

Figure 1.4. Typical acceptor molecules for CT complex. [7(c)]

Charge-transfer (CT) crystal is a solid-state organic functional material composed of electron rich molecule (donor) and electron deficient molecule (acceptor). Extensive studies have been conducted on CT crystal due to its unique electrochemical, and magnetic properties, such as electrical conductivity (e.g. TTF-TCNQ), superconductivity (e.g. $(TMTSF)_2PF_6$), ferroelectricity (e.g. TTF-CA), photoconductivity (e.g. BuV-PyTs, PVK-TNF) and electrical semiconductivity (e.g. BEDT-TTF or DBTTF-TCNQ)[8]. Based on such peculiar properties, CT crystal has raised much attention for application to organic electronics, especially field-effect transistor, semiconducting active element or metallic conducting electrode.[1,9]

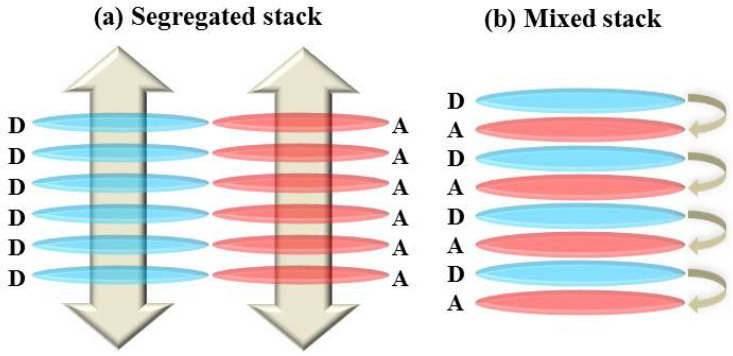

Figure 1.5. Stacking arrangement of donor and acceptor molecules in two different types of CT complexes; (a) segregate stack, and (b) Mixed stack.

CT crystals can take two different stacking arrangement of electron donor and acceptor, segregated stacking and mixed stacking (as shown in Figure 1.5). In the segregated stacking mode, donor and acceptor molecules form separate D- and A- columnar stacks, which essentially promotes metallic conducting property. In the mixed stacking mode, on the other hand, adjacent donor and acceptor molecules stack alternatively with face-to-face arrangement, which normally results in the electrically insulating or semiconducting properties. [8] Normally, π-conjugated aromatic molecules are most suitable donor and acceptor molecules for the formation of CT complexes, because those π-conjugated molecules have strong π-π interaction together with the D/A CT interaction, and they are easy to make columnar stacks. [10]

1.4 Organic electronics

Organic optoelectronic devices using organic molecules as an active layer, like organic light-emitting diodes (OLEDs), organic photovoltaics (OPVs), organic field-effect transistors (OFETs), organic memory devices, and so on, have been extensively studied over the last 20 because of benefits of organic materials, such as light weight, low cost fabrication, easy processing with good solubility, good mechanical property and structural flexibility.[11] Recently, studies about organic devices using small molecules are investigated with increased interest compared to polymeric organic devices, because small molecule have numerous advantages such as simple synthesis and purification, monodispersity, and well-defined structures compared to polymer.[12]

1.4.1 Organic field-effect transistors (OFETs)

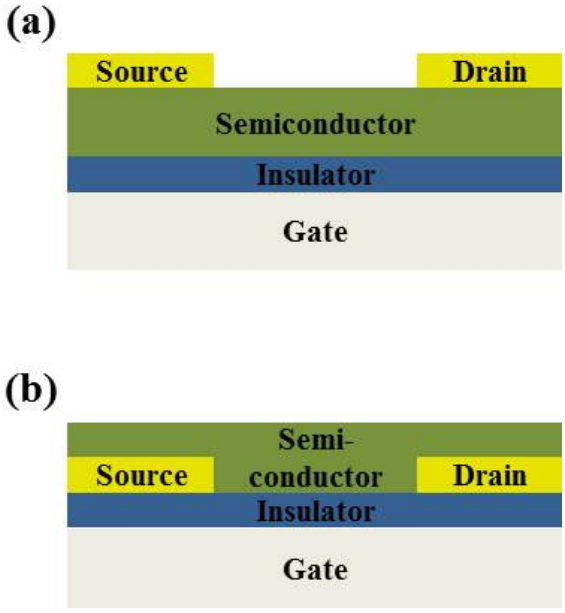

Figure 1.6. Device structure of OFET; (a) top contact (b) bottom contact.

Field-effect transistors are most important logic units in electronic devices, used as switching or amplifier devices. In 1986, polythiophene film was used as an active layer in OFETs, showing mobility of 10^{-5} $cm^2V^{-1}s^{-1}$, which was the first of ever report of OFET. 4 years later, π-conjugated small molecule, sexithiophene was used in OFETs with mobility of 10^{-3} $cm^2V^{-1}s^{-1}$. In these days, enormous progress has been made in the field of OFETs, with hole mobility up to 31 $cm^2V^{-1}s^{-1}$ (average value of 16.4 $cm^2V^{-1}s^{-1}$) and electron mobility of 11 $cm^2V^{-1}s^{-1}$(average value of 5.2 $cm^2V^{-1}s^{-1}$), quite comparable to those of amorphous silicon (~1 $cm^2V^{-1}s^{-1}$) and polycrystalline silicon (10~100 $cm^2V^{-1}s^{-1}$).[13]

In view of the device performance, long-range order and alignment of molecules in organic active elements significantly control the mobility of charge carriers. Charge carrier transport in polymer-based OFETs exhibit is limites by the high molecular disorder and low crystallinity in the film, resulting in the low charge carrier mobility. However, organic single-crystal has less structural defects than their amorphous or polycrystalline counterparts.[14] In these days, high device performances of single-crystal OFETs have been reported, of which the state-of-the-art of mobility is 18 $cm^2V^{-1}s^{-1}$ in devices using rebrene.[15]

Even though single-crystal OFETs (sc-OFETs) have disadvantages that fabrication is difficult for technological application, enormous efforts have been focused toward large-area fabrication of sc-OFET with high device performance through method of aligning single-crystals in large-area substrate.[14(a)]

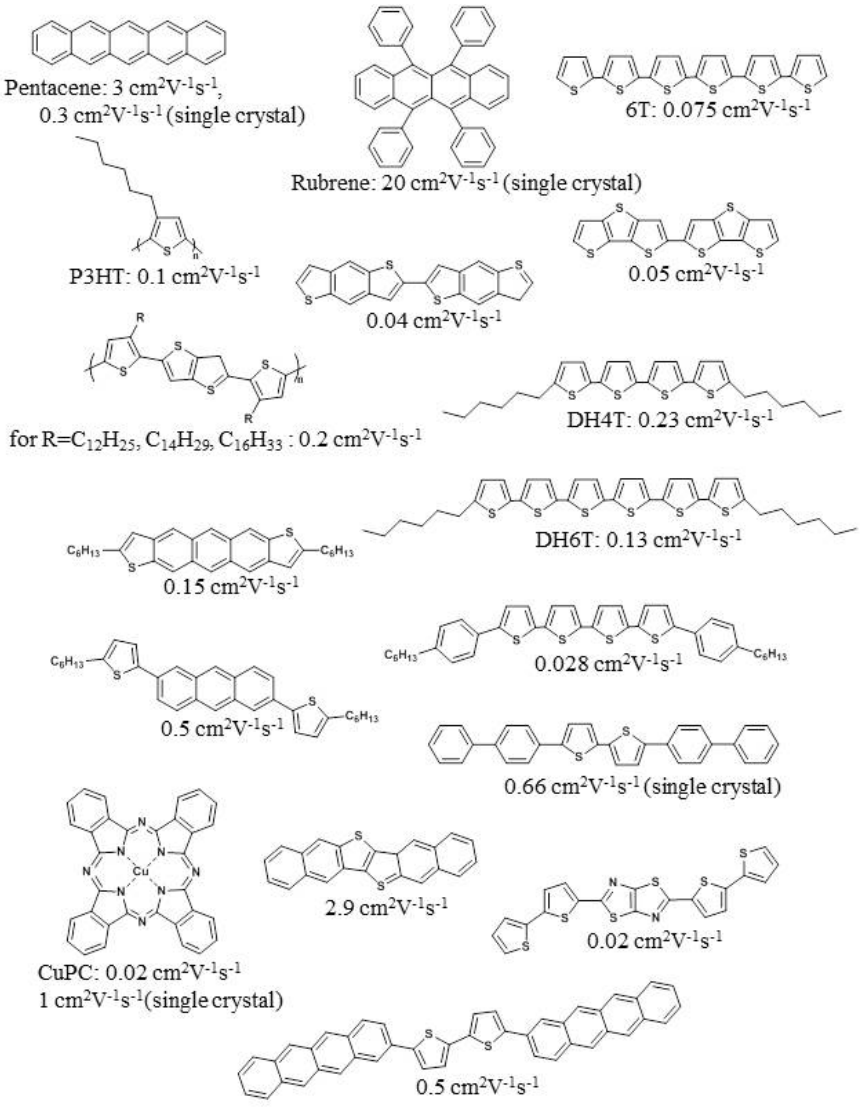

Figure 1.7. p-type charge transporting organic molecules for OFET. [16]

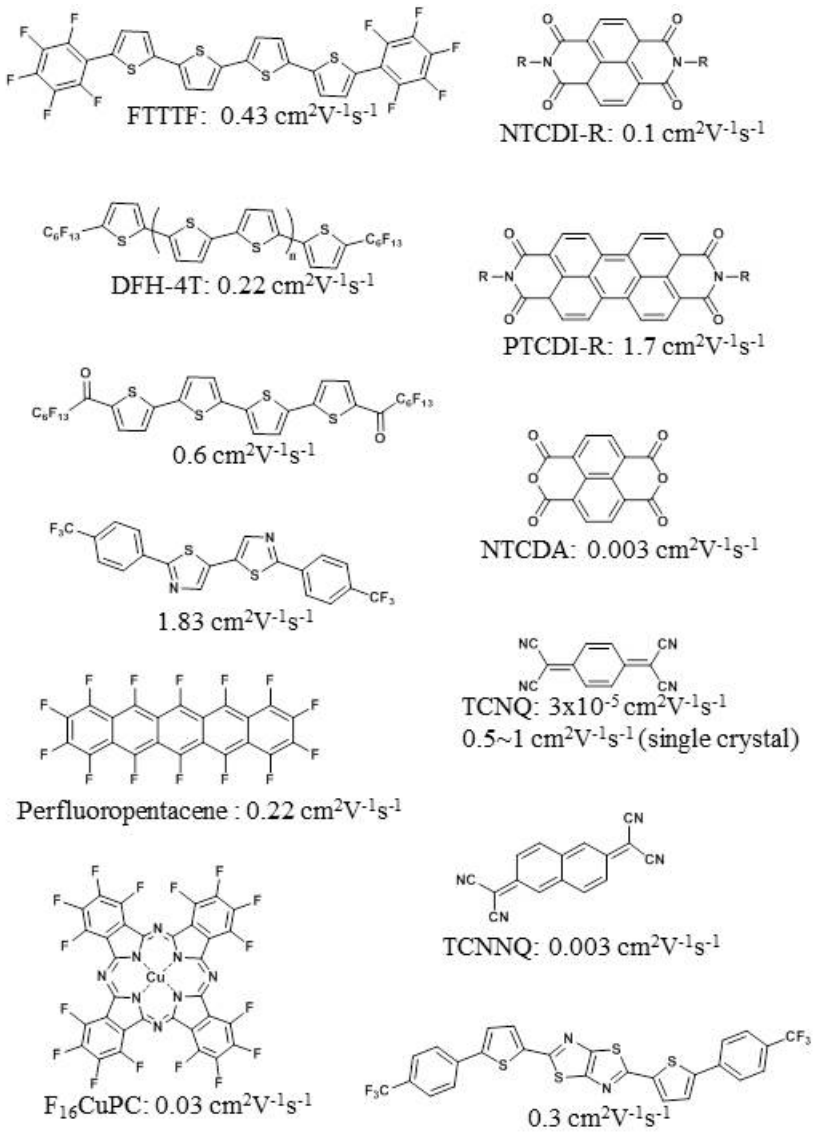

Figure 1.8. n-type charge transporting organic molecules for OFET. [16]

Most widely used p-type, and n-type organic semiconductors, based on oligothiophene, acene, and heteroacene, are shown in Figure 1.7 and Figure 1.8.[16]

Although organic molecules in Figure 1.7 and Figure 1.8 show high mobility, fabrication of integrated circuit through unipolar approach (p-type or n-type) has several limits. Using unipolar charge transport molecules, lots of process steps are required, resulting in complex process, and increased manufacturing cost for fabrication of integrated circuit. However, ambipolar charge transporting materials have advantages compared to unipolar molecules. Using ambipolar charge transporting materials in OFETs could make not only complementary-like inverters without advanced patterning techniques are enabled, but also devices work in both positive and negative supply voltage. Typically used single-component ambipolar organic semiconductor are shown in Figure 1.9.[17]

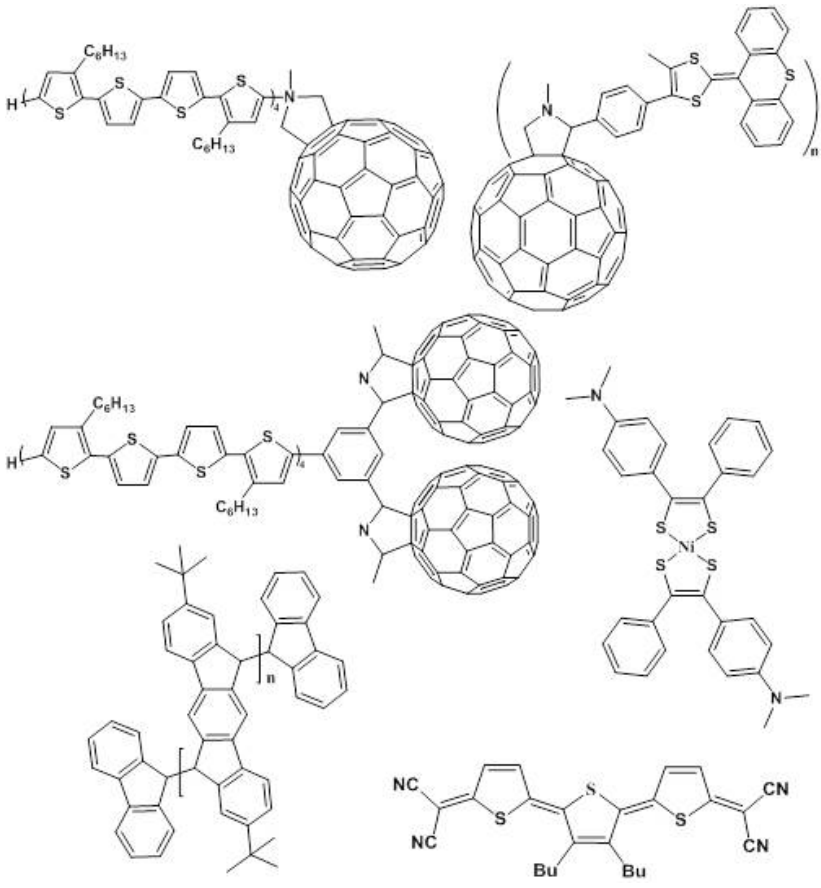

Figure 1.9. Ambipolar charge transporting organic molecules for OFET. [16]

Organic field-effect transistors (OFETs) consist of source and drain electrodes, gate electrode, an insulator, and an organic semiconductor as an active element as shown in Figure 1.6. Operation process of OFETs is as follows. When there is no voltage applied to the gate electrode, only small current flows between source and drain, and this is called “off-state” of transistor. When negative voltage is applied to the gate electrode, hole carriers injected from grounded electrodes (normally source electrode) are accumulated at the interface between organic semiconducting layer and dielectric layer, developing p-type channel between source and drain conductors, and this is called “on-state” of transistor. When positive voltage is applied to the gate voltage, electrons are accumulated at the interface of organic/dielectric layers, making n-channel between source and drain conductors, which results in flowing current, I_{SD}. In teams of energy level, when negative voltage is applied to gate electrode, energy levels (HOMO and LUMO) of the organic materials shift up to the Fermi level(E_F) of the metal. If the HOMO becomes resonant with E_F, hole carriers could flow between the HOMO and the metal, resulting in current flowing between source and drain. In this case, the flow of holes makes current between electrodes, and materials are called as a p-type semiconductor. In n-type semiconductors, opposite processes are carried out. When positive voltage is applied, HOMO and LUMO levels will shift down to E_F of metal, resulting in resonance between LUMO and E_F and electrons flow. Consequently, current flows between source and drain electrode. [18]

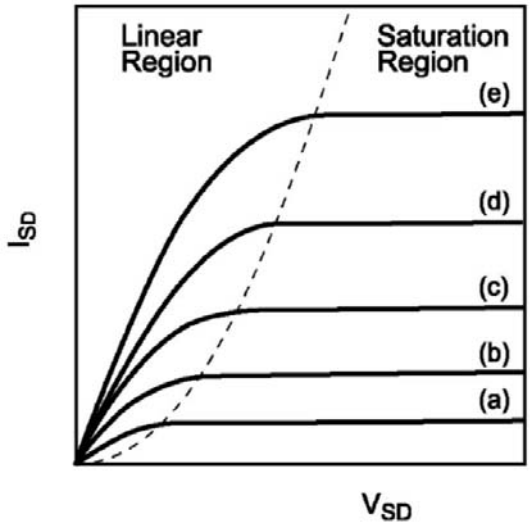

Figure 1.10. Typical electrical characteristics obtained in OFET. [11(d)]

The current (I_{SD}) flowing between source and drain electrodes at a given gate voltage (V_G) in the linear region and saturation region are given as follows,

$$I_{SD,lenear} = \frac{C_i W \mu_{FET}}{L}(V_G - V_T)V_{SD}$$

$$I_{SD,sat} = \frac{C_i W \mu_{FET}}{2L}(V_G - V_T)^2$$

, where μ_{FET} is the field-effect mobility of the charge carrier, L is the length of the channel, W is the width of the channel, C_i is the capacitance per unit area of the gate dielectric, and V_T is the threshold voltage.

The most important parameters indicating device performance of OFETs are the charge carrier mobility (μ_{FET}), current on/off ratio ($I_{on/off}$), and the threshold voltage (V_T), where μ_{FET} could be calculated from slope of plots of $I_{SD}^{1/2}$-V_G, $I_{on/off}$ is the ratio of drain current in on-state and the drain current of off-state at a particular gate voltage, and V_T could be extracted from the linear fit to zero yields in transfer curve.

.

1.4.2 Organic photovoltaics (OPVs)

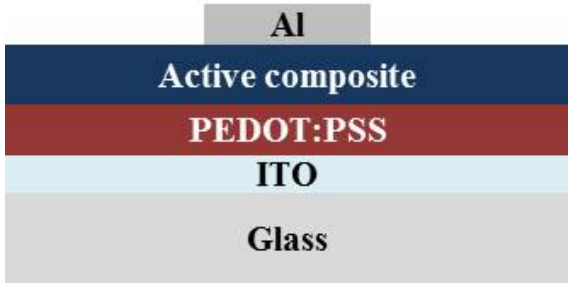

Figure 1.11. Device structure of OSCs.

Organic photovoltaics (OPVs) are one of the most promising ways of providing green energy, through conversion from solar energy to electrical energy. Photovoltaics using organic materials as an active layer have several advantages compared to the inorganic photovoltaics, such as light weight, flexibility, low materials and fabrication cost.[11] However, efficiencies of OPVs are lower than those of inorganic devices due to the small exciton diffusion length, low quantum yield for photogeneration of charge carriers, and high bulk resistance of OPVs,[19] while the state-of-the-art device performance of inorganic PVs is over 20%, that of polymer solar cells (PSCs) is currently just beyond 10%, [20] and also that of small molecule organic solar cells (SMOSCs) is around 8%.[9] Based on the advantages of organic materials, OSCs have been significantly investigated and progressed in last several years through chemical modification of materials and developing new device structures.

Solar cells using polymeric materials exhibit lots of benefits compared to small molecule organic solar cells, such good film quality, low materials consumption with large extinction coefficient, and excellent mechanical flexibility.[19] Based on those properties, many research groups have reported high efficiency device performances. However, enormous progress has been reported on small molecule organic solar cells as well, due to the ease of purification and synthesis, high intrinsic carrier mobility, and tendency to self-assemble for long-range order. [21]

Organic photovoltaics consist of thin films of organic active materials sandwiched between two electrode materials. (Figure 1.11) ITO with high work function around 4.7 eV is used as an anode in OPV, while metals with low work function are used as a cathode to provide Ohmic contacts

at the cathode-active layer interface. PEDOT:PSS with work function around 5.0 eV is a typical p-type interface layer which forms an Ohmic contact with the active layer for the effective charge collection.

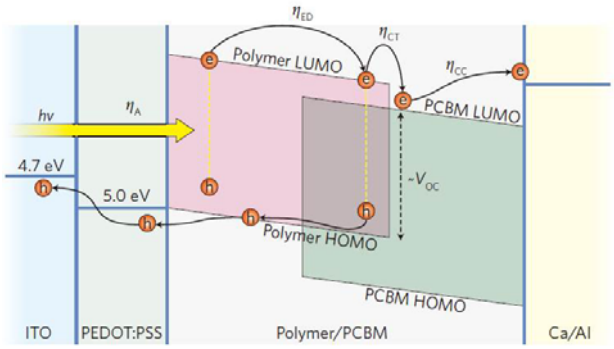

Figure 1.12. Operating mechanism of OSCs. [19]

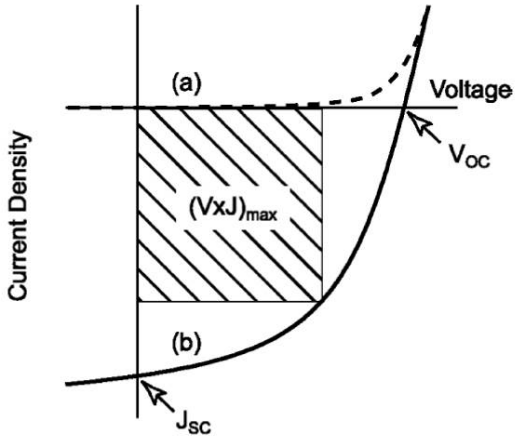

Figure 1.13. Typical J-V curve obtained from OSCs. [11(d)]

The mechanism for operation of OPVs is as follows: (a) light absorption and exciton formation, (b) exciton migration, (c) exciton dissociation at the donor-acceptor interface with generation of charge carrier and (d) charge transport and charge collection. Schematic operating mechanism of solar cells is shown in Figure 1.12.

In 1979, bilayer planar heterojunction solar cells were first reported exhibiting around 1% of PCE (power conversion efficiency), but this device structure has limitation of small surface area between donor and acceptor, and requires long charge carrier life time.[19] Bulk heterojunction (BHJ) OSCs, including a mixed layer with interpenetrating network of donor and acceptor, solve the problem of bilayer planar junction OSCs. By maximizing interface between donor and acceptor molecules, excitons are easy to reach the interface of donor and acceptor. [3]

The device performance of OPVs is evaluated by fill factor (FF), power conversion efficiency (η), as follows,

$$\mathrm{FF} = \frac{(VJ)_{max}}{V_{OC}J_{SC}}$$

$$\eta = \frac{(VJ)_{max}}{I}$$

where, J_{sc} (short-circuit current density) is the current density extracted from OSCs under light illumination (AM 1.5G) without bias voltage, and V_{oc} (open-circuit voltage) is affected by the energy difference between the LUMO of the acceptor and the HOMO of the donor, providing the driving force for charge separation.[22] Typical *J-V* curve of OSCs is shown in Figure 1.13.

Another important parameter is EQE (external quantum efficiency), which is function of wavelength (λ), defined as followed equation:

$$\mathrm{EQE}(\lambda) = \eta_A(\lambda) \times \eta_{ED}(\lambda) \times \eta_{CS}(\lambda) \times \eta_{CC}(\lambda)$$

, where $\eta_A(\lambda)$ is the efficiency of light absorption, $\eta_{ED}(\lambda)$ is the efficiency of exciton diffusion, $\eta_{CS}(\lambda)$ is the efficiency of charge separation, and $\eta_{CC}(\lambda)$ is the efficiency of charge collection.[23]

Materials used in small molecule organic solar cells (SMOSCs) are divided into electron-rich molecules (donor) and electron-deficient molecules (acceptor). In OSCs, fullerene derivatives, such as $PC_{61}BM$, $PC_{71}BM$, $BisPC_{71}BM$, ICBA, are mostly used as an acceptor due to their deep-lying and degenerate LUMO level, and high electron mobility. [23(b)] Molecules used as active elements is OSCs are needed for several properties, i.e., ease of charge transfer to donor or acceptor, effective formation of π-overlap between the molecules for charge transport, and especially, low bandgap energy is critical for broad light absorption.[1]

1.5 Research objectives

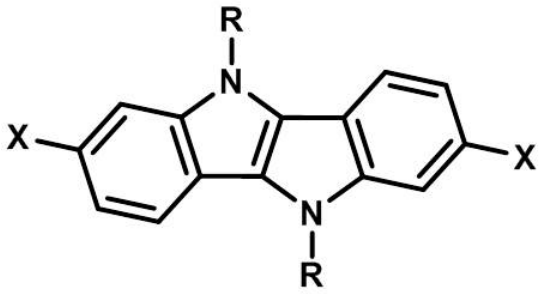

Scheme 1.1. Chemical structure of indolo[3,2-b]indole backbone where X is aromatic group and R is alkyl solubilizing group.

Herein, I designed and synthesized indolo[3,2-b]indole (IDID) derivatives shown in Scheme 1.1. IDID aromatic system has strong electron donating property originating from low ionization potential. Rigid, planar backbone of IDID unit makes strong π-π interaction and face-to-face molecular configuration between adjacent molecules. [24] Furthermore, by substitution of alkyl side groups on nitrogen atoms, solubility of the material is to be increased. Moreover, substitution of aromatic groups to 2,7-position of IDID may extend π-conjugation of entire system.

Based on such molecular design strategy, I studied different series of IDID molecules and investigated their electronic and optoelectronic properties. In chapter 2, basic properties of IDID is explored by comparison with carbazole by UV/vis spectroscopy and measurement of energy level. I explored fundamental electron donating property of them

based on energy level tuning, and successfully demonstrated the formation of CT complexes when IDID derivatives are interacted with electron acceptor molecules, i.e., 2,4-dinitro-9-fluorenone (DNF), 2,4,7-trinitro-9-fluorenone (TNF), and 7,7,8,8-tetracyanoquinodimethane (TCNQ) by secondary interaction. And I characterized photophysical properties of CT complexes by UV-vis spectroscopic measurement, and of single-crystal OFETs using CT co-crystals.

In chapter 3, I designed and synthesized A-D-A and D-A-D type triad small molecules using IDID as a donor moiety and diketopyrrolopyrrole (DPP) as an acceptor moiety, which show strong intramolecular charge transfer (ICT) character and possesses low bandgap. By comparing A-D-A and D-A-D triad molecules through optical and electrochemical property, suitable molecular structure for high efficiency OSC device was clearly identified. Consequently, I demonstrated different photovoltaic properties when indoloindole derivatives are blended with $PC_{61}BM$ acceptor.

1.6 Bibliography

1. J. Anthony, *Chem. Rev.*, **2006**, 103, 5028

2. (a) K. Niimi, S. Shinamura, I. Osaka, E. Miyasaki, K. Takimiya, *JACS*, **2011**, 133, 8732 (b) H. Ebata, T. Izawa, E. Miyasaki, K. Takimiya, M. Ikeda, H. Kuwabara, T. Yui, *JACS*, **2007**, 129, 15732 (c) M. Nakano, H. Mori, S. Shinamura, K. Takimiya, *Chem. Mater*., **2012**, 24, 190 (d) C. Wang, H. Dong, W. Hu, Y. Liu, D. Zhu, *Chem. Rev.*, **2012**, 112, 2208

3. M.D.Perez, C.Borek, S.R.Forrest, and M.E.Thompson, *JACS,* **2009,** 131, 9281

4. (a) J.R. Kirtley, J. Mannhart, *nature materials*, **2008**, 7, 520 (b) D. Jérome, *Solid State Sciences*, **2008**, 10, 1692 (c) H. Yamochi, J. Hagiwara, M. Soeda, G. Saito, *J.Mater.Chem*., **2006**, 16, 550 (d) S. Horiuchi, Y. Tokura, *nature materials*, **2008**, 7, 357 (e) W. Yu, X.-Y. Wang, J. Li, Z.-T. Yan, W. Wang, J. Pei, *Chem. Comm*., **2013**, 29, 54

5. Z.G. Soos, *Annual Review of Physical Chemistry*, **1974**, 25, 121

6. (a) X.Lin, Y.Tani, R.Kanda, K.-i.Nakayama, S.Yagai, *J. Mater. Chem. A*, **2013**, 1, 14686, (b)Y. Zou, D.Gendron, R. Badrou-Aı¨ch, A.Najari, Y.Tao, M.Leclerc, *Macromolecules,* **2009**, 42, 2891, (c)J. Jo, D. Gendron, A.Hajari, J.S.Moon, S.Cho, M.Leclerc, A.J.Heeger, *Applied physics letters*, **2010**, 97, 203303 (d) J.-S.Wu, C.-T.Lin, C.-L.Wang, Y.-J.Cheng, C.-S.Hsu, *Chem.Mater*., 2012, 24, 2391

7. (a) A.A. Sagade, K.V. Rao, S.J. George, A. Datta, G.U. Kulkarni, *Chem.Commun.*, **2013**,49,5847 (b) S. Horiuchi, H. Yamochi, G. Saito, K. Sakaguchi, M. Kusunoki, *JACS*, **1996**, 118, 8604 (c) T. Mori,

Chem. Lett., **2011**, 40, 428

8. V. Podzorov, *Nature Materials*, **2010**, 9, 616

9. (a) E. Menard, V.Podzorov, S.-H.Hur, A.Gaur, M.E.Gershenson, and J.A.Rogers, *Adv.Mater*, **2004**, 16, 2097. (b) S.K.Park, S.Varghese, J.H.Kim, S.-Jun.Yoon, O.K.Kwon, B.-K.An, J.Gierschner, S.Y.Park, *JACS*, **2013**, 135, 4757. (c) Y.Takahashi, T.Hasegawa, Y.Abe, Y.Tokura, K.Nishimura, and G.Saito, *Appl.Phys.Lett*., **2005**, 86, 063504 (d) Y.Takahashi, T.Hasegawa, Y.Abe, Y.Tokura, and G.Saito, *Appl.Phys.Lett*, **2006**, 88, 073604 (e) A.K.K. Kyaw, D.H. Wang, V. Gupta, J. Zhang, S. Chand, G.C. Bazan, and A.J. Heeger, *Adv.Mater*., **2013**, 25, 2397

10. J.Zhang, H.Geng, T.S.Virk, Y.Zhao, J.Tan, C.Di, W.Zu, K.Singh, W.Hu, Z.Shuai, Y.Liu, and D.Zhu, *Adv.Mater*, **2012**, 24, 2603

11. (a) M. Mas-Torrent, C. Rovira, *Chem.Soc.Rev.*, **2008**, 37, 827 (b) E. Menard, M. A. Meitl, Y. Sun, J.-U. Park, D.J.-L. Shir, Y.-S. Nam, S. Jeon, and J.A. Rogers, *Chem.Rev*., **2007**, 107, 1117. (c) S. Allard, M. Forster, B. Souharce, H. Thiem, and U. Sherf, *Angew.Chem.Int.Ed*., **2008**, 47, 4070. (d) Y. Shirota, H. Kageyama, *Chem.Rev*, **2007**, 107, 953 (e) H. Ma, H.-L. Yip, F. Huang, and A.K.-Y. Jen, *Adv.Funct.Mater.*, **2010**, 20, 1371

12. Y. Liu, X. Wan, F. Wang, J. Zhou, G. Long, J. Tian, J. You, Y. Yang, Y. Chen, *Adv, Energy Mater*., **2011**, 1, 771

13. (a) H. Minemawari, T. Yamada, H. Matsui, J. Tsutsumi, S. Haas, R. Chiba, R. Kumai, and T. Hasegawa, *Nature*, **2011**, 475, 364. (b) H.Y Li, B.C.K. Tee, J.J. Cha, Y. Cui. J.W. Chung, S.Y. Lee, and Z.N. Bao, *JACS*, **2012**, 134, 2760

14. (a) I.G.Lezama, and A.F.Morpurgo, *MRS Bulletin*, **2013**, 38, 51. (b) H.Li, G.Giri, J.B.-H.Tok, Z.Bao, *MRS Bulletin*, **2013**, 38, 34

15. J.Zaumseil, and H.Sirringhaus, *Chem.Rev*., **2007**, 107, 1296

16. T. Mori, *J.Phys.:Condens.Matter*., **2008**, 20, 184010

17. E.J.Meijer, D.M.de Leeuw, S. Setayesh, E.van Veenendaal, B.-H. Huisman, P.W.M. Blom, J.C. Hummelen, J. Scherf, and T.M. Klapwijk, *nature materials*, **2003**, 2, 678

18. (a) M. Mas-Torrent, C. Rovira, *Chem.Soc.Rev.*, **2008**, 37, 827 (b) Y. Shirota, H. Kageyama, *Chem.Rev*, **2007**, 107, 953

19. G. Li, R. Zhu, Y. Yang, *Nature Photonics***, 2012**, 6, 153

20. J. You, L. Dou, K. Yoshimura, T. Kato, K. Ohya, T. Moriarty, K. Emery, Ch.-C. Chen, J. Gao, G. Li, and Y. Yan, *nature communications*, **2013**, 4, 1446

21. P.M. Beaujuge, J.M.J. Fréchet., *JACS*, **2011**, 133, 20009

22. J.-L.Brédas, J.E.Norton, J. Cornil, V. Coropceanu*, Accounts of Chemical Research*, **2009**, 42, 11, 1691

23. (a) Y. Shirota, H. Kageyama, *Chem.Rev*, **2007**, 107, 953 (b) B.C.Thopmson, J.M.J. Fréchet, *Angew.Chem.Int.Ed*., **2008**, 47, 58

24. (a) Z.R.Owczrczyk, W.A.Braunecker, A.Garcia, R.Larsen, A.M.Nardes, N.Kopidakis, D.S.Ginley, D.C.Olson, *Macromolecules*, **2013**, 46, 1350 (b) Y.-Y.Lai, J.-M.Yeh, C.-E.Tsai, Y.-J.Cheng, *Eur.J.Org.Chem.*, **2013**, 5076

Chapter 2. Charge-Transfer complex based on Novel Electron Donor Indoloindole Derivatives for Ambipolar Single-Crystal Organic Field-Effect Transistors (sc-OFETs)

2.1 Introduction

Organic optoelectronics have attracted much attention in recent years due to their flexibility, low-cost, potential to large-area electronic devices, and structural tunability with chemical modification. In particular, much interest has been focused on organic filed-effect transistors (OFETs) with their applicability to organic circuits, and organic light-emitting transistors (OLETs). Among them, single-crystal OFETs (sc-OFETs) have advantages of uniform charge transporting properties compared to polymeric thin-film devices.[1]

Specially, ambipolar charge transporting OFETs have triggered significant interest as alternatives for complementary-like circuits with simplified fabrication.[2] Based on these tendency of research, multicomponent organic system has been suggested for active elements in ambipolar OFETs instead of single-component system, with significantly simplified synthesis and fabrication processes. [3]

Charge-transfer complex, composed of donor (D) and acceptor (A) combined by charge transfer interaction, exhibits novel characteristics different from individual donor and acceptor molecules, such as magnetic property[4], electrical conductivity[5], superconductivity[6], ferroelectricity[7], photoconductivity[8], and electrical semiconductivity[9]. Those unique

characteristics are affected, and controlled by energy levels of D and A molecules, stacking arrangement of D and A[10], and degree of charge transfer (ionicity). Until now, most of research for electrical properties of CT complex has been investigated about TTF-TCNQ CT complex and their analogues, and only a few of them shows ambipolar semiconducting property.[11] Thus, it is highly desired to explore novel CT complexes with ambipolar semiconducting properties.

In this work, novel electron donating molecule, indolo[3,2-b]indole (IDID) derivatives are used as a donor of CT complex, where 2 nitrogen atoms substituted heteroacene (pyrrole-containing heteroacene system) exhibits strong electron-donating nature. Compared to carbazole, IDID possesses more fused pyrrole rings in backbone, which results stronger electron donating property. By substituting several electron donating or accepting functional groups to IDID, energy levels of IDID derivatives are effectively tuned. To explore electron donating nature of IDID, CT complexes, using carbazole, and IDID derivatives as a donor and DNF, TNF, TCNQ as an acceptor, were demonstrated and investigated in photophysical study.

Among IDID derivatives, IDIDp was used for optoelectronic application for sc-OFETs. CT co-crystals of IDIDp-TCNQ were successfully grown in PMMA matrix and used as the active elements in sc-OFETs. Consequently, IDIDp-TCNQ CT co-crystals exhibited the ambipolar semiconducting property in sc-OFET devices, while IDIDp single crystal OFETs exhibited unipolar p-type charge transport property.

2.2 Experimental

2.2.1 Design concept and target materials

For the formation of CT complexes, 2,7-dinitro-9-fluorenone (DNF), 2,4,7-trinitro-9-fluorenone(TNF), and 7,7,8,8-tetracyanoquinodimethane (TCNQ) were chosen, which were commonly used as an acceptor. (as shown in Scheme 2.2) And to explore electron donating nature of IDID, I designed and synthesized IDID derivatives (as shown in Scheme 2.1). Pyrrole-containing heteroacene backbone unit exhibits significantly strong electron donating property and ladder-type planar structure, resulting in enhancement of the face-to-face charge transfer interaction between adjacent molecules. Furthermore, due to the planar structure of backbone unit, donor and acceptor could be easily stacked and charge transport property is considerably improved in columnar stacks. Aromatic groups attached on 2,7-position of IDID extend π-conjugation, and 2 alkyl side groups attached on nitrogen atoms enhance solubility of molecule.

Herein, E-CBZ, 2HIDID, and IDIDp (in Scheme 2.1 a) were studied as the reference molecules. By comparison of E-CBZ and 2HIDID, enhanced electron donating nature of IDID could be studied. And by substituting phenyl rings on 2,7-position of IDID backbone, I could investigate the effect of extended π-conjugation on the formation of CT complexes. By direct substitution of electron donating group and electron withdrawing group to IDID backbone unit (Scheme 2.1.b), electron donating nature of IDID derivatives was effectively tuned. Furthermore, para-phenylene type electron donating groups and electron withdrawing groups are attached on 2,7-position of IDID. (Scheme 2.1 c,d) With comparing the photophysical

properties of IDID derivatives in Scheme 2.1 c,d, I could understand the effect of supramolecular structures on the property of CT complexes.

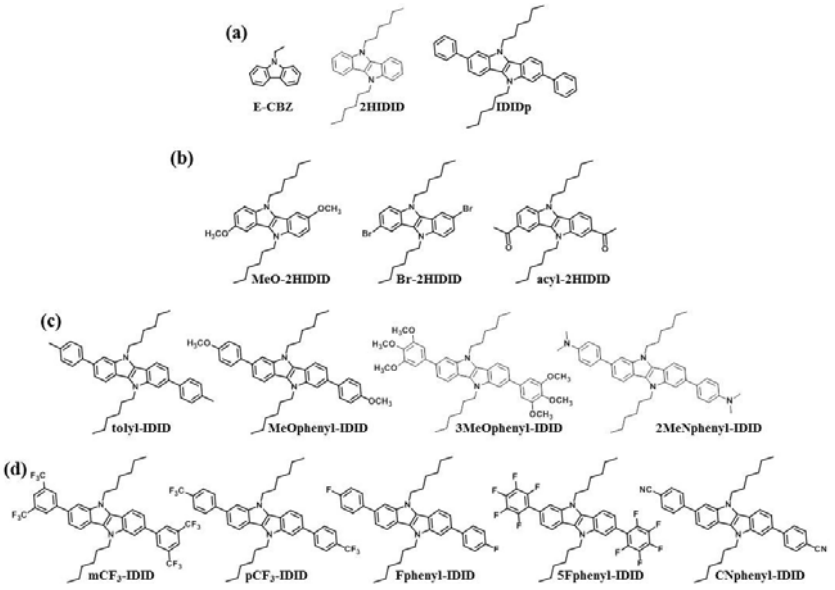

Scheme 2.1. Donor molecules (a) reference molecules (E-CBZ, 2HIDID, IDIDp), (b) functional groups directly attached indoloindole derivatives (c) electron donating group attached indoloindole derivatives, and (d) electron withdrawing group attached indoloindole derivatives.

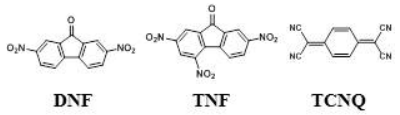

Scheme 2.2. Acceptor molecules (DNF, TNF, and TCNQ).

2.2.2 Synthesis

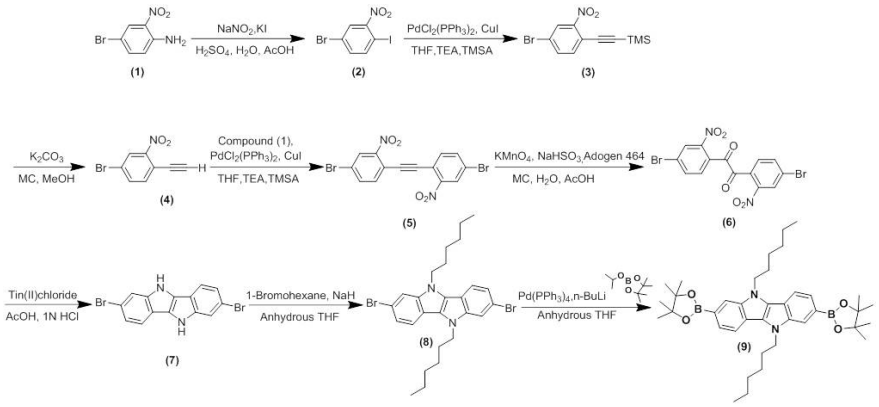

Scheme 2.3. Synthesis of indoloindole core.

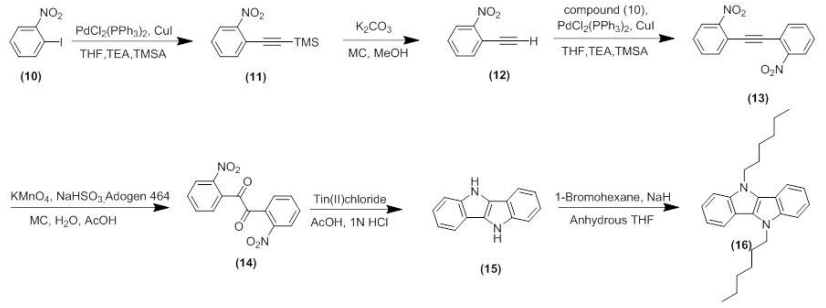

Scheme 2.4. Synthesis of non-brominated indoloindole (2HIDID).

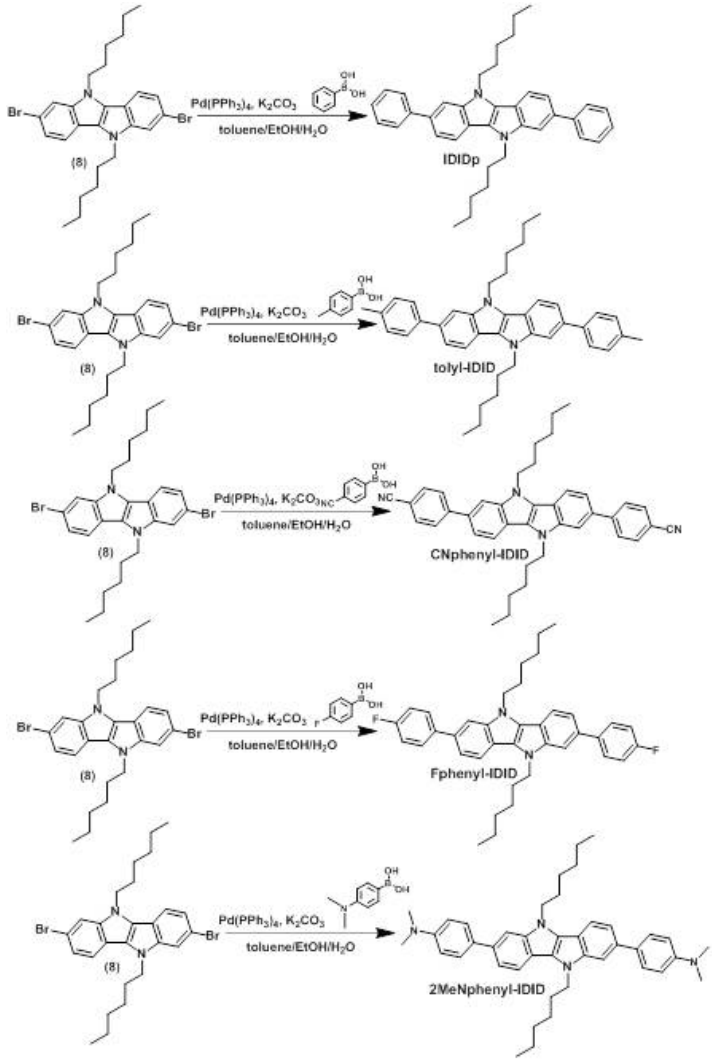

Scheme 2.5. Synthesis of indoloindole derivatives (1).

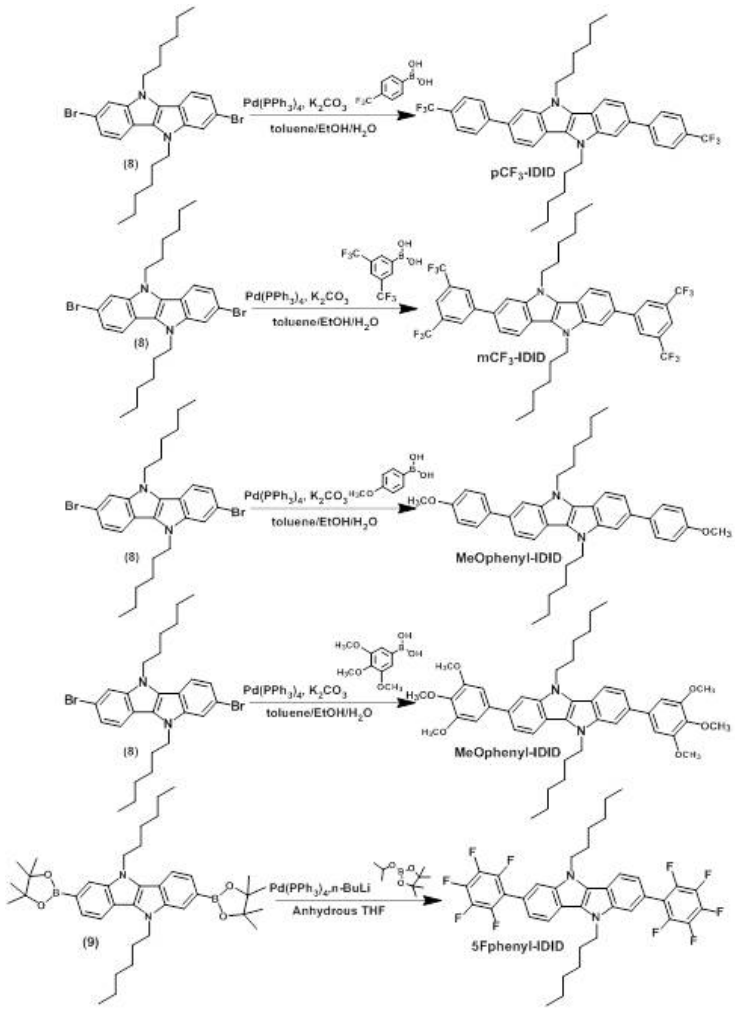

Scheme 2.6. Synthesis of indoloindole derivatives (2).

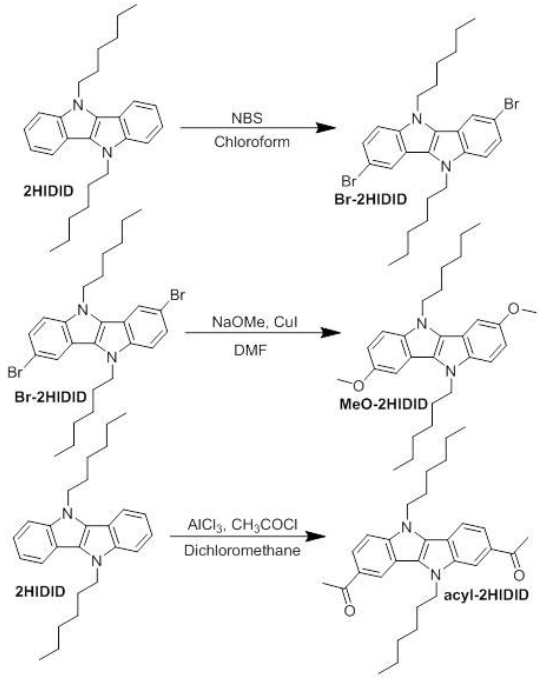

Scheme 2.7. Synthesis of indoloindole derivatives (3).

Final products were synthesized according to the procedure shown in Scheme 2.3~2.7. Unless stated otherwise, all reagents were purchased at Sigma Aldrich, TCI, and Alfa Aesar.

DNF, TNF, and TCNQ were purchased from Aldrich Chemical Company.

4-bromo-1-iodo-2-nitrobenzene (2)

A 500 mL two-neck round-bottom flask, equipped with a magnetic stirrer bar and a dropping funnel was charged with water (38 mL) and H_2SO_4 (35 mL), acetic acid (35 mL), and 4-bromo-2-nitroaniline (1) (10.851 g, 50 mmol) were added at 0°C. Afterwards, a solution of $NaNO_2$

(3.795 g, 55 mmol, in 15mL H2O) was added dropwise slowly. After completion of the addition the mixture was stirred an hour, and a solution of KI (9.960 g 60 mmol, in 15 mL H_2O) was added dropwise. After completion of the addition the mixture was heated to 60 °C for 3 hour, cool down to 0°C again, and methylene chloride was added until all precipitate was dissolved. The reaction mixture was poured into saturated $NaHCO_3$ aqueous solution 400 mL in ice bath and extraction with methylene chloride. The organic phase were washed with brine and saturated $Na_2S_2O_3$ aqueous solution (250 mL x 2, each), dried over $MgSO_4$, filtered, and concentrated. The residue was recrystallized from ethanol to give compound (2) as orange powder (14.560, 77.1%).

1H-NMR (300 MHz, $CDCl_3$, δ): 7.99 (s, 1H), 7.90-7.88 (d, 1H), 7.41-7.38 (d, 1H)

(4-bromo-2-nitro-phenylethynyl)-trimethyl-silane (3)

A 100 mL two-neck round-bottom flask, equipped with a magnetic stirrer bar was added the 4bromo-1-iodo-2-nitrobenzene (2) (5 g, 15.248 mmol), bis(triphenylphosphine)palladium(II) dichloride (0.535 g, 0.762 mmol), and copper(I) iodide (0.290 g, 1.525 mmol). The vessel was then sealed with a rubber septum, evacuated and backfilled with Ar gas. The THF (40 mL) was added as a solvent, and the trimethylsilylacetylene (1.500 g, 15.248 mmol) and triethylamine (10 mL) was added. After 3 hours stirring at room temperature, the reaction mixture filtered through a silica plug. The concentrated filtrate purified by column chromatography (ethyl acetate/n-hexane; 1:9, v/v) to give compound (3) as brown oil (4.120 g, 90.6%).

1H-NMR (300 MHz, $CDCl_3$, δ): 8.16 (s, 1H), 7.69-7.66 (d, 1H), 7.52-7.49 (d, 1H), 0.27 (s, 9H)

4-bromo-1-ethynyl-2-nitrobenzene (4)

A 250 mL round-bottom flask, equipped with a magnetic stirrer bar was added the (4-bromo-2-nitro-phenylethyneyl)-trimethyl-silane (3) (3.770 g, 15.642 mmol), K_2CO_3 (1.922 g, 13.906 mmol), and a co-solvent of methylene chloride (80 mL) was added followed by the methanol (20mL). After 10 hours stirring at room temperature, the reaction mixture poured in to water (300 mL), and extracted with methylene chloride. The organic layer was washed with brine (x2) and dried over $MgSO_4$. Flash column chromatography (ethyl acetate/n-hexane; 1:3, v/v) gave compound (4) as brown powder (2.791 g, 97.6%).

1H-NMR (300 MHz, $CDCl_3$, δ): 8.21 (s, 1H), 7.74-7.71 (d, 1H), 7.57-7.54 (d, 1H), 3.57 (s, 1H)

4,4'-dibromo-2,2'-dinitrotolane (5)

Synthesis of 4,4'-dibromo-2,2'-dinitrotolane took same synthetic procedure with (4-bromo-2-nitro-phenylethynyl)-trimethyl-silane. Used were 4-bromo-1-ethynyl-2-nitrobenzene (4) (3.020 g, 13.361 mmol), 4-bromo-1-iodo-2-nitrobenzene (2) (4.382 g, 13.361 mmol), bis(triphenylphosphine)palladium(II) dichloride (0.469 g, 0.668 mmol), copper(I) iodide (0.250 g, 1.336 mmol), THF (60 mL), and triethylamine (12mL). Flash column chromatography (CHCl3) and recrystallization ($CHCl_3$) afforded the compound (5) as brown solid (2.573 g, 45%).

1H-NMR (300 MHz, $CDCl_3$, δ): 8.31 (s, 2H), 7.81-7.78 (d, 2H), 7.69-

7.67 (d, 2H)

4,4'-dibromo-2-2'-dinitrobenzil (6)

A 250 mL round-bottom flask, equipped with a magnetic stirrer bar was added the potassium permanganate (2.815 g, 17.816 mmol), Adogen 464 (catalytic amount), water (60 mL), methylene chloride (80 mL), and acetic acid (3 mL). The mixture was stirred and evacuated and backfilled with Ar gas. The mixture was added the 4,4'-dibromo-2,2'dinitrotolane (5) and then gently refluxed for 5 hours, cooled, and decolorized using $NaHSO_3$. The resulting two clear phases were separated, and the yellow organic phase was dried over $MgSO_4$ and filtered through a silica plug. The yellow filtrate was concentrated, and the resulting solid was washed with methanol to give compound (6) as yellow crystalline solid (2.454 g, 91%).

1H-NMR (300 MHz, $CDCl_3$, δ): 8.41 (s, 2H), 8.03-8.00 (d, 2H), 7.54-7.52 (d, 2H)

2,7-dibromo-5,10-dihydroindolo[3,2-b]indole (7)

A 250 mL round-bottom flask, equipped with a magnetic stirrer bar was added the 4,4'-dibromo-2,2'-dinitrobenzil (6) (2.811 g, 6.218 mmol), and warm acetic acid (50 mL). With vigorous stirring, the reaction vessel was added the filtrate of stannous chloride (24.700 g, 124.375 mmol), acetic acid (60 mL), and 1 N HCl (24 mL) mixed solution. The vessel gently refluxed for 5 hours at 80°C. The resulting precipitate was filter, and washed with acetic acid, 1 N HCl, water, and ethanol. Flash column chromatography (ethyl acetate) and washing ($CHCl_3$) afford the compound (7) as gray solid (1.223 g, 54%).

1H-NMR (300 MHz, Acetone-d_6, δ): 10.51 (s, 2H), 7.74 (d, 2H), 7.73-7.72 (d, 2H), 7.25-7.22 (d, 2H)

2,7-dibromo-5,10-dihexyl-5,10-dihydroinolo[3,2-b]indole (8)

A 100 mL round-bottom flask, equipped with a magnetic stirrer bar and reflux condenser was baked under reduced pressure and Ar backfilled (x3). The baked reaction vessel was added 2,7-dibromo-5,10-dihydroindolo[3,2-b]indole (7) (1.500 g, 4.120 mmol), anhydrous THF (40 mL), NaH (0.390 g, 16.482 mmol). After 10 minutes at room temperature, 2.720g (16.482, mmol) of 1-bromohexane was added to the reaction mixture. After being stirring 10 minutes, the vessel gently refluxed 48hours, the reaction mixture poured into brine (200 mL). The organic layer separated, washed (water, x3), dried with $MgSO_4$, and concentrated. Resulting crude product was purified by flash column chromatography (ethyl acetate/n-hexane; 1:4, v/v) and recrystallization (ethyl acetate) to give compound (8) as white crystalline solid (1.652 g, 75%)

1H-NMR (300 MHz, $CDCl_3$, δ): 7.66-7.63 (d, 2H), 7.58 (s, 2H), 7.28 (d, 2H), 4.42-4.37 (t, 4H), 1.95-1.88 (m, 4H), 1.39-1.23 (m, 12H), 0.87-0.83 (t, 6H)

5,10-dihexyl-2,7-bis(4,4,5,5-tetramethyl-1,3,2-dioxaborolan-2-yl)-5,10-dihydroindolo[3,2-b]indole (9)

A 100 mL round-bottom flask, equipped with a magnetic stirrer bar and reflux condenser was baked under reduced pressure and Ar backfilled (x3). The baked reaction vessel was added 2,7-dibromo-5,10-dihexyl-5,10-

dihydroinolo[3,2-b]indole (8) (0.400g, 0.831 mmol) and Anhydrous THF(70mL) in dry ice and acetone bath. After 1 hour stirring, n-Butyllithium solution 1.6M in hexane (0.266 g, 4.154 mmol) was gently injected. And after 1 hour stirring, 2-isopropoxy-4,4,5,5-tetramethyl-1,3,2-dioxaborolane (3.804g, 4.154 mmol) was injected. The solution was stirred at room temperature for 2 hours. After reaction finished, reaction mixture quenched with brine (300 mL), and extracted with methylene chloride. The combined organic phase was concentrated under reduced pressure. The crude product was purified by column chromatography (ethyl acetate/n-hexane; 1:100, v/v) to afforded 5,10-dihexyl-2,7-bis(4,4,5,5-tetramethyl-1,3,2-dioxaborolan-2-yl)-5,10-dihydro indolo[3,2-b]indole (9) as white oilish liquid (0.180g, 35%)

1H-NMR (300 MHz, DMSO, δ): 7.93 (s, 2H), 7.91-7.88 (d, 2H), 7.46-7.44 (d, 2H), 4.60-4.58 (t, 4H), 1.88-1.84 (m,4H) , 1.34 (s, 24H), 1.23-1.08 (m, 12H), 0.79-0.41-0.79 (m, 6H),

trimethyl((2-nitrophenyl)ethynyl)silane (11)

A 100 mL two-neck round-bottom flask, equipped with a magnetic stirrer bar was added the 1-iodo-2-nitrobenzene (10) (4 g, 17.697 mmol), bis(triphenylphosphine)palladium(II) dichloride (0.621 g, 0.885 mmol), and copper(I) iodide (0.337 g, 1.770 mmol). The vessel was then sealed with a rubber septum, evacuated and backfilled with Ar gas. The THF (40 mL) was added as a solvent, and the trimethylsilylacetylene (1.738 g, 17.697 mmol) and triethylamine (10 mL) was added. After 3 hours stirring at room temperature, the reaction mixture filtered through a silica plug. The concentrated filtrate purified by column chromatography (ethyl

acetate/n-hexane; 1:9, v/v) to give compound (11) as brown oil (2.705 g, 70%).

1H-NMR (300 MHz, $CDCl_3$, δ): 8.03-7.99 (d, 1H), 7.67-7.64 (d, 1H), 7.58-7.53 (t, 1H), 7.48-7.42 (t, 1H), 0.29 (s, 9H)

1-ethynyl-2-nitrobenzene (12)

A 250 mL round-bottom flask, equipped with a magnetic stirrer bar was added the trimethyl((2-nitrophenyl)ethynyl)silane (11) (2.705 g, 12.334 mmol), K_2CO_3 (1.875 g, 13.568 mmol), and a co-solvent of methylene chloride (80 mL) was added followed by the methanol (20mL). After 10 hours stirring at room temperature, the reaction mixture poured in to water (300 mL), and extracted with methylene chloride. The organic layer was washed with brine (x2) and dried over $MgSO_4$. Flash column chromatography (ethyl acetate/n-hexane; 1:3, v/v) gave compound (12) as orange powder (1.734 g, 95.6%).

1H-NMR (300 MHz, $CDCl_3$, δ): 8.07-8.04 (d, 1H), 7.72-7.69 (d, 1H), 7.62-7.57 (t, 1H), 7.54-7.48 (t, 1H), 3.51 (s, 1H)

1,2-bis(2-nitrophenyl)ethyne (13)

Synthesis of 4,4'-dibromo-2,2'-dinitrotolane took same synthetic procedure trimethyl((2-nitrophenyl)ethynyl)silane (11). Used were 1-ethynyl-2-nitrobenzene (12), (1.734 g, 11.799 mmol1-iodo-2-nitrobenzene (10) (2.937 g, 11.793 mmol), bis(triphenylphosphine)palladium(II) dichloride (0.414 g, 0.590 mmol), copper(I) iodide (0.225 g, 1.180 mmol), THF (24 mL), and triethylamine (6mL). Flash column chromatography ($CHCl_3$) and recrystrallization (EA) afforded the compound (13) as brown

solid (1.728 g, 55%).

1H-NMR (300 MHz, $CDCl_3$, δ): 8.16-8.13 (d, 2H), 7.85-7.82 (d, 2H), 7.69-7.63 (t, 2H), 7.57-7.51 (t, 2H)

1,2-bis(2-nitrophenyl)ethane-1,2-dione (14)

A 250 mL round-bottom flask, equipped with a magnetic stirrer bar was added the potassium permanganate (3.054 g, 19.327 mmol), Adogen 464 (catalytic amount), water (60 mL), methylene chloride (80 mL), and acetic acid (3 mL). The mixture was stirred and evacuated and backfilled with Ar gas. The mixture was added 1,2-bis(2-nitrophenyl)ethyne (13) and then gently refluxed for 5 hours, cooled, and decolorized using $NaHSO_3$. The resulting two clear phases were separated, and the yellow organic phase was dried over $MgSO_4$ and filtered through a silica plug. The yellow filtrate was concentrated, and the resulting solid was washed with methanol to give compound (14) as yellow crystalline solid (1.738 g, 90%).

1H-NMR (300 MHz, $CDCl_3$, δ): 8.30 (d, 2H), 7.92-7.87 (t, 2H), 7.79-7.74 (t, 2H), 7.69-7.67(d, 2H).

5,10-dihydroindolo[3,2-b]indole (15)

A 250 mL round-bottom flask, equipped with a magnetic stirrer bar was added the 1,2-bis(2-nitrophenyl)ethane-1,2-dione (14) (1.738 g, 5.788 mmol), and warm acetic acid (30 mL). With vigorous stirring, the reaction vessel was added the filtrate of stannous chloride (22 g, 115.78 mmol), acetic acid (60 mL), and 1 N HCl (17 mL) mixed solution. The vessel gently refluxed for 5 hours at 80°C. The resulting precipitate was filter,

and washed with acetic acid, 1 N HCl, water, and ethanol. Flash column chromatography (ethyl acetate) and washing ($CHCl_3$) afford the compound (15) as gray solid (0.72 g, 60.3%).

1H-NMR (300 MHz, Acetone-d_6, δ): 10.24 (s, 2H), 7.78-7.75 (d, 2H), 7.53-7.51(d, 2H), 7.20-7.15 (t, 2H), 7.10-7.05 (t, 2H).

5,10-dihexyl-5,10-dihydroindolo[3,2-b]indole (16, 2HIDID)

A 100 mL round-bottom flask, equipped with a magnetic stirrer bar and reflux condenser was baked under reduced pressure and Ar backfilled (x3). The baked reaction vessel was added 5,10-dihydroindolo[3,2-b]indole (15) (0.4 g, 1.94 mmol), anhydrous THF (40 mL), NaH (0.230 g, 9.70 mmol). After 10 minutes at room temperature, 1.6g (9.70 mmol) of 1-bromohexane was added to the reaction mixture. After being stirring 10 minutes, the vessel gently refluxed 48hours, the reaction mixture poured into brine (200 mL). The organic layer separated, washed (water, x3), dried with $MgSO_4$, and concentrated. Resulting crude product was purified by flash column chromatography (ethyl acetate/n-hexane; 1:9, v/v) and recrystallization (ethyl acetate) to give compound (16) as white crystalline solid (0.52 g, 72%)

1H-NMR (300 MHz, Acetone-d6, δ): 7.97-7.92(d, 2H), 7.59-7.57(d, 2H), 7.28-7.23(t, 2H), 7.15-7.02(t, 2H), 4.59-4.42(t, 4H), 1.99-1.91(m, 4H), 1.47-1.28(m, 12H), 0.92-0.61(m, 6H).

2,7-diphenyl -5,10-dihexyl-5,10-dihydroindolo[3,2-b]indole (IDIDp)

A 100 mL round-bottom flask, equipped with a magnetic stirrer bar was added 2,7-dibromo-5,10-dihexyl-5,10-dihydroinolo[3,2-b]indole (8)

(0.200 g, 0.376 mmol), phenylboronic acid (0.096 g, 0.789 mmol), tetrakis(triphenylhosphine)palladium(0) (0.065g, 0.056 mmol), 2N K_2CO_3 aqueous solution (10 mL), toluene (20 mL), and ethanol (5mL) under Ar atmosphere. The solution was stirred at 115℃, for 40 hours. After reaction finished, reaction mixture quenched with 1N HCl aqueous solution (300 mL), and extracted with methylene chloride. The combined organic phase was dried with $MgSO_4$ and concentrated under reduced pressure. The crude product was purified by flash column chromatography (chloroform/ethyl acetate/n-hexane; 2.5:0.5:7, v/v) and recrystallization (ethyl acetate) to afforded 2,7-diphenyl -5,10-dihexyl-5,10-dihydroindolo[3,2-b]indole (IDIDp) as yellow solid (0.142 g, 72%)

1H-NMR (300 MHz, DMSO, δ): 7.98 (d, 2H), 7.92 (s, 2H), 7.82-7.80 (d, 4H), 7.53-7.48 (t, 4H), 7.45-7.44 (d, 2H), 7.38-7.33 (t, 2H), 4.67-4.63 (t, 4H), 1.95-1.88 (m, 4H), 1.35-1.23 (m, 12H), 0.80-0.75 (t, 6H)

Elemental Analysis calculated for $C_{38}H_{42}N_2$: C 86.64, H 8.04, N 5.32; found: C 86.67, H 8.03, N 5.22.

5,10-dihexyl-2,7-di-p-tolyl-5,10-dihydroindolo[3,2-b]indole (tolyl-IDID)

A 100 mL round-bottom flask, equipped with a magnetic stirrer bar was added 2,7-dibromo-5,10-dihexyl-5,10-dihydroinolo[3,2-b]indole (8) (0.200 g, 0.376 mmol), p-tolylboronic acid (0.107 g, 0.789 mmol), tetrakis(triphenylhosphine)palladium(0) (0.065g, 0.056 mmol), 2N K2CO3 aqueous solution (10 mL), toluene (20 mL), and ethanol (5mL) under Ar atmosphere. The solution was stirred at 115℃, for 40 hours. After reaction finished, reaction mixture quenched with 1N HCl aqueous

solution (300 mL), and extracted with methylene chloride. The combined organic phase was dried with $MgSO_4$ and concentrated under reduced pressure. The crude product was purified by flash column chromatography (chloroform/ethyl acetate/n-hexane; 1.5:0.5:8, v/v) and recrystallization (ethyl acetate) to afforded 5,10-dihexyl-2,7-di-p-tolyl-5,10-dihydroindolo[3,2-b]indole (tolyl-IDID) as yellow crystalline solid (0.142 g, 67%)

1H-NMR (300 MHz, DMSO, δ): 7.94-7.92(d, 2H), 7.87(s, 2H), 7.71-7.69(d, 4H), 7.44-7.42(d, 2H), 7.32-7.29(d, 4H), 4.65-4.61(t, 4H), 2.37(s, 6H), 1.91-1.87(m, 4H), 1.34-1.17((m 12H), 0.80-0.75(t, 6H)

5,10-dihexyl-2,7-bis(4-methoxyphenyl)-5,10-dihydroindolo[3,2-b]indole (MeOphenyl-IDID)

A 100 mL round-bottom flask, equipped with a magnetic stirrer bar was added 2,7-dibromo-5,10-dihexyl-5,10-dihydroinolo[3,2-b]indole (8) (0.150 g, 0.282 mmol), (4-methoxyphenyl)boronic acid (0.090 g, 0.592 mmol), tetrakis(triphenylhosphine)palladium(0) (0.049g, 0.042 mmol), 2N K2CO3 aqueous solution (10 mL), toluene (20 mL), and ethanol (5mL) under Ar atmosphere. The solution was stirred at 115℃, for 40 hours. After reaction finished, reaction mixture quenched with 1N HCl aqueous solution (300 mL), and extracted with methylene chloride. The combined organic phase was dried with $MgSO_4$ and concentrated under reduced pressure. The crude product was purified by flash column chromatography (chloroform/ethyl acetate/n-hexane; 1.5:0.5:8, v/v) and recrystallization (ethyl acetate) to afforded 5,10-dihexyl-2,7-bis(4-methoxyphenyl)-5,10-dihydroindolo[3,2-b]indole (MeOphenyl-IDID) as yellow solid (0.14 g,

64%)

1H-NMR (300 MHz, THF, δ): 7.86-7.84(d, 2H), 7.67(s, 2H), 7.65-7.62(d, 4H), 7.35-7.33(d, 2H), 6.99-6.96(d, 4H), 4.62-4.57(t, 4H), 3.81(s, 6H), 2.02-1.92(m, 4H), 1.49-1.16((m, 12H), 0.88-0.81(t, 6H)

5,10-dihexyl-2,7-bis(3,4,5-trimethoxyphenyl)-5,10-dihydro-indolo[3,2-b]indole (3MeOphenyl-IDID)

A 100 mL round-bottom flask, equipped with a magnetic stirrer bar was added 2,7-dibromo-5,10-dihexyl-5,10-dihydroinolo[3,2-b]indole (8) (0.150 g, 0.282 mmol), (3,4,5-trimethoxyphenyl)boronic acid (0.125 g, 0.592 mmol), tetrakis(triphenylhosphine)palladium(0) (0.049g, 0.042 mmol), 2N K_2CO_3 aqueous solution (10 mL), toluene (20 mL), and ethanol (5mL) under Ar atmosphere. The solution was stirred at 115℃, for 40 hours. After reaction finished, reaction mixture quenched with 1N HCl aqueous solution (300 mL), and extracted with methylene chloride. The combined organic phase was dried with MgSO4 and concentrated under reduced pressure. The crude product was purified by flash column chromatography (chloroform/ethyl acetate/n-hexane; 1.5:0.5:8, v/v) and recrystallization (ethyl acetate/n-hexane) to afforded 5,10-dihexyl-2,7-bis(3,4,5-trimethoxyphenyl)-5,10-dihydro-indolo[3,2-b]indole (3MeOphenyl-IDID) as yellow solid (0.11 g, 55%)

1H-NMR (300 MHz, THF, δ): 7.88-7.85(d, 2H), 7.68(s, 2H), 7.37-7.34(d, 2H), 6.93(s, 4H), 4.63-4.58(t, 4H), 3.89(s, 12H), 3.76(s, 6H), 2.04-1.95(m, 4H), 1.49-0.16(m, 12H), 0.86-0.81(t, 6H)

4,4'-(5,10-dihexyl-5,10-dihydroindolo[3,2-b]indole-2,7-diyl)bis(N,N-

dimethylaniline) (2MeNphenyl-IDID)

A 100 mL round-bottom flask, equipped with a magnetic stirrer bar was added 2,7-dibromo-5,10-dihexyl-5,10-dihydroinolo[3,2-b]indole (8) (0.150 g, 0.282 mmol), (4-(dimethylamino)phenyl)boronic acid (0.098 g, 0.592 mmol), tetrakis(triphenylhosphine)palladium(0) (0.049g, 0.042 mmol), 2N K_2CO_3 aqueous solution (10 mL), toluene (20 mL), and ethanol (5mL) under Ar atmosphere. The solution was stirred at 115℃, for 40 hours. After reaction finished, reaction mixture quenched with 1N HCl aqueous solution (300 mL), and extracted with methylene chloride. The combined organic phase was dried with $MgSO_4$ and concentrated under reduced pressure. The crude product was purified by flash column chromatography (ethyl acetate/n-hexane; 4:6, v/v) and recrystallization (ethyl acetate) to 4,4'-(5,10-dihexyl-5,10-dihydroindolo[3,2-b]indole-2,7-diyl)bis(N,N-dimethylaniline) (2MeNphenyl-IDID) as yellow solid (0.11 g, 64%)

1H-NMR (300 MHz, THF, δ): 7.81(m, 2H), 7.63(s, 2H), 7.58-7.55(d, 4H), 7.34-7.32(d, 2H), 6.83-6.80(d, 4H), 4.57(m, 4H), 2.97(s, 12H), 2.04-1.93(m, 4H), 1.49-1.42((m, 12H), 0.88-0.82(m, 6H)

4,4'-(5,10-dihexyl-5,10-dihydroindolo[3,2-b]indole-2,7-diyl)dibenzonitrile (CNphenyl-IDID)

A 100 mL round-bottom flask, equipped with a magnetic stirrer bar was added 2,7-dibromo-5,10-dihexyl-5,10-dihydroinolo[3,2-b]indole (8) (0.200 g, 0.376 mmol), (4-cyanophenyl)boronic acid (0.116 g, 0.789 mmol), tetrakis(triphenylhosphine)palladium(0) (0.065g, 0.056 mmol), 2N K_2CO_3 aqueous solution (8 mL), toluene (16 mL), and ethanol (4mL)

under Ar atmosphere. The solution was stirred at 115℃, for 40 hours. After reaction finished, reaction mixture quenched with 1N HCl aqueous solution (300 mL), and extracted with methylene chloride. The combined organic phase was dried with $MgSO_4$ and concentrated under reduced pressure. The crude product was purified by flash column chromatography (ethyl acetate/n-hexane; 4:6, v/v) and recrystallization (ethyl acetate) to 4,4'-(5,10-dihexyl-5,10-dihydroindolo[3,2-b]indole-2,7-diyl)bis(N,N-dimethylaniline) (2MeNphenyl-IDID) as orange crystalline solid (0.97 g, 45%)

1H-NMR (300 MHz, DMSO, δ): 8.08-8.01(m, 8H), 7.96-7.93(d, 4H), 7.57-7.55(d, 2H), 4.70-4.66(m, 4H), 1.92-1.87(m, 4H), 1.31-1.19(m, 12H), 0.78-0.74(t, 6H)

2,7-bis(4-fluorophenyl)-5,10-dihexyl-5,10-dihydroindolo[3,2-b]indole (Fphenyl-IDID)

A 100 mL round-bottom flask, equipped with a magnetic stirrer bar was added 2,7-dibromo-5,10-dihexyl-5,10-dihydroinolo[3,2-b]indole (8) (0.300 g, 0.564 mmol), (4-fluorophenyl)boronic acid (0.166 g, 1.183 mmol), tetrakis(triphenylhosphine)palladium(0) (0.098g, 0.085 mmol), 2N K_2CO_3 aqueous solution (10 mL), toluene (20 mL), and ethanol (5mL) under Ar atmosphere. The solution was stirred at 115℃, for 40 hours. After reaction finished, reaction mixture quenched with 1N HCl aqueous solution (300 mL), and extracted with methylene chloride. The combined organic phase was dried with $MgSO_4$ and concentrated under reduced pressure. The crude product was purified by flash column chromatography (ethyl acetate/n-hexane; 4:6, v/v) and recrystallization (ethyl acetate) to

2,7-bis(4-fluorophenyl)-5,10-dihexyl-5,10-dihydroindolo[3,2-b]indole (Fphenyl-IDID) as orange crystalline solid (0.21 g, 66%)

1H-NMR (300 MHz, THF, δ): 7.92-7.89(d, 2H), 7.76-7.70(t, 6H), 7.38-7.35(d, 2H), 7.20-7.13(m, 4H), 4.64-4.59(t, 4H), 2.03-1.91(m, 4H), 1.49-1.11(m, 12H), 0.88-0.81(t, 6H)

5,10-dihexyl-2,7-bis(perfluorophenyl)-5,10-dihydroindolo[3,2-b]indole (5Fphenyl-IDID)

A 100 mL round-bottom flask, equipped with a magnetic stirrer bar was added 5,10-dihexyl-2,7-bis(4,4,5,5-tetramethyl-1,3,2-dioxaborolan-2-yl)-5,10-dihydroindolo[3,2-b]indole (9) (0.226 g, 0.360 mmol), 1,2,3,4,5-pentafluoro-6-iodobenzene (0.222 g, 0.756 mmol), tetrakis(triphenylhosphine)palladium(0) (0.042 g, 0.036 mmol), 2N K_2CO_3 aqueous solution (10 mL), toluene (20 mL), and ethanol (5mL) under Ar atmosphere. The solution was stirred at 115℃, for 40 hours. After reaction finished, reaction mixture quenched with 1N HCl aqueous solution (300 mL), and extracted with methylene chloride. The combined organic phase was dried with $MgSO_4$ and concentrated under reduced pressure. The crude product was purified by flash column chromatography (ethyl acetate/n-hexane; 4:6, v/v) and recrystallization (ethyl acetate) to 5,10-dihexyl-2,7-bis(perfluorophenyl)-5,10-dihydroindolo[3,2-b]indole (5Fphenyl-IDID) as orange crystalline solid (0.16 g, 63%)

1H-NMR (300 MHz, THF, δ): 8.03-7.97(d, 2H), 7.66(s, 2H), 7.27-7.20(d, 2H), 4.62-4.58(t, 4H), 2.03-1.89(m, 4H), 1.45-1.23(m, 12H), 0.88-0.81(t, 6H)

19F-NMR (300 MHz, DMSO, δ): -144.99~-145.11(m, 4H), -158.67~-

158.85(t, 2H), -164.67~-164.87 (m, 4H).

5,10-dihexyl-2,7-bis(4-(trifluoromethyl)phenyl)-5,10-dihydroindolo[3,2-b]indole (pCF_3-IDID)

A 100 mL round-bottom flask, equipped with a magnetic stirrer bar was added 2,7-dibromo-5,10-dihexyl-5,10-dihydroindolo[3,2-b]indole (8) (0.250 g, 0.470 mmol), (4-(trifluoromethyl)phenyl)boronic acid (0.187 g, 0.986 mmol), tetrakis(triphenylhosphine)palladium(0) (0.054 g, 0.047 mmol), 5N NaOH aqueous solution (10 mL), toluene (20 mL), and ethanol (5mL) under Ar atmosphere. The solution was stirred at 115℃, for 40 hours. After reaction finished, reaction mixture quenched with 1N HCl aqueous solution (300 mL), and extracted with methylene chloride. The combined organic phase was dried with $MgSO_4$ and concentrated under reduced pressure. The crude product was purified by flash column chromatography (ethyl acetate/n-hexane; 4:6, v/v) and recrystallization (ethyl acetate) to 5,10-dihexyl-2,7-bis(4-(trifluoromethyl)phenyl)-5,10-dihydroindolo[3,2-b]indole (pCF_3-IDID) as yellow crystalline solid (0.21 g, 67%)

1H-NMR (300 MHz, THF, δ): 8.07-8.01(t, 4H), 7.85-7.83(d, 2H), 7.56-7.53(d, 1H), 4.75-4.68(t, 4H), 2.13-1.91(m, 4H), 1.55-1.23(m, 12H), 0.92-0.81(t, 6H)

2,7-bis(3,5-bis(trifluoromethyl)phenyl)-5,10-dihexyl-5,10-dihydroindolo[3,2-b]indole (mCF_3-IDID)

A 100 mL round-bottom flask, equipped with a magnetic stirrer bar was added 2,7-dibromo-5,10-dihexyl-5,10-dihydroindolo[3,2-b]indole (8)

(0.500 g, 0.939 mmol), (3,5-bis(trifluoromethyl)phenyl)boronic acid (0.497 g, 1.930 mmol), tetrakis(triphenylhosphine)palladium(0) (0.065 g, 0.056 mmol), 5N NaOH aqueous solution (15 mL), toluene (24 mL), and ethanol (6mL) under Ar atmosphere. The solution was stirred at 115℃, for 40 hours. After reaction finished, reaction mixture quenched with 1N HCl aqueous solution (300 mL), and extracted with methylene chloride. The combined organic phase was dried with $MgSO_4$ and concentrated under reduced pressure. The crude product was purified by flash column chromatography (ethyl acetate/n-hexane; 4:6, v/v) and recrystallization (ethyl acetate) to 5,10-dihexyl-2,7-bis(4-(trifluoromethyl)phenyl)-5,10-dihydroindolo[3,2-b]indole (mCF_3-IDID) as yellow crystalline solid (0.37 g, 49%)

1H-NMR (300 MHz, THF, δ): 8.32(s, 4H), 8.05-8.03(d, 2H), 7.95(d, 2H), 7.55-7.52 (d, 2H), 4.75-4.69(t, 4H), 2.13-1.94(m, 4H), 1.50-1.29(m, 12H), 0.87-0.82(t, 6H)

3,8-dibromo-5,10-dihexyl-5,10-dihydroindolo[3,2-b]indole (Br-2HIDID)

A 250 mL round-bottom flask, equipped with a magnetic stirrer bar was added 5,10-dihexyl-5,10-dihydroindolo[3,2-b]indole (16, 2HIDID) (0.300 g, 0.800 mmol) and chloroform(100mL) solution, followed by gentle injection of NBS (0.299 g, 1.682 mmol) in ice bath under Ar atmosphere with light shielding. The solution was stirred for 3 hours. After reaction finished, reaction mixture was poured into brine solution, and extracted with methylene chloride. The combined organic phase was dried with $MgSO_4$ and concentrated under reduced pressure. The crude product was

purified by flash column chromatography (ethyl acetate/n-hexane; 4:6, v/v) and recrystallization (ethyl acetate) to 3,8-dibromo-5,10-dihexyl-5,10-dihydroindolo[3,2-b]indole (Br-2HIDID) as white crystalline solid (0.25 g, 58%)

1H-NMR (300 MHz, THF, δ): 7.76-7.73(d, 2H), 7.72(s, 2H), 7.23-7.20(d, 2H), 4.52-4.48(t, 4H), 1.96-1.86(m, 4H), 1.44-1.22(m, 12H), 0.85-0.81(t, 6H)

5,10-dihexyl-3,8-dimethoxy-5,10-dihydroindolo[3,2-b]indole (MeO-2HIDID)

CuI(0.150g, 0.789mmol) was added to the solution of Br-2HIDID (0.100g, 0.188mmol) in DMF(3mL), followed by NaOMe in methanol (25wt%, 0.86mL, 3.757mmol) in a sealed tube. The mixture was heated under microwave at 120℃ for 10h. After reaction finished, the resulting crude mixture was diluted by EA, and washed with saturated K_2CO_3 solution. The combined organic phase was dried with $MgSO_4$ and concentrated under reduced pressure. The crude product was purified by flash column chromatography (ethyl acetate/n-hexane; 2:8, v/v) and recrystallization (ethyl acetate) to 5,10-dihexyl-3,8-dimethoxy-5,10-dihydroindolo[3,2-b]indole (MeO-2HIDID) as light violet crystalline solid (0.28 g, 34%)

1H-NMR (300 MHz, THF, δ): 7.55-7.50(d, 2H), 6.89(s, 2H), 6.67-6.64(d, 2H), 4.36-4.31(t, 4H), 3.77(s, 6H), 1.71-1.65(m, 4H), 1.37-1.22(m, 12H), 0.87-0.82(t, 6H)

1,1'-(5,10-dihexyl-5,10-dihydroindolo[3,2-b]indole-2,8-diyl)bis(ethan-1-one) (acyl-2HIDID)

A 100 mL round-bottom flask was flame based for 3 times, and after Ar purged, the mixture of $AlCl_3$(0.084g, 1.335mmol), CH_3COCl in methylene chloride solution(1M) (1.1mL, 1.068mmol) and anhydrous methylene chloride was injected into flask, followed by dropwise injection of 3,8-dibromo-5,10-dihexyl-5,10-dihydroindolo[3,2-b]indole (Br-2HIDID) (0.100g, 0.267mmol) in anhydrous methylene chloride(10mL) solution. The solution was stirred at room temperature for overnight. After reaction finished, reaction mixture was poured into brine solution in ice water, followed by stirring for 5 hours, and extracted with methylene chloride. The combined organic phase was concentrated under reduced pressure, and the crude product was purified by flash column chromatography (ethyl acetate/n-hexane; 1:19, v/v) and recrystallization (ethyl acetate) to 1,1'-(5,10-dihexyl-5,10-dihydroindolo[3,2-b]indole-2,8-diyl)bis(ethan-1-one) (acyl-2HIDID) as yellow crystalline solid (0.06 g, 49%)

1H-NMR (300 MHz, THF, δ): 8.59(s, 1H), 8.25(s, 1H), 7.99-7.98(d,1H), 7.93-7.90(d, 1H), 7.82-7.78(d, 1H), 7.60-7.57(d, 1H), 4.74-4.69(t, 2H), 4.63-4.58(t, 4H), 2.63-2.62(d, 6H), 2.04-1.92(m, 4H), 1.50-1.21(m, 12H), 0.86-0.80(t, 6H)

2.2.3 Instruments and measurements

Chemical structures were identified with 1H NMR (Bruker, Avance-300) in $CDCl_3$, Acetone-d_6, DMSO-d_6, and THF-d_6 solutions, GC-Mass (JEOL, JMS-700), and elemental analysis (EA1110, CE Instrument). The melting temperatures of the compounds were determined using DSC under the N_2 atmosphere, using a TA instruments Q1000 model.

UV-vis absorption spectra were recorded on a Shimadzu UV-1650PC and Cary-5000(Varian). HOMO levels were obtained from the cyclic voltammetry measurement using a 273 A (Princeton Applied Research) with a one-component electrolysis cell consisting of a platinum working electrode, a platinum wire counter-electrode, and a quati Ag+/Ag electrode as a reference. Measurements were performed in a 0.5 mM acetonitrile solution with tetrabutylammonium tetrafluoreborate as the supporting electrolyte, at a scan rate 100 mV/s. Each oxidation potential was calibrated using ferrocene as a reference. LUMO levels were obtained from the edge of the absorption spectra and HOMO levels from cyclo-voltammetry measurement.

Optical microscopic observation of the crystals was carried out with a Leica Mikroskopie & System GmbH Wetzier.

2.2.4 Fabrication and characterization of single-crystal organic field effect transistors (sc-OFETs)

Before fabricating devices, Si/SiO_2 substrates were rinsed with acetone and isopropyl alcohol, respectively, for 10 min in ultrasonicator, followed by UV(360nm) O_3 exposure for 20 min. IDIDp, TCNQ and PMMA (Mw~15000) were dissolved in methylene chloride (1.0 wt% of PMMA, 0.05, 0.10, 0.15wt% of IDIDp and TCNQ (1:1 molar ratio) for CT co-crystal devices, and 1.0wt% of PMMA, 0.05, 0.10wt% of IDIDp for p-type devices). Then solution was spin-coated at 2500 rpm for 1 min. For the SVA process, 5mL of methylene chloride was injected in 8mL vial and covered with a spin-coated film for 10 min. For the top-contact sc-OFETs, 50nm of Au were thermally deposited through a metal mask in a vacuum chamber. The I-V characteristics of individual devices were measured using a Keithley 4200SCS. Metal vacuum deposition and device performance measurements were carried out in a N_2-fulled glovebox.

2.3 Results and discussion

2.3.1 Optical and electrochemical properties of indoloindole derivatives

Absorbance spectra of E-CBZ and IDID derivatives in solution and film states are shown in Figure 2.1 and 2.2, respectively. Absorption spectra of E-CBZ and IDID derivatives which functional groups are directly substituted to IDID core are in panel (a) in both Figure 2.1 and 2.2. Absorbance spectra of para-phenylene type electron donating group-attached indoloindole derivatives are shown in panel (b), and those of para-phenylene electron withdrawing group-attached IDID derivatives are shown in panel (c), in both Figure 2.1 and 2.2.

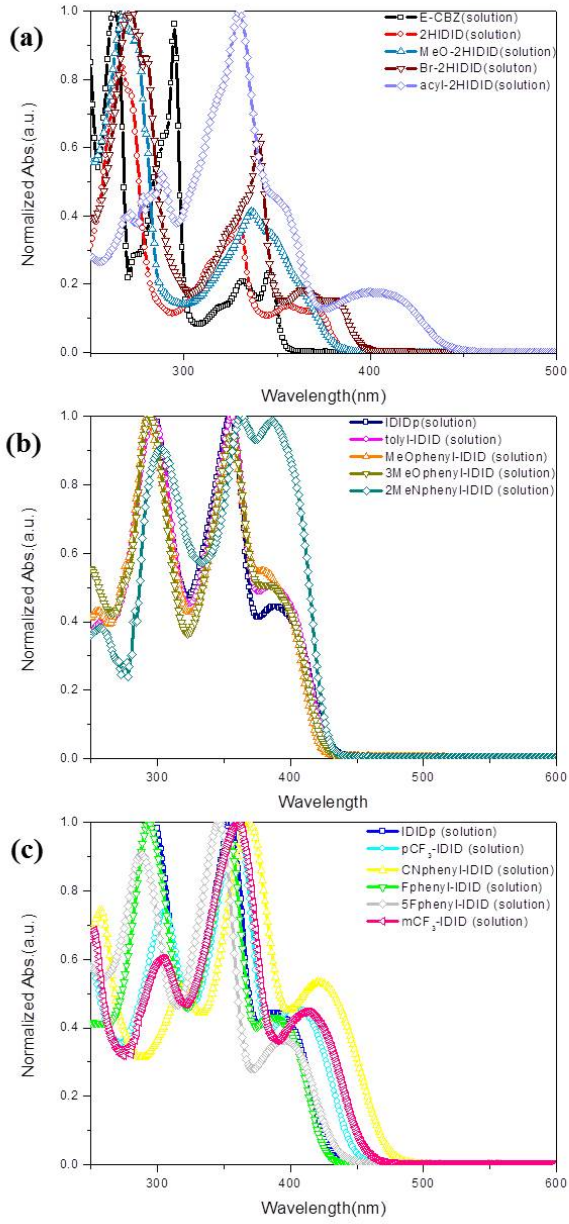

Figure 2.1. Normalized UV/vis absorption spectra of (a) reference molecules and directly functional groups substituted indoloindole derivatives (b) para-phenylene electron donating group attached indoloindole derivatives and (c) para-phenylene electron withdrawing group attached indoloindole derivatives in THF solution.

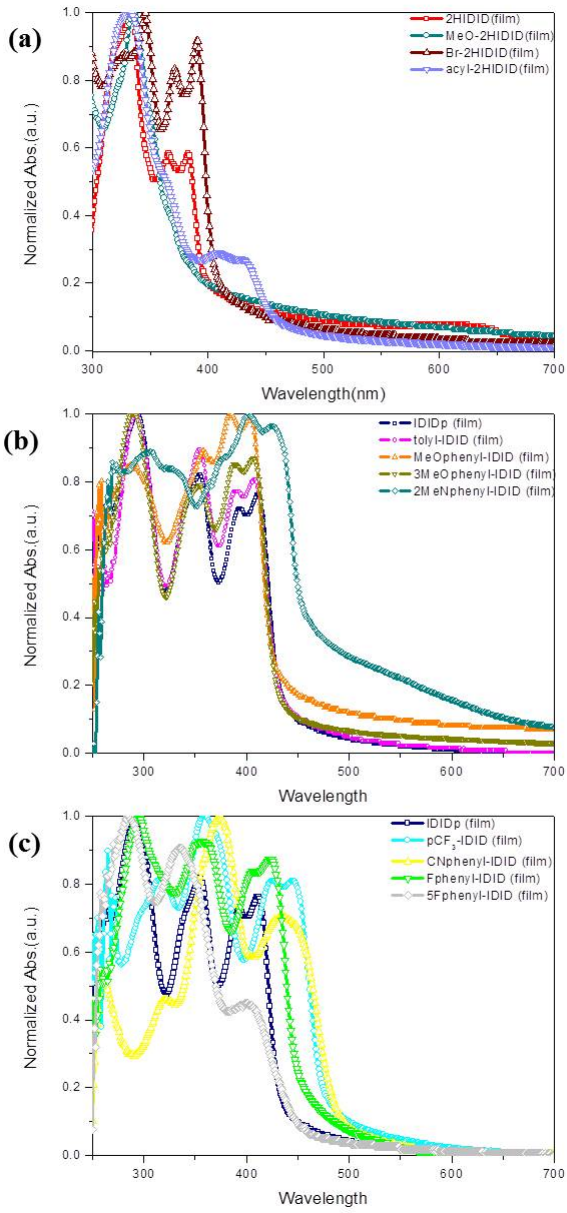

Figure 2.2. Normalized UV/vis absorption spectra of (a) reference molecules and directly functional groups substituted indoloindole derivatives (b) para-phenylene electron donating group attached indoloindole derivatives and (c) para-phenylene electron withdrawing group attached indoloindole derivatives in spin-coated film.

Table 2.1. Optical properties of IDIDp in solution and film state.

Compound	λ_{abs} (nm)	λ_{onset} (nm)	λ_g [c] (eV)
E-CBZ(sol) [a]	332, 347	355	3.49
2HIDID(sol) [a]	330, 355, 372	383	3.24
MeO-2HIDID(sol) [a]	268, 336	380	3.26
MeO-2HIDID(film) [b]	279, 337	391	3.17
Br-2HIDID(sol) [a]	272, 340, 364, 378	396	3.13
Br-2HIDID(film) [b]	268, 327, 345, 371, 391	406	3.05
acyl-2HIDID(sol) [a]	288, 330, 401	440	2.82
acyl-2HIDID(film) [b]	288, 332, 409, 429	463	2.68
IDIDp(sol)[a]	294, 355, 387	425	2.91
IDIDp(film)[b]	295, 354, 392, 411	432	2.87
tolyl-IDID(sol) [a]	257, 297, 356, 386	424	2.92
tolyl-IDID(film) [b]	296, 355, 390, 408	432	2.87
MeOphenyl-IDID(sol) [a]	256, 293, 358, 379	421	2.94
MeOphenyl-IDID(film) [b]	287, 357, 384, 403	428	2.90
3MeOphenyl-IDID(sol) [a]	294, 358, 384	425	2.92
3MeOphenyl-IDID(film) [b]	292, 355, 389, 406	430	2.88
2MeNphenyl-IDID(sol) [a]	257, 302, 363, 387	428	2.90
2MeNphenyl-IDID(film) [b]	307, 329[d], 376[d], 401, 426	461	2.69
pCF_3-IDID(sol) [a]	306, 360, 405	447	2.77

pCF_3-IDID(film) [b)]	316, 358, 4245, 445	479	2.59
CNphenyl-IDID(sol) [a)]	257, 320, 369, 421	470	2.64
CNphenyl-IDID(film) [b)]	262, 320, 373, 434, 444[d)]	494	2.51
Fphenyl-IDID(sol) [a)]	294, 354, 3887	425	2.92
Fphenyl-IDID(film) [b)]	294, 356, 405, 422	452	2.74
5Fphenyl-IDID(sol) [a)]	288, 346, 395	434	2.86
5Fphenyl-IDID(film) [b)]	284, 335, 400	448	2.77
mCF_3-IDID(sol) [a)]	252, 304, 361, 414	456	2.72

a) Measured in THF solution of concentration of 10^{-5}M. b) Spin-coated 0.5wt% using 1,2-dichloroethane solution.(1000rpm/30s) c) Optical band gap was obtained from absorption edge. d)not apparent peak, shoulder near absorption band.

Figure 2.1 shows normalized UV-vis absorption spectra of E-CBZ, 2HIDID as the reference molecules, and directly functional groups substituted IDID derivatives (MeO-2HIDID, Br-2HIDID, and acyl-2HIDID) in THF solution. In view of the chemical structure of 2 molecules, carbazole is composed of 3 aromatic rings including 2 benzene and 1 pyrrole rings, while IDID backbone unit is composed of 2 benzene and 2 pyrrole rings. 2HIDID has longer π-conjugation which results broader light absorbance and lower bandgap than E-CBZ. Compared to 2HIDID, MeO-2HIDID, Br-2HIDID and acyl-2HIDID show different absorption spectra. In case of MeO-2HIDID, light absorption wavelength range was similar to 2HIDID. However, due to electron donating nature of both IDID core and end functional groups, MeO-2HIDID does not show intramolecular charge transfer interaction. On the other hand, Br atoms attached to 2HIDID withdraw electron density from electron-rich IDID core, resulting in broader light absorbance and lower bandgap energy originating from intramolecular charge transfer. In case of acyl-2HIDID, electron withdrawing effect of substituted functional groups is increased, resulting in significantly broader and more red-shifted light absorption spectrum than Br-2HIDID.

In Figure 2.1(b), para-phenylene type electron donating groups are attached on IDID backbone. Because IDID core is an strong electron donating backbone unit, attached electron donating groups could not significantly affect the electron donating strength of IDID derivatives. However, in Figure 2.1(c), para-pheneylene type electron withdrawing groups are attached on 2,7-position of IDID backbone, resulting in intramolecular charge transfer(ICT) characteristics between core electron

donating moiety and lateral-attached electron withdrawing groups. As a result, absorption spectra of those molecules are red-shifted compared to absorption of the reference molecule, IDIDp. And as electron withdrawing strength of attached aromatic groups is increased, absorption spectrum is more red-shifted, resulting in lower bandgap.

In film state (Figure 2.2), similar phenomena are shown with solution state. Compared to 2HIDID, Br-2HIDID and acyl-2HIDID films exhibit more-red shifted absorption spectra. When para-phenylene type electron donating groups are attached on IDID backbone, entire electron donating strength is not significantly affected due to extremely strong electron donating strength of IDID core. And when para-phenylene type electron withdrawing groups are attached on IDID backbone unit, spectra of those molecules show bathochromic shift compared to that of IDIDp due to the intramolecular charge-transfer transition between IDID and lateral-attached moieties.

The shape of film absorption and that of solution absorption are quite similar, but an aggregation-induced vibronic peak in longer wavelength region is shown in the absorption spectrum of the film state. In film state, secondary interaction between adjacent molecules induces aggregation, which prohibits the rotation of end moieties, resulting in extended π-conjugation. When intramolecular charge-transfer transition occurred, π-conjugation is efficiently extended with large bathochromic shift in absorption spectra (as shown in CNphenyl-IDID, pCF_3-IDID, and Fphenyl-IDID). However, in case of 2MeNphenyl-IDID including attached electron donating groups on 2,7-position of IDID core, dimethylaniline groups have extremely stronger electron donating strength

than IDID core. In this reason, IDID core withdraws electron density from lateral 2 dimethylaniline groups, with opposite direction of charge transfer compared to other examples, such as CNphenyl-IDID, pCF_3-IDID, and Fphenyl-IDID.

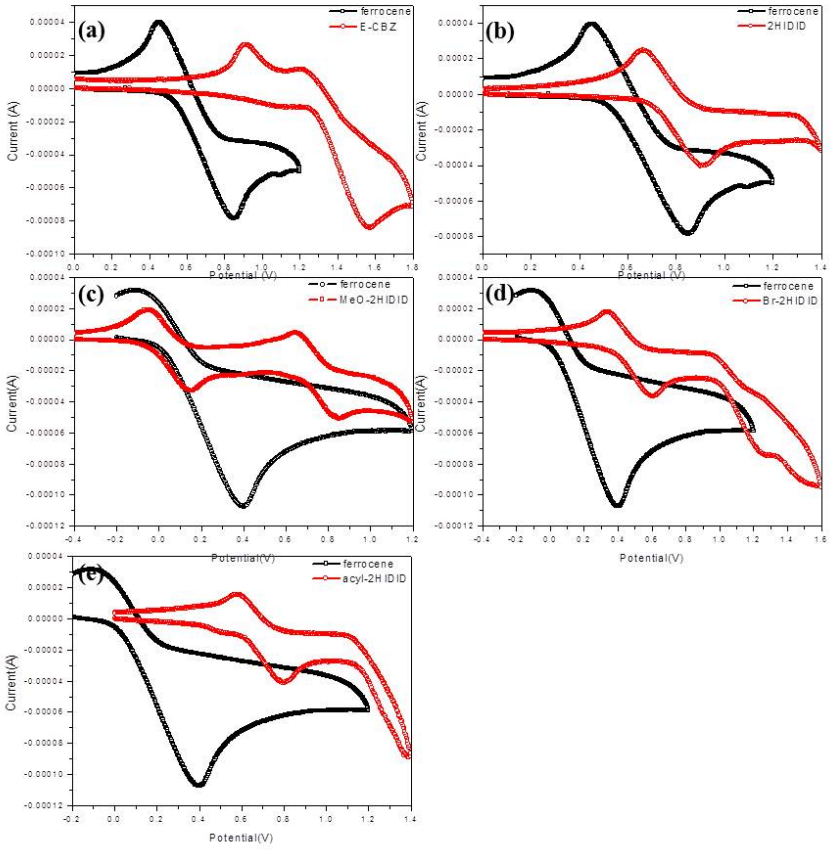

Figure 2.3. The cyclic voltammograms of carbazole and indoloindole derivatives where functional groups are directly substituted (red) in solution and ferrocene (black) with TBATFB in acetonitrile as the supporting electrolyte.

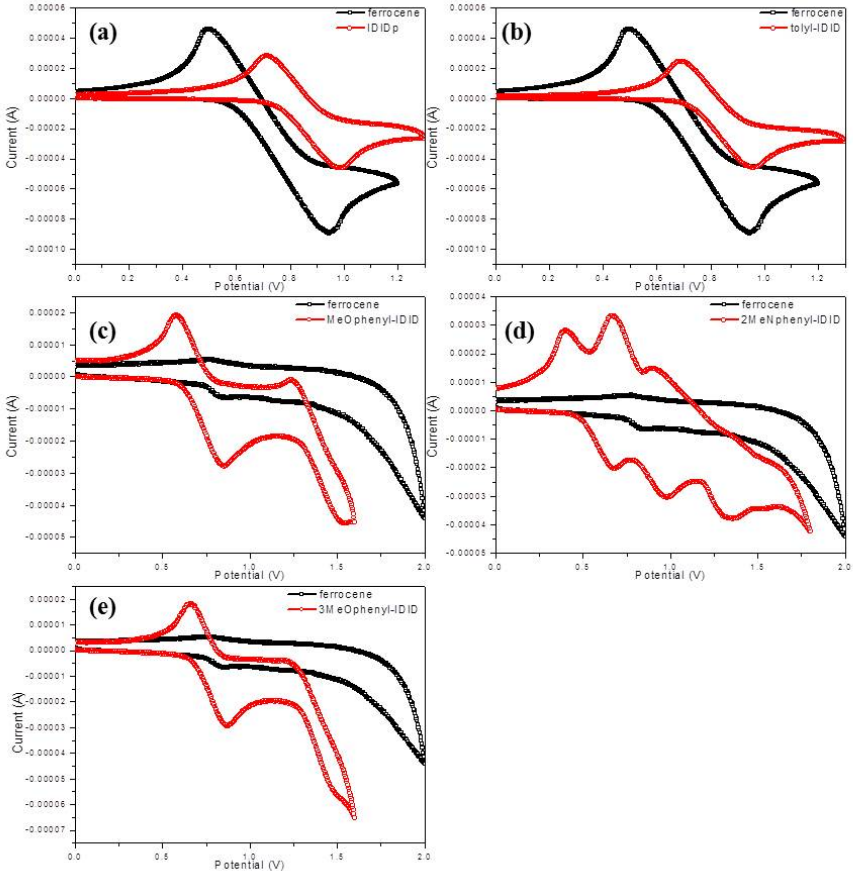

Figure 2.4. The cyclic voltammograms of para-phenylene electron donating group attached indoloindole derivatives (red) in solution and ferrocene (black) with TBATFB in acetonitrile as the supporting electrolyte.

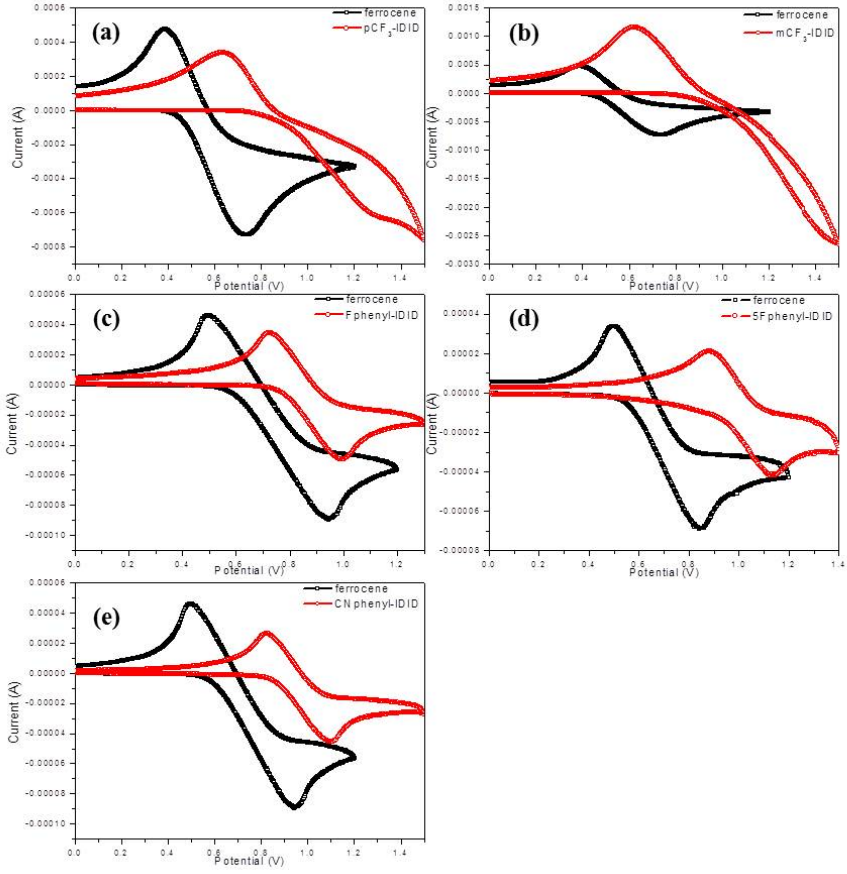

Figure 2.5. The cyclic voltammograms of para-phenylene electron withdrawing group attached indoloindole derivatives (red) in solution and ferrocene (black) with TBATFB in acetonitrile as the supporting electrolyte.

Table 2.2. Electrochemical properties of IDID derivatives in solution.

Compound	λ_g [a] (eV)	E_{HOMO} [b] (eV)	E_{LUMO} [c] (eV)
E-CBZ	3.49	-5.48	-1.99
2HIDID	3.24	-4.96	-1.72
MeO-2HIDID	3.26	-4.73	-1.46
Br-2HIDID	3.13	-5.14	-2.01
acyl-2HIDID	2.82	-5.36	-2.55
IDIDp	2.91	-4.95	-2.04
tolyl-IDID	2.92	-4.92	-2.00
MeOphenyl-IDID	2.94	-4.90	-1.96
3MeOphenyl-IDID	2.92	-4.95	-2.03
2MeNphenyl-IDID	2.90	-4.76	-1.86
pCF3-IDID	2.77	-4.95	-2.27
mCF3-IDID	2.72	-5.12	-2.40
CNphenyl-IDID	2.64	-5.06	-2.42
Fphenyl-IDID	2.92	-4.97	-2.05
5Fphenyl-IDID	2.86	-5.13	-2.27

a) Optical band gap was obtained from films absorption edge. b) HOMO level calculated by eqaution : $E_{HOMO} = \left[-\left(E_{onset} - E_{ferrocene}\right) - 4.8\right]$ c) LUMO level was calculated from optical band gap and HOMO level.

The electrochemical properties of IDID derivatives were measured by cyclic-voltammetry (LUMO level is calculated from optical bandgap of UV/vis absorption spectrum and electrochemically measured HOMO level, Table 2.2, Figure 2.3, 2.4, and 2.5). The oxidation potential for molecules was measured in relation to ferrocene (Fc/Fc^{+}=4.8eV), typically used as reference. The HOMO and LUMO levels of molecules are shown in Table 2.2, Figure 2.6, and 2.7.

Compared to carbazole, IDID has stronger electron donating nature originating from 2 pyrrole rings included in heteroacene backbone, resulting in higher-lying HOMO level. Furthermore, with longer π-conjugation extension, IDID has lower bandgap than carbazole. Based on those properties, 2HIDID has higher-lying HOMO level and lower bandgap than E-CBZ. In case of MeO-2HIDID, attached methoxy groups increase electron density of molecule, resulting in higher-lying HOMO level compared to 2HIDID. On the other hand, electron withdrawing groups decrease electron density of molecules with lowering HOMO level. HOMO level of Br-2HIDID is lowered about 0.2 eV compared to 2HIDID, and stronger electron withdrawing acyl groups significantly lowered HOMO level about 0.4 eV compared to 2HIDID. Furthermore, with electron withdrawing groups, bandgap energy is decreased, resulting in lowering LUMO levels, also. With strongest electron withdrawing effect of acyl groups, LUMO level of acyl-2HIDID is significantly lowered to -2.55eV. In short, with controlling directly attached functional groups, energy levels of IDID are significantly tuned. (as shown in Figure 2.6)

In para-phenylene type substituted IDID derivatives, IDID core dominantly determines the entire electron donating nature. Therefore,

HOMO levels of IDID derivatives (as shown in Figure 2.7) are almost fixed at the level of -4.9 ~ -5.0 eV. And LUMO levels are more tuned than HOMO levels with controlled bandgap energy. However, when para-phenylene type electron withdrawing groups are attached on IDID, absorption spectra are red-shifted, resulting in lowering bandgap and LUMO levels. Furthermore, when extremely strong electron withdrawing groups (para-phenylene type) are attached on IDID, electron donating nature of entire molecule is decreased, which results lower-lying HOMO level. However, energy level tuning range with para-phenylene type substituted IDID derivatives is much smaller than directly functional groups substituted IDID derivatives as shown in Figure 2.6 and 2.7.

As a conclusion, IDID has significantly higher-lying HOMO level and lower bandgap compared to carbazole, which is originating from extended π-conjugation and increased electron donating property from pyrrole rings. Basically, IDID core unit determines HOMO levels of IDID derivatives, and end-attached electron donating or electron withdrawing groups result in tuning of HOMO level. With strong electron donating end-groups, HOMO level is raised; while, with strong electron accepting end-groups, HOMO level is lowered. With significantly efficient ICT transition, bandgap is lowered, and also LUMO level is tuned with controlled bandgap. Energy level tuning range is significantly controllable with different functional groups attached to IDID core.

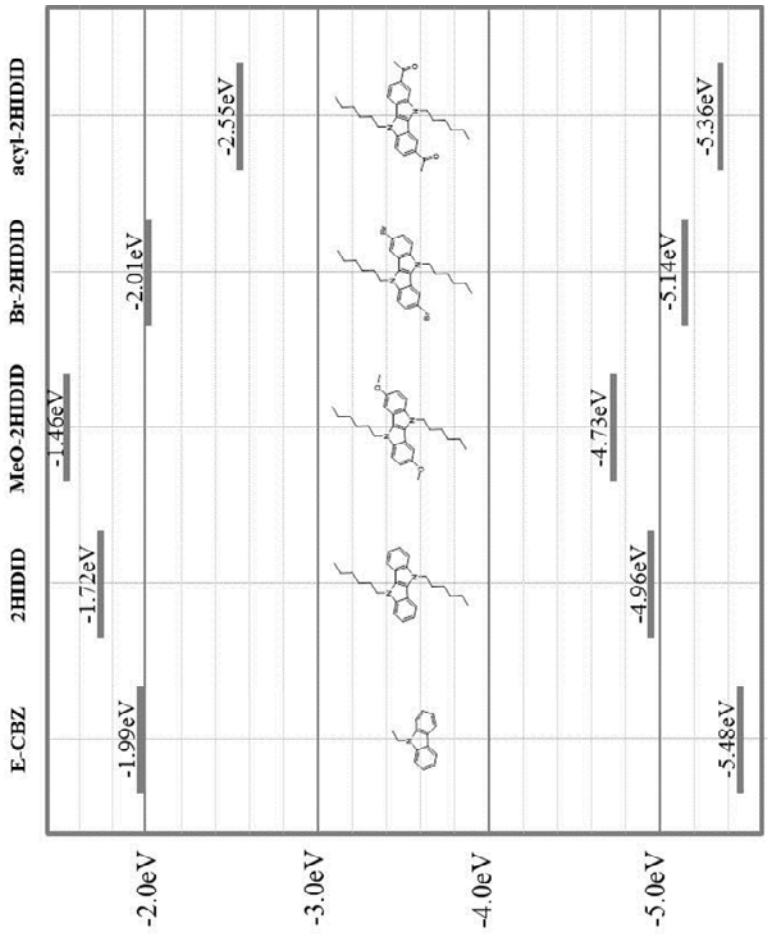

Figure 2.6. Energy diagrams of carbazole and indoloindole derivatives where functional groups are directly substituted.

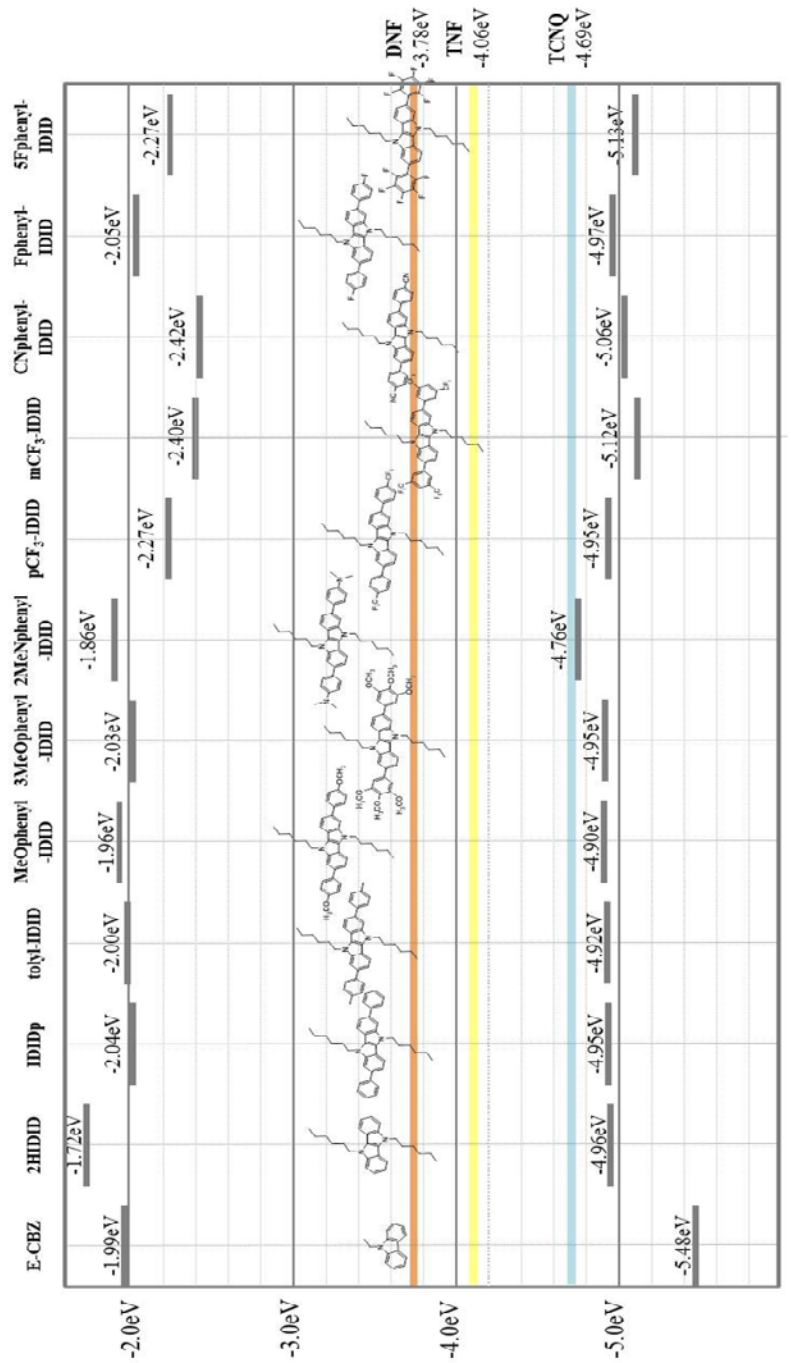

Figure 2.7. Energy diagrams of donor(indoloindole derivatives) and acceptor molecules.

2.3.2 Optical properties of CT complexes

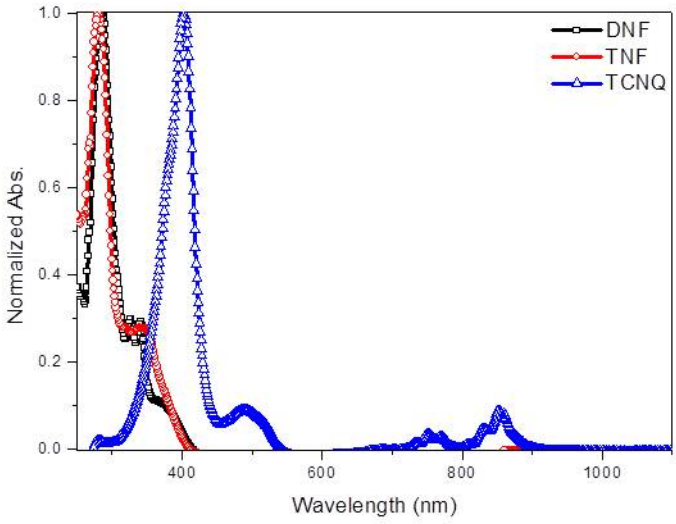

Figure 2.8. Normalized UV/vis absorption spectra of DNF (black), TNF (red) and TCNQ (blue) in THF solution.

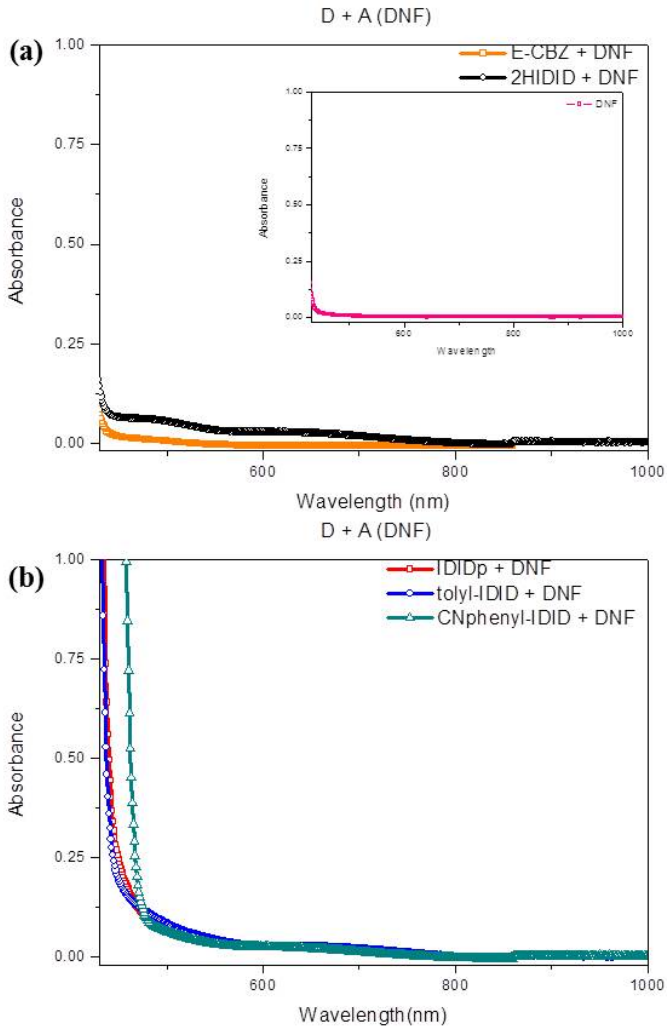

Figure 2.9. UV/vis absorption spectra of (a) E-CBZ+DNF (orange) and 2HIDID+DNF (black) $5x10^{-3}$M solution in THF and (b) IDIDp+DNF (red), tolyl-IDID+DNF (blue), and CNphenyl-IDID+DNF (green) $5x10^{-3}$M solution in THF solution. Inset is absorbance of DNF (magenta) $1x10^{-2}$M in THF solution.

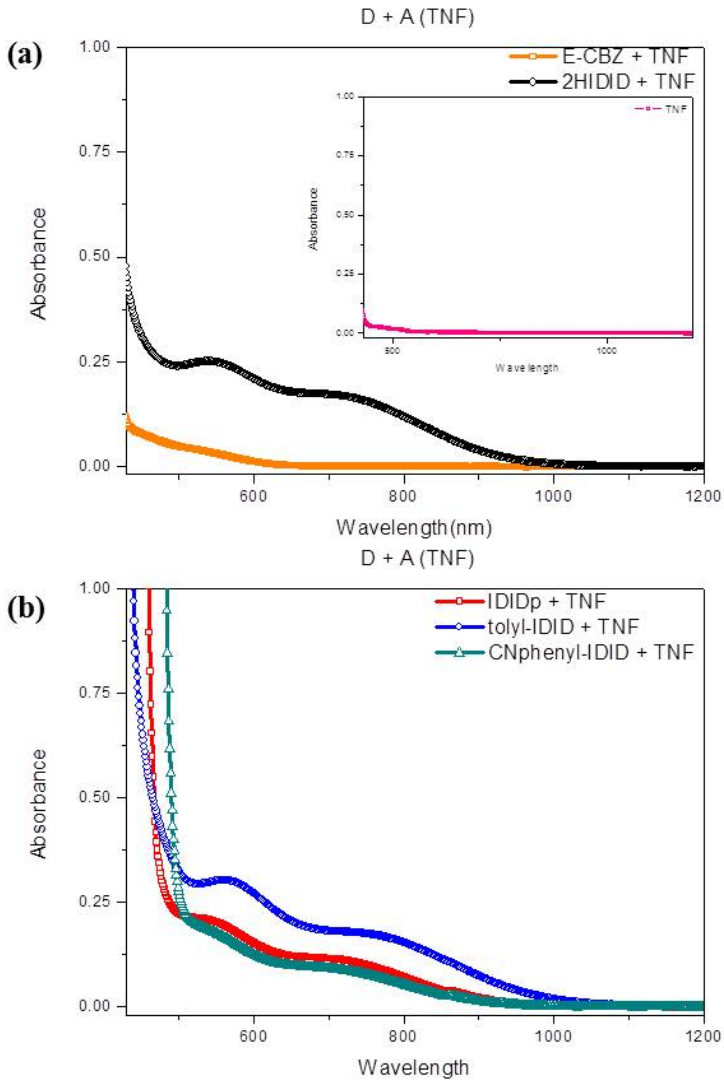

Figure 2.10. UV/vis absorption spectra of (a) E-CBZ+TNF (orange) and 2HIDID+TNF (black) $5x10^{-3}$M solution in THF and (b) IDIDp+TNF (red), tolyl-IDID+TNF (blue), and CNphenyl-IDID+TNF (green) $5x10^{-3}$M solution in THF solution. Inset is absorbance of TNF (magenta) $1x10^{-2}$M in THF solution.

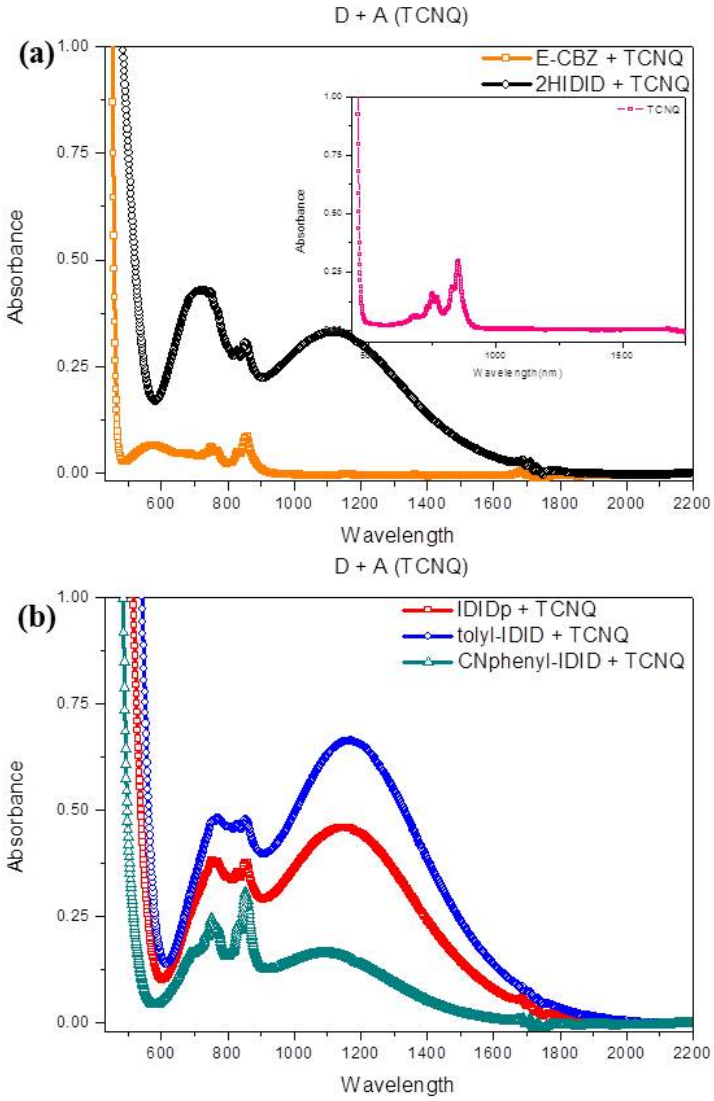

Figure 2.11. UV/vis absorption spectra of (a) E-CBZ+TCNQ (orange) and 2HIDID+TCNQ (black) $5x10^{-3}$M solution in THF and (b) IDIDp+TCNQ (red), tolyl-IDID+TCNQ(blue), and CNphenyl-IDID+TCNQ (green) $5x10^{-3}$M solution in THF solution. Inset is absorbance of TCNQ (magenta) $1x10^{-2}$M in THF solution.

Based on different electron donating strength and energy levels of materials, 5 molecules were selected for donor materials, E-CBZ, 2HIDID, IDIDp, tolyl-IDID, and CNphenyl-IDID. To explore intrinsic electron donating nature of IDID, E-CBZ and 2HIDID were chosen. And to investigate the effect of end-functional attached groups on electron donating property of IDID derivatives, IDIDp, CNphenyl-IDID, and tolyl-IDID were selected, which have similar chemical structures but different electron donating strength. Three different molecules, DNF, TNF, and TCNQ were used as acceptors for the formation of CT complex, with different electron accepting strength.

As shown in Figure 2.9~2.11, new CT bands were shown with the formation of CT complexes, which are not shown in donor solution or acceptor solution absorbance spectra (as shown in Figure 2.1 and 2.8). By comparing 2HIDID and E-CBZ, intrinsic electron donating character of IDID could be investigated. CT complexes of 2HIDID and acceptor (DNF, TNF, and TCNQ) always form 2 broad CT bands; while E-CBZ and acceptors form 1 broad CT band. Furthermore, CT bands of 2HIDID - acceptor (DNF, TNF, TCNQ) CT complexes always show higher intensity and longer wavelength region than those of E-CBZ - acceptor (DNF, TNF, TCNQ) CT complexes. Those phenomena are due to more efficient formation of CT complex between 2HIDID and acceptors, originating from stronger electron donating property of 2HIDID.

Different end-substituted functional groups affect electron donating strength of IDID derivatives, and tendency to form CT complex with acceptors. IDIDp, tolyl-IDID, and CNphenyl-IDID always exhibit 2 CT bands when mixed with acceptors (DNF, TNF, TCNQ). However, tolyl-

IDID always has highest intensity of CT bands, and CNphenyl-IDID always exhibits lowest intensity of CT bands among 3 molecules. Because tolyl-IDID includes electron donating group attached on IDID, and CNphenyl-IDID include electron withdrawing group attached on IDID, IDID derivatives show different electron donating strength, which results different intensity of CT bands when mixed with acceptors.

Additionally, by controlling electron accepting strength of acceptor molecules, the tendency to form CT complex could be modulated. DNF is the weakest electron acceptor and TCNQ is the strongest electron acceptor among 3 acceptors. In this reason, when donor molecules are mixed with DNF, newly formed CT bands have small intensity of absorbance, and the wavelength region of CT bands is up to 580nm for E-CBZ, and 800nm for IDID derivatives. In case of TNF, tendency to form CT complex is more increased than DNF. Intensity of CT bands is higher and wavelength region of CT bands are broader (up to 650nm for E-CBZ, and 1000nm for IDID derivatives) compared to those of CT bands in case of DNF. The strongest acceptor, TCNQ, shows strongest tendency to form CT complexes with donor molecules. In this case, as shown in Figure 2.9~2.11, intensity of CT bands is highest among 3 acceptors, and wavelength region of CT bands is significantly broadened (up to 1000nm for E-CBZ, and 1800nm for IDID derivatives).

As a summary, CT complexes are effectively formed when donor (E-CBZ, 2HIDID, IDIDp, tolyl-IDID, CNphenyl-IDID) and acceptor (DNF, TNF, TCNQ) are mixed, resulting in newly formed CT band in absorption spectrum. By comparing absorbance of mixed solution of donor and acceptor, several facts were confirmed with different intensity and

wavelength region of the CT bands. IDID has stronger electron donating nature compared to carbazole, and tendency to form CT complex is affected by electron donating strength of IDID derivatives (finely tuned with lateral-substituted groups) and electron accepting strength of acceptors. When CT interaction between donor and acceptor is stronger, efficient charge transfer from donor to acceptor occurs, which results higher intensity and broader wavelength region of newly formed CT band.

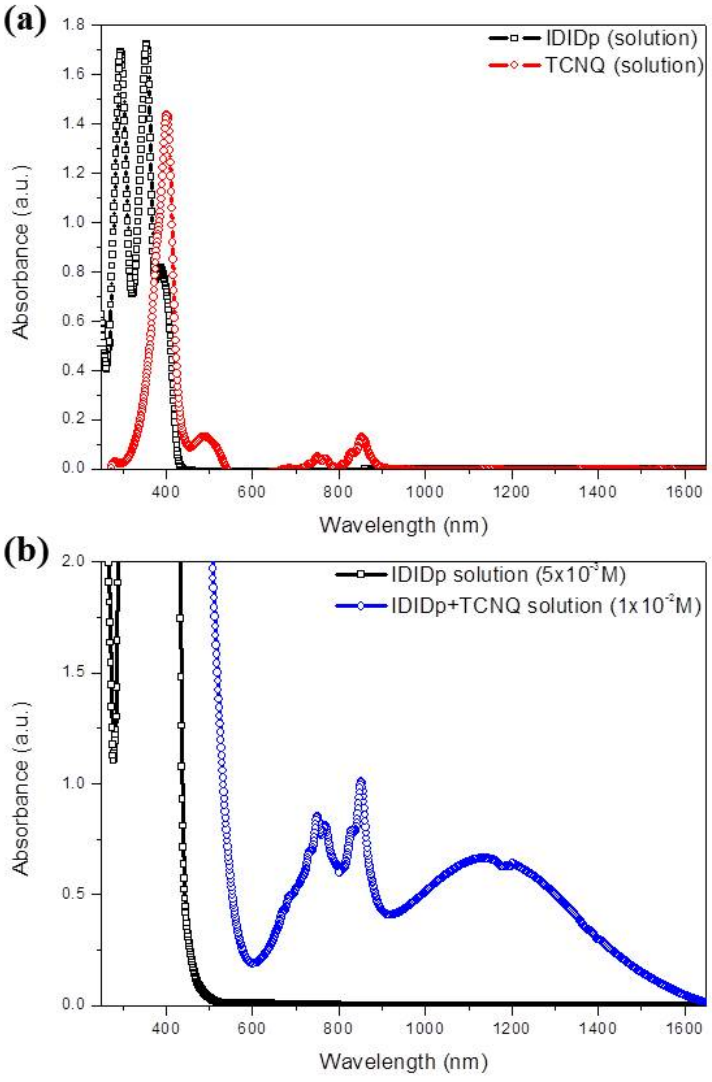

Figure 2.12. UV/vis absorption spectra of (a) IDIDp (black) and TCNQ (red) $1x10^{-5}$M solution in THF and (b) IDIDp $5x10^{-3}$M solution (black) in THF and IDIDp+TCNQ(1:1 molar ratio) $1x10^{-2}$M solution (blue) in THF.

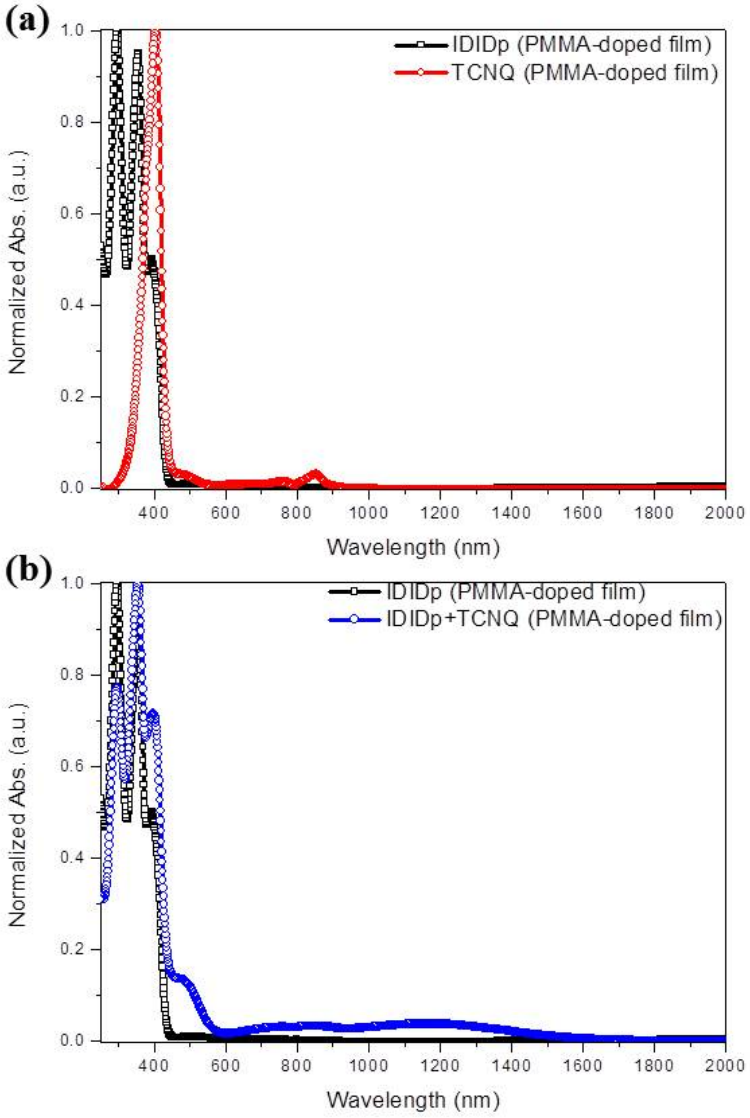

Figure 2.13. Normalized UV/vis absorption spectra of (a) IDIDp (black) and TCNQ (red) –doped in PMMA film and (b) IDIDp (black) and IDIDp+TCNQ (1:1 molar ratio)-doped in PMMA film.

Based on those fundamental studies of CT complex, IDIDp and TCNQ are selected as a donor and acceptor to study CT complex in film state.

Absorbance spectra of IDIDp, TCNQ, and D-A mixture-doped PMMA film are shown in Figure 2.13. IDIDp-doped PMMA film shows absorbance from 250nm to 400nm, and TCNQ-doped PMMA film shows absorbance from 250nm to 440nm with vibronic peaks in the region of 700nm to 900nm. Similar to TCNQ solution absorbance (in Figure 2.11), vibronic peaks originating from TCNQ anions are shown in TCNQ-doped PMMA film absorbance. In addition, D-A mixture-doped PMMA film shows broad absorption band, but no vibronic peaks are shown in region of 700 to 900nm. As noticed by comparing TCNQ absorbance in solution and PMMA-doped film, the amount of TCNQ anions in D-A mixture is less in PMMA-doped film than in solution. Based on D-A mixture absorption spectrum, CT state of donor and acceptor is confirmed in film state.

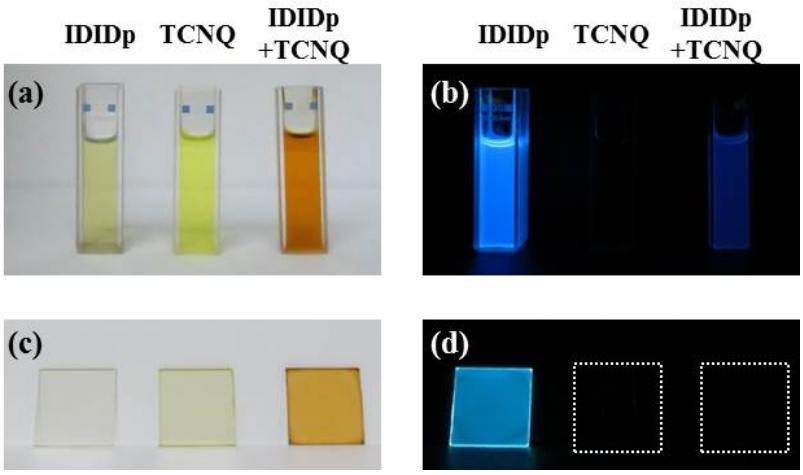

Figure 2.14. Solutions of IDIDp, TCNQ, IDIDp+TCNQ under (a) room light, and (b) 365nm UV light. PMMA-doped films of IDIDp, TCNQ, IDIDp+TCNQ under (c) room light, and (d) 365nm UV light.

As a conventional method of realizing CT state, D-A mixed solution shows different optical property with donor or acceptor. As shown in Figure 2.14, each solution of donor and acceptor shows light yellow color, and donor solution shows bright blue fluorescence under 365nm UV light. But when donor and acceptor are mixed, solution is dark orange because newly obtained charge-transfer state of D-A complex forms small energy gap between HOMO of donor and LUMO of acceptor(Figure 2.14 (a)), and because of new charge-transfer state, fluorescence of donor is highly quenched in mixed solution (Figure 2.14 (b)). Similar phenomenon is shown in PMMA-doped film state. IDIDp-doped PMMA film and TCNQ-doped PMMA film are light yellow, but D-A complex-doped PMMA film is dark orange (Figure 2.14 (c)). And fluorescence of IDIDp-doped PMMA film is bright light blue, but fluorescence of D-A complex-doped PMMA film is significantly quenched (Figure 2.14 (d)). Through UV/vis spectroscopy, optical properties of donor, acceptor, and CT complex were measured in solution and film state.

2.3.3 OFET properties

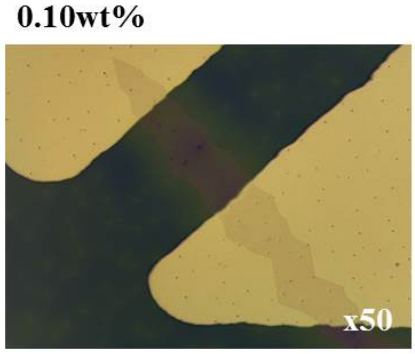

Figure 2.15. Optical microscope image of a single-crystal OFET of IDIDp fabricated by SVA.

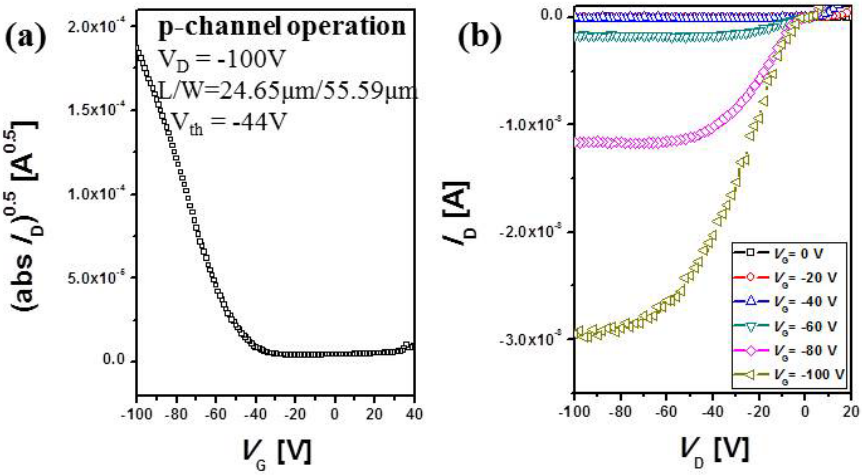

Figure 2.16. (a) Transfer and (b) output characteristics of the single-crystal OFET of IDIDp fabricated by SVA.

Table 2.3. Hole mobility of single-crystal OFET of IDIDp fabricated by SVA.

	$\mu_{h,avg}$ ($cm^2V^{-1}s^{-1}$)	$\mu_{h,max}$ ($cm^2V^{-1}s^{-1}$)
p-type mobility	$1.73x10^{-2}$	$2.29x10^{-2}$

As shown in Figure 2.15, flat plate-type IDIDp single crystal is successfully grown in PMMA matrix by solvent vapor annealing method, used as the active elements of sc-OFETs. By modulating the concentration of IDIDp solution, the size and thickness of crystals were easily controlled. Transfer and output characteristics of sc-OFET of IDIDp are shown in Figure 2.16. At hole-enhancement mode, p-type charge transport behavior is apparent at given V_G of -100 V due to high-lying HOMO level of IDIDp. Average value of the hole mobility is $1.73x10^{-2}$ $cm^2V^{-1}s^{-1}$ (maximum value of $2.29x10^{-2}$ $cm^2V^{-1}s^{-1}$) and threshold voltage was -44 V.

(a) 0.15wt%

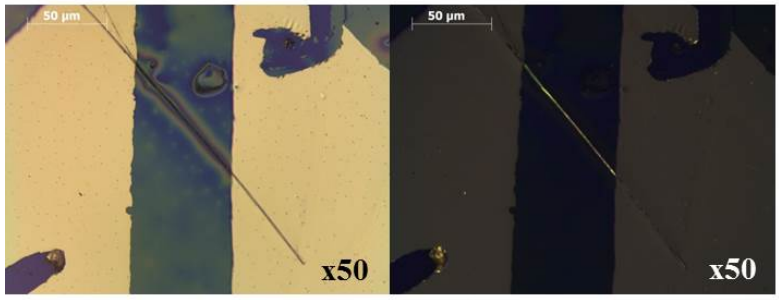

(b) 0.05wt%

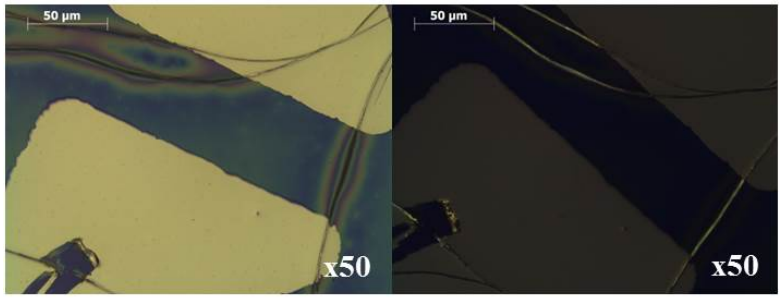

Figure 2.17. Optical microscope image of a single-crystal OFET of IDIDp and TCNQ fabricated by SVA.

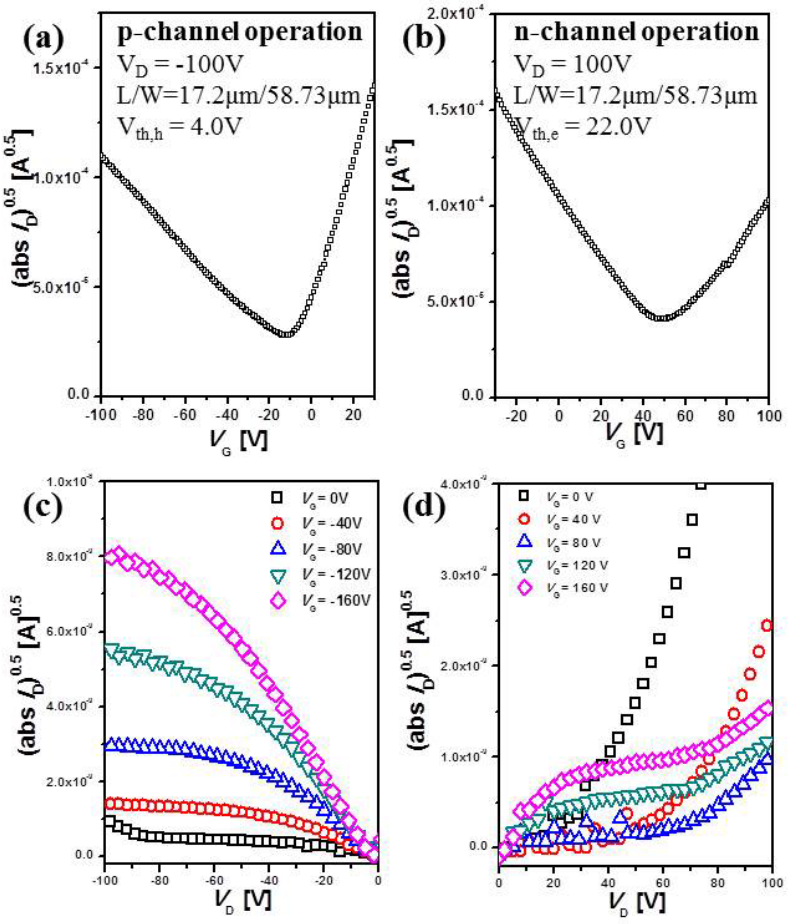

Figure 2.18. (a) p-channel operated transfer, (b) n-channel operated transfer, (c) p-channel operated output, and (d) n-channel operated output characteristics of the single-crystal OFET of IDIDp fabricated by SVA.

Table 2.4. Device performances of single-crystal OFET of IDIDp-TCNQ CT co-crystals fabricated by SVA.

		μ_{avg} ($cm^2V^{-1}s^{-1}$)	μ_{max} ($cm^2V^{-1}s^{-1}$)
Only n-type shown devices		$1.85x10^{-2}$	$6.00x10^{-2}$
Ambipolar devices	n-type	$1.19x10^{-2}$	$3.40x10^{-2}$
	p-type	$2.02x10^{-4}$	$1.27x10^{-3}$

Because of strong electron donating property of IDIDp, CT co-crystals were grown using IDIDp and TCNQ in PMMA matrix by solvent vapor annealing method, used as the active elements of sc-OFETs. As shown in Figure 2.17, 1-dimensional rod-type black crystal is formed, which is significantly different from either plate-type yellow single crystal of IDIDp or well-known bright orange single-crystal of TCNQ. [13]

Among 18 channel measurements, 11 channels show only n-type electron transport behavior, showing average electron mobility of $1.85x10^{-2}$ $cm^2V^{-1}s^{-1}$ (maximum value of $6.00x10^{-2}$ $cm^2V^{-1}s^{-1}$). And 7 channels show ambipolar charge transport behavior, showing average hole mobility of $2.02x10^{-4}$ $cm^2V^{-1}s^{-1}$ (maximum value of $1.27x10^{-3}$ $cm^2V^{-1}s^{-1}$) and electron mobility of $1.19x10^{-2}$ $cm^2V^{-1}s^{-1}$ (maximum value of $3.40x10^{-2}$ $cm^2V^{-1}s^{-1}$).

Ambipolar characteristics of devices are shown in Figure 2.18. V-shape transfer curves clearly indicate the ambipolarity of charge transport in both hole and electron enhancement modes, where one arm indicates hole-transport and the other indicates electron-transport (Figure 2.18 (a), (b)). Threshold voltages for hole and electron are 4.0 V and 22.0 V, respectively.

Output curve is a superposition of a saturated behavior of one main charge carrier, and a superlinear behavior at low V_G and high V_D due to the injection of the opposite charge carriers from the metal electrodes. Due to the ambipolar charge carrier transport property of IDIDp-TCNQ CT co-crystals, both holes and electrons could be transported through channels of holes and electrons, and at high V_D, injected opposite charge carriers could be transported showing superlinear behavior (Figure 2.18 (c), (d)).

Due to proper energy levels of IDIDp and TCNQ (-5.16 eV for the HOMO of IDIDp, -4.69 eV for the LUMO of TCNQ), strong CT interaction between donor and acceptor forms CT co-crystals, which are suitable for the active elements in sc-OFETs, and appropriate energy alignment takes places for charge injection from the metal electrodes and transport in the active elements. TCNQ is reported as n-type semiconducting material, where sc-OFETs using TCNQ exhibit electron mobility of μ_e=0.5 $cm^2V^{-1}s^{-1}$.[12] And synthesized IDIDp is a p-type semiconducting material, sc-OFETs using IDIDp exhibit hole mobility of μ_h=1.72x10^{-2} $cm^2V^{-1}s^{-1}$. By the formation of CT complexes, sc-OFETs using CT co-crystals of IDIDp and TCNQ exhibit ambipolar charge transport characteristics, with μ_e=1.19x10^{-2} $cm^2V^{-1}s^{-1}$ and μ_h=2.02x10^{-4} $cm^2V^{-1}s^{-1}$.

2.3 Conclusion

In conclusion, to explore strong electron donating nature of IDID, I investigated the optical and electrochemical properties of carbazole, and IDID derivatives. By comparing with carbazole, IDID is clearly confirmed as a strong electron donor, and the electron donating strength is effectively tuned by structural modification. CT complexes of IDID derivatives and acceptors were demonstrated. Their energy levels were measured and calculated from UV/vis absorption and cyclo-voltammetry. Through newly obtained CT bands in absorption spectra, color change in solution and film states, and change of color and shape of crystal state, formation of the CT complexes of IDIDp and TCNQ was clearly confirmed.

Single-crystal OFETs, fabricated using CT co-crystals of IDIDp and TCNQ by SVA method, exhibit ambipolar charge carrier transport properties, with μ_h of 2.02×10^{-4} $cm^2V^{-1}s^{-1}$ (maximum value of 1.27×10^{-3} $cm^2V^{-1}s^{-1}$) and μ_e of 1.19×10^{-2} $cm^2V^{-1}s^{-1}$ (maximum value of 3.40×10^{-2} $cm^2V^{-1}s^{-1}$), while sc-OFETs using IDIDp by SVA exhibit p-type charge carrier transport properties with μ_h of 1.72×10^{-2} $cm^2V^{-1}s^{-1}$ (maximum value of $2.29 \times 10^{-2} cm^2V^{-1}s^{-1}$).

2.4 Bibliography

1. M.E. Gershenson, V. Podzorov, and A.F. Morpurgo, *Rev.Mod.Phys.*, **2006**, 78, 973.

2. (a) T. D. Anthopoulos, S. Setayesh, E. Smits, M. Cölle, E. Cantatore, B. de Boer, P. W. M. Blom, and D. M. de Leeuw, *Adv. Mater.*, **2006**, 18, 1900. (b) E. J. Meijer, D. M. de Leeuw, S. Setayesh, E. van Veenendaal, B.-H. Huisman, P.W.M. Blom, J.C. Hummelen, U.Scherf, and T.M. Klapwijk, *nature materials*, **2003**, 2, 678.

3. J.Zhang, H. Geng, T. S. Virk, Y. Zhao, J. Tan, C. Di, W. Xu, K. Singh, W. Hu, Z. Shuai, Y. Liu, and D. Zhu, *Adv. Mater*, **2012**, 24, 2603.

4. (a) T. Enoki, and A. Miyazaki, *Chem.Rev.*, **2004**, 104, 5449. (b) G. Saito, and Y. Yoshida, *Bull.Chem.Soc.Jpn.*, **2007**, 80, 1.

5. (a) G. Saito, S.-S. Pac, and O.O. Drozdova, *Synthetic Metals*, **2001**, 120, 667. (b) M.J. Cohen, L.B. Coleman, A.F. Garito, and A.J. Heeger, *Physical Review B*, **1974**, 10, 1298.

6. D. Jérome, *Solid State Sciences*, **2008**, 10, 1692.

7. (a) S. Horiuchi, and Y. Tokura, *nature materials*, **2008**, 7, 357. (b) A.K. Tayi, A.K. Shveyd, A.C.-H. Sue, J.M. Swarko, B.S. Rolczynski, D.Cao, T.J. Kennedy, A.A. Sarjeant, C.L. Stern, W.F. Paxton, W. Wu, S.K. Dey, A.C. Fahrenbach, J.R. Guest, H. Mohseni, L.X. Chen, K.L. Wang, J.F. Stoddart and S.I. Stupp, *nature*, **488**, 485.

8. Wei, Yu, X.-Y. Wang, J. Li, Z.-T. Li, Y.–K. Yan, W. Wang, and J. Pei, *Chem. Commun*, **2013**, 49, 54.

9. (a) A.A. Sagade, K.V. Rao, S.J. Geroge, A. Datta, and G.U. Kulkarni,

Chem. Commun, **2013**, 49, 5847. (b) S.K. Park, S. Varghese, J.H. Kim, S.-J.Yoon, O.K. Kwon, B.-K. An, J. Gierschner, and S.Y. Park, *JACS*, **2013**, 135, 4757. (c) A.A. Sagade, K.V. Rao, U. Mogera, S.J. Geroge, A. Datta, and G.U. Kulkarni, *Adv.Mater*., **2013**, 25, 559. (d) Y. Takahshi, T. Hasegawa, Y. Abe, Y. Tokura, G. Saito, *Appl.Phys.Lett.*, **2006**, 88, 073504.

10. (a) L. Zhu, Y. Yi, Y. Li, E.-G. Kim, V. Coropceanu, and J.-L. Brédas, *JACS*, **2012**, 134, 2340. (b) P. García, S. Dahaoui, P. Fertey, E. Wenger, and C. Lecomte, *Physial Review B.*, **2005**, 72, 104115.

11. (a) T. Hasegawa, and J. Takeya, Sci. Technol. *Adv. Mater.*, **2009**, 10, 024314. (b) M. Sakai, H. Sakuma, Y. Ito, A. Saito, M. Nakamura, and K. Kudo, *Physical Review B*, **2007**, 76, 045111. (c) Y. Takahashi, T. Hasegawa, Y. Abe, Y. Tokura, K. Nishimura, and G. Saito, *Appl. Phys. Lett*, **2005**, 86, 063504. (d) H. Yamochi, J. Hagiwara, M. Soeda, and G. Saito, *J. Mater.Chem.*, **2006**, 16, 550. € S. horiuchi, H. Yamohi, G. Saito, K. Sakaguchi, and M. Kusunoki, *JACS*, **1996**, 118, 8604.

12. H.T. Jonkman, and J. Kommandeur, *Chemical Physics Letters*, **1972**, 15, 496.

13. (a) M. Yamagishi, Y. Tominari, T. Uenura, and J. Takeya, *Appl. Phys. Lett.*, **2009**, 94, 053305. (b) E. Menard, V. Podzorov, S.-H. Hur, A. Gaur, M.E. Gershenson, and J.A. Rogers, *Adv.Mater.*, **2004**, 16, 2097. (c) J.R. Kirtley, and J. Mannhart, *nature materials*, **2008**, 7, 520.

Chapter 3. A-D-A/D-A-D Type Indoloindole Derivatives for Bulk-heterojunction Small Molecule Organic Solar Cells (SMOSCs)

3.1 Introduction

Solution-processed organic solar cells (OSCs) have been intensively investigated as a competitive technology of green energy with low cost of fabrication, light weight, and great mechanical flexibility. Polymeric solar cells (PSCs) have advantages of better film forming quality compared to small molecule OSCs, and over 10% of PCEs are already reported with polymeric photovoltaics.[1] Although small molecule OSCs(SMOSCs) have been less investigated than PSCs, SMOSCs have benefits of synthetic reproducibility from the ease of synthesis and purification, and greater tendency to self-assemble for charge transport. Furthermore, SMOSCs do not suffer from batch-to-batch variation with well-defined structure and definite molecular weight. Based on these advantages, over 7% of efficiencies have been reported for small molecule bulk-heterojunction OSCs.[2] However, device performances of SMOSCs are still lower than PSCs. Therefore, further works are needed to design molecular structure for improving device performances of SMOSCs.

Push-pull structure, normally A-D-A or D-A-D type triad molecules, is considered as the promising candidates for organic molecules to obtain high efficiency of OSCs. In push-pull structure, electron donating group and electron withdrawing group are effectively combined by covalent

bonding. And, this structure exhibits intramolecular charge transfer characteristics, resulting in lowered bandgap with effectively tuned HOMO and LUMO levels of molecule. Several kinds of dyes, such as tryarylamine[3], diketopyrrolopyrrole (DPP)[4], isoindigo[5], rhodanine[6], and so on, are considered as the promising materials for high performance of OSCs due to their high absorption coefficients. Among them, DPP derivatives are excellent candidates for a promising acceptor moiety with strong light absorption, photochemical stability, excellent charge carrier mobility, and easy synthesis process. With those advantages of DPP, benzodithiophene-DPP derivative is reported with PCE of 5.79%, the highest device performance among DPP-based SMOSCs.[7]

In this work, novel A-D-A type (HD-IDID-EH-DPP) and D-A-D type (HD-DPP-EH-IDID) triad organic small molecules were designed and synthesized, where IDID, novel electron donating moiety, and DPP, an electron accepting moiety, are covalently attached as shown in Figure 3.1.a. Strong intramolecular charge transfer (ICT) characteristics were exhibited due to strong electron donating property of IDID and strong electron accepting property of DPP. The solution-processed OSCs based on HD-IDID-EH-DPP/HD-DPP-EH-IDID and $PC_{61}BM$ were fabricated, with chloroform and chlorobenzene. With high absorption coefficient of HD-IDID-EH-DPP, devices fabricated using chloroform showed high J_{SC} up to 13.02 mA/cm^2 (maximum value of PCE=3.61%), and devices fabricated using chlorobenzene show high fill factor up to 55.6% (maximum value of PCE=4.15%). While, devices using HD-DPP-EH-IDID as a donor in active layer exhibit relatively poor device performance of PCE of 1.94% with low J_{SC} and V_{OC}, due to low light absorption and

high-lying HOMO level.

Finally, I could demonstrate high efficiency OSCs with extremely high J_{SC}, by using HD-IDID-EH-DPP as a donor. Furthermore, A-D-A type IDID-DPP derivative is identified as a suitable donor molecule for high efficiency OSCs through comparison of device performances between A-D-A and D-A-D type molecules, clearly correlated with molecular structure and optical, electrochemical properties.

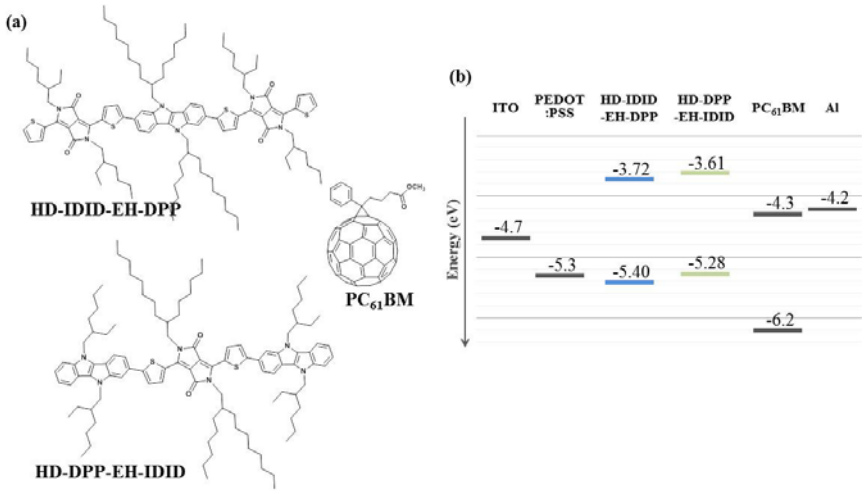

Figure 3.1. (a) Molecular structure of HD-IDID-EH-DPP, HD-DPP-EH-IDID and $PC_{61}BM$ and (b) energy levels.

3.2 Experimental

3.2.1 Design concept and target materials

To induce efficient intramolecular charge transfer transition in molecule, I designed A-D-A type (HD-IDID-EH-DPP) and D-A-D type (HD-DPP-EH-IDID) triad small molecules as shown in Figure 3.1 (a), where IDID is selected as a donor unit, and DPP is selected as an acceptor unit. DPP moieties are attached on 2- or 2,7-position of IDID to extend π-conjugation by covalent bond.

Pyrrole-containing fused aromatic backbone, IDID, has a planar conformation beneficial to π-π interaction for charge transport, and exhibits strong electron-donating property. Furthermore, substitution of aromatic groups on 2- or 2,7-position of IDID allow π-conjugation extension to attached aromatic unis. DPP is selected as an acceptor moiety based on strong electron withdrawing property, which induces strong intramolecular charge transfer with IDID, and large molar extinction coefficient for high light absorption of devices. 6 bulky alkyl groups attached on nitrogen atoms of IDID and DPP, 2 hexyldecyl groups on core unit and 4 ethylhexyl groups on end-capped units, allow great solubility to common organic solvents and good film forming quality.

Based on these strategies, push-pull type HD-IDID-EH-DPP and HD-DPP-EH-IDID were designed to explore electron donating property of IDID, and investigate structural effect on optical, electrochemical, and device properties.

3.2.2 Synthesis

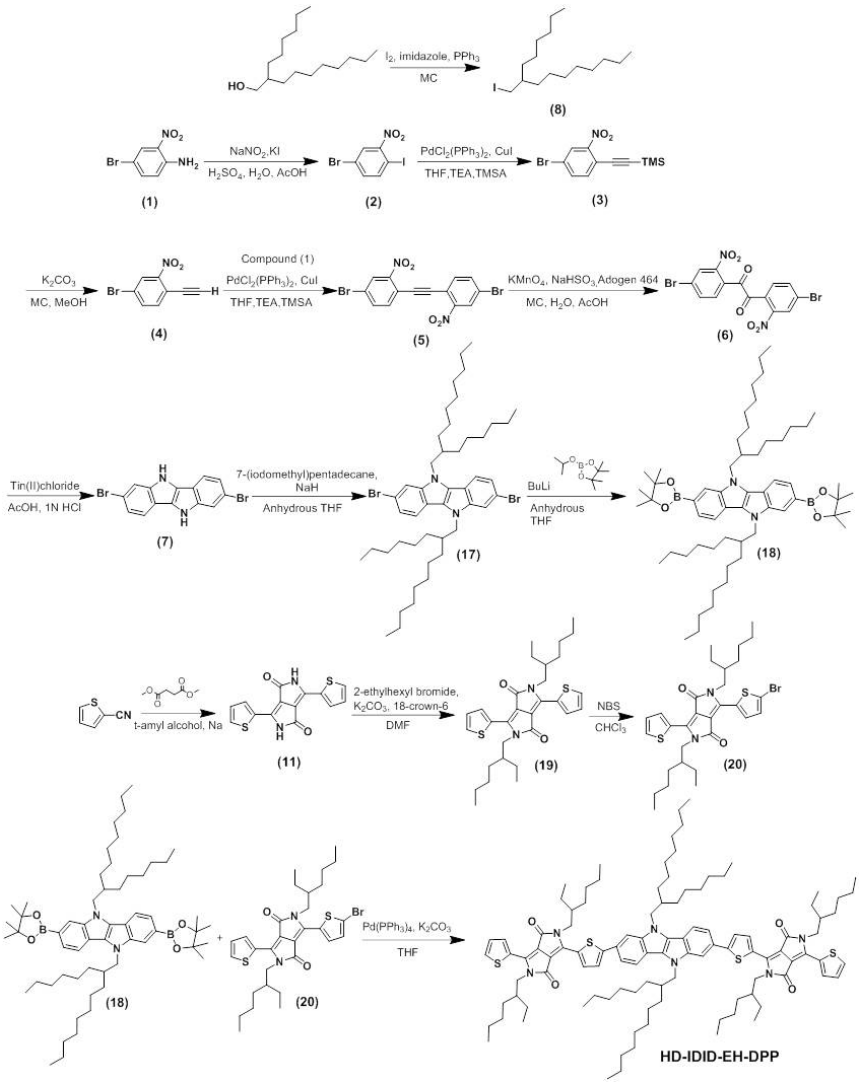

Scheme 3.1. Synthesis of HD-IDID-EH-DPP.

Synthesis methods of (1)~(7) are exactly same with methods of (1)~(7) in **2.2.1 Synthesis** in **Chapter 2**.

7-(iodomethyl)pentadecane (8)

Iodine (13.128 g, 51.724mmol) was added to a solution of 2-hexyldecan-1-ol (10.45 g, 43.103mmol), triphenylphosphine (13.567 g, 51.724 mmol), and imidazole (3.520 g, 51.724 mmol) in 60 mL of methylene chloride in the ice bath (0°C). After stirring for 30 min, the temperature went up to room temperature for overnight. After reaction is over, organic solution is poured into water and methylene chloride. After 20 mL of saturated Sodium metabisulfite ($Na_2S_2O_5$) (aq) was added, organic solution were separated, dried with $MgSO_4$, and concentrated by evaporation. The organics were purified by flash column chromatography (chloroform/ethyl acetate/n-hexane; 0.5;0.5:9, v/v) to give compound (8) as transparent oilish liquid (8.1g, 62%)

1H-NMR (300 MHz, $CDCl_3$, δ): 3.2-3.26 (d, 2H), 2.02-1.97 (t, 1H), 1.43-1.12 (m, 25H), 0.90-0.86 (m, 6H).

2,7-dibromo-5,10-bis(2-hexyldecyl)-5,10-dihydroindolo[3,2-b]indole (17)

A 100 mL round-bottom flask, equipped with a magnetic stirrer bar and reflux condenser was baked under reduced pressure and Ar backfilled (x3). The baked reaction vessel was added 2,7-dibromo-5,10-dihydroindolo[3,2-b]indole (7) (0.650 g, 1.786 mmol), anhydrous THF (70 mL), NaH (0.257 g, 10.713 mmol). After 10 minutes at room temperature, 3.775g (10.713 mmol) of 7-(iodomethyl)pentadecane (8) was

added to the reaction mixture. After being stirring 10 minutes, the vessel gently refluxed 48 hours, the reaction mixture poured into brine (200 mL) and methylene chloride. The organic layer separated, washed (water, x 3), dried with $MgSO_4$, and concentrated. Resulting crude product was purified by flash column chromatography (ethyl acetate/n-hexane; 1:100, v/v) to give compound (17) as yellow oilish liquid (0.910 g, 62%)

1H-NMR (300 MHz, THF, δ): 7.74-7.72 (d, 2H), 7.69 (s, 2H), 7.23-7.20 (d, 2H), 4.39-4.37 (t, 4H), 1.39~1.18 (m, 50H), 0.88-0.80 (m, 12H)

5,10-bis(2-hexyldecyl)-2,7-bis(4,4,5,5-tetramethyl-1,3,2-dioxaborolan-2-yl)-5,10-dihydroindolo[3,2-b]indole (18)

A 100 mL round-bottom flask, equipped with a magnetic stirrer bar and reflux condenser was baked under reduced pressure and Ar backfilled (x3). The baked reaction vessel was added 2,7-dibromo-5,10-bis(2-hexyldecyl)-5,10-dihydroindolo[3,2-b]indole (17) (0.900g, 1.095 mmol) and Anhydrous THF(70mL) in dry ice and acetone bath. After 1 hour stirring, n-Butyllithium solution 1.6M in hexane (0.351 g, 5.475 mmol) was gently injected. And after 1 hour stirring, 2-isopropoxy-4,4,5,5-tetramethyl-1,3,2-dioxaborolane (1.019g, 5.475 mmol) was injected. The solution was stirred at room temperature for 2 hours. After reaction finished, reaction mixture quenched with brine (300 mL), and extracted with methylene chloride. The combined organic phase was concentrated under reduced pressure. The crude product was purified by column chromatography (ethyl acetate/n-hexane; 1:100, v/v) to afforded 5,10-bis(2-hexyldecyl)-2,7-bis(4,4,5,5-tetramethyl-1,3,2-dioxaborolan-2-yl)-5,10-dihydroindolo[3,2-b]indole (18) as yellow oilish liquid (0.310g, 31%)

1H-NMR (300 MHz, THF, δ): 7.93 (s, 2H), 7.84-7.81 (d, 2H), 7.52-7.49 (d, 2H), 4.47-4.44 (t, 4H), 1.39 (s, 24H), 1.35-1.18 (m, 50H), 0.87-0.79 (m, 12H),

3,6-di(thiophen-2-yl)-2,5-dihydropyrrolo[3,4-c]pyrrole-1,4-dione (11)

Sodium metal (1.21 g, 52.64mmol) immersed in mineral oil was washed with hexane and cut into small pieces. Sodium metal pieces were slowly added to the solution of tert-amyl alcohol (40mL) under Ar atmosphere. The mixture was slowly heated to 120℃ and stirred for overnight. Then 2-thiophenecarbonitrile (2.18g, 26.32mmol) was added and dimethylsuccinate (1.83g, 10.53mmol) was added dropwise to the reaction mixture for 1hour. The mixture was stirred at 120℃ for 3hours and then cooled to room temperature. The contents were poured into acidic methanol (200mL methanol and 10mL HCl) in ice bath and stirred for 1.5hour. Filtration of the suspension yielded a purple solid (2.13g, 33.9%), which was used in next step without further purification.

2,5-bis(2-ethylhexyl)-3,6-di(thiophen-2-yl)-2,5-dihydropyrrolo[3,4-c]pyrrole-1,4-dione (19)

A 250 mL round-bottom flask, equipped with a magnetic stirrer bar was added the 3,6-di(thiophen-2-yl)-2,5-dihydropyrrolo[3,4-c]pyrrole-1,4-dione(11) (5 g, 16.647 mmol), potassium carbonate (7.597 g, 54.936 mmol), DMF (150 mL). After being stirring 1 hour at 120℃, 2-ethylhexyl bromide (9.645 g, 49.942 mmol), and 18-crown-6 (1 g, 3.783 mmol) were gently injected, and temperature went up to 150℃. After the vessel was gently refluxed for 24hours, the reaction mixture was poured into water

(400 mL). The crude solid precipitate was filtered with reduced pressure. Resulting crude product was purified by flash column chromatography (chloroform/ethyl acetate/n-hexane; 3:0.4:6.6, v/v) and then precipitated using methanol and methylene chloride to give compound (19) as purple solid. (1.48 g, 17%)

1H-NMR (300 MHz, $CDCl_3$, δ): 8.76 (s, 2H), 7.61 (d, 2H), 7.27 (d, 2H), 4.03-3.93 (m, 4H), 1.84 (m, 2H), 1.40-1.23 (m, 16H), 0.91-0.83 (m, 12H)

3-(5-bromothiophen-2-yl)-2,5-bis(2-ethylhexyl)-6-(thiophen-2-yl)-2,5-dihydropyrrolo[3,4-c]pyrrole-1,4-dione (20)

A 250 mL round-bottom flask, equipped with a magnetic stirrer bar was added the 2,5-bis(2-ethylhexyl)-3,6-di(thiophen-2-yl)-2,5-dihydropyrrolo[3,4-c]pyrrole-1,4-dione (19) (1.05 g, 2.001 mmol), chloroform (200 mL). After being stirring 1 hour at 0℃, NBS (0.374 g, 2.101 mmol) was gently injected, and temperature went up to room temperature. The solution was stirred for 2 hours in light shielded environment. The reaction mixture was poured into water (200 mL) and methylene chloride. The organic layer was separated, washed (water, x3), dried with $MgSO_4$, and concentrated. Resulting crude product was purified by flash column chromatography (chloroform/ethyl acetate/n-hexane; 3:0.2:6.8, v/v) and then precipitated using methanol and methylene chloride to give compound (20) as dark red solid. (1.48 g, 39.7%)

1H-NMR (300 MHz, $CDCl_3$, δ): 8.90 (d, 1H), 8.65-8.62(t, 1H), 7.65-7.63 (d, 1H), 7.29-7.27 (d, 1H), 7.23-7.22 (d, 1H), 4.03-3.96 (m, 4H), 1.87 (m, 2H), 1.38-1.20 (m, 16H), 0.94-0.83 (m, 12H)

6,6'-((5,10-bis(2-hexyldecyl)-5,10-dihydroindolo[3,2-b]indole-2,8-diyl)bis(thiophene-5,2-diyl))bis(2,5-bis(2-ethylhexyl)-3-(thiophen-2-yl)-2,5-dihydropyrrolo[3,4-c]pyrrole-1,4-dione) (HD-IDID-EH-DPP)

A 100 mL round-bottom flask, equipped with a magnetic stirrer bar was added 5,10-bis(2-hexyldecyl)-2,7-bis(4,4,5,5-tetramethyl-1,3,2-dioxaborolan-2-yl)-5,10-dihydroindolo[3,2-b]indole (10) (0.342 g, 0.443 mmol), 3-(5-bromothiophen-2-yl)-2,5-bis(2-ethylhexyl)-6-(thiophen-2-yl)-2,5-dihydropyrrolo[3,4-c]pyrrole-1,4-dione (13) (0.480 g, 0.929 mmol), tetrakis(triphenylhosphine)palladium(0) (0.077g, 0.066 mmol), 2N K_2CO_3 aqueous solution (40 mL), and THF (80 mL). The vessel was than sealed with rubber septum, evacuated and backfilled with Ar gas and then gently refluxed for 48 hours at 70℃. After reaction finished, reaction mixture quenched with 1N HCl aqueous solution (300 mL), and extracted with methylene chloride. The combined organic phase was dried with $MgSO_4$ and concentrated under reduced pressure. The crude product was purified by flash column chromatography (chloroform/ethyl acetate/n-hexane; 4:0.007:5.993, v/v) and reprecipitated with methanol and methylene chloride to afforded 6,6'-((5,10-bis(2-hexyldecyl)-5,10-dihydroindolo[3,2-b]indole-2,8-diyl)bis(thiophene-5,2-diyl))bis(2,5-bis(2-ethylhexyl)-3-(thiophen-2-yl)-2,5-dihydropyrrolo[3,4-c]pyrrole-1,4-dione) (HD-IDID-EH-DPP) as goldish dark blue solid (0.16 g, 25%)

1H-NMR (300 MHz, THF, δ): 9.23-9.21(d, 2H), 9.06-9.05(d, 2H), 7.90-7.87(d, 2H), 7.86(s, 2H), 7.79-7.69(d, 2H), 7.68-7.67(d, 2H), 7.57-7.52(d, 2H), 7.29-7.26(t, 2H), 4.49-4.46(d, 4H), 4.14-4.05(m, 8H), 2.03-1.88(m, 6H), 1.43-1.19(m, 80H), 0.93-0.78(m, 36H).

Elemental Analysis calculated for $C_{106}H_{150}N_6O_4S_4$: C 74.86, H 8.89, N 4.94, O 3.76, S, 7.54; found: C 74.89, H 8.95, N 4.87, O 3.82, S 7.51.

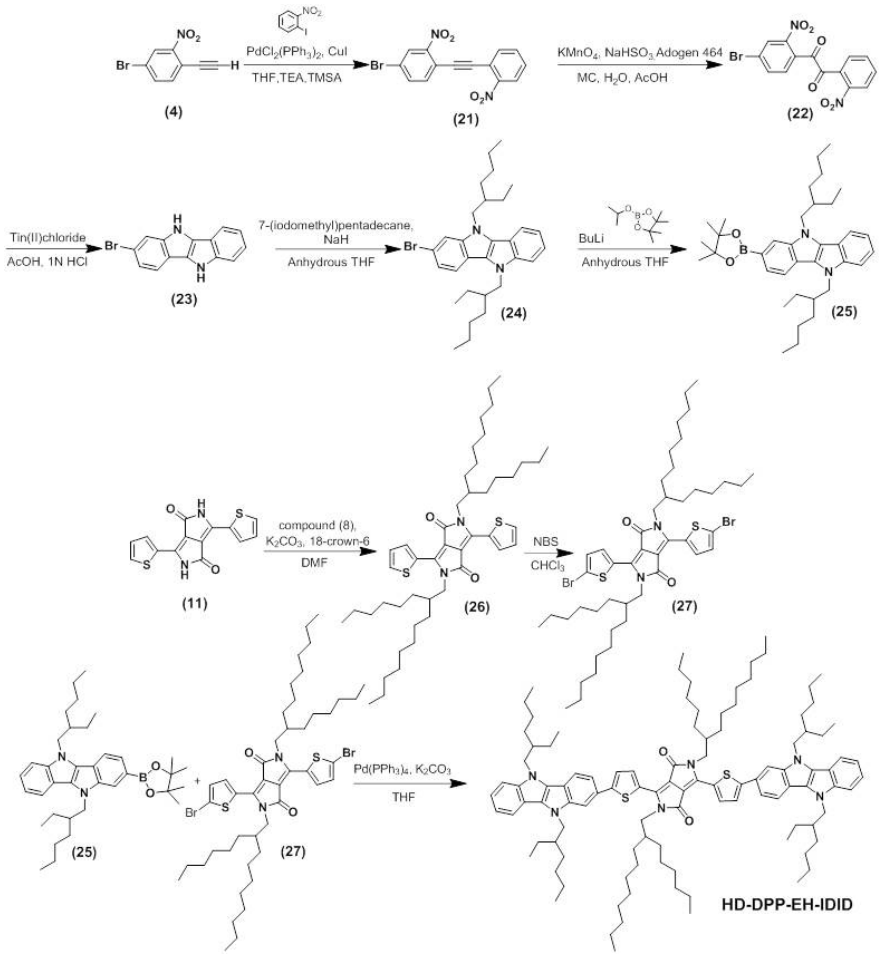

Scheme 3.2. Synthesis of HD-DPP-EH-IDID.

Synthesis of HD-DPP-EH-IDID is as follows.

4-bromo-2-nitro-1-((2-nitrophenyl)ethynyl)benzene (21)

Synthesis of 4,4'-dibromo-2,2'-dinitrotolane took same synthetic procedure with (4-bromo-2-nitro-phenylethynyl)-trimethyl-silane. Used were 4-bromo-1-ethynyl-2-nitrobenzene (4) (2.751 g, 12.171 mmol), 1-iodo-2-nitrobenzene (3.031 g, 12.171 mmol), bis(triphenylphosphine)

palladium(II) dichloride (0.427 g, 0.609 mmol), copper(I) iodide (0.232 g, 1.217 mmol), THF (80 mL), and triethylamine (20mL). Flash column chromatography ($CHCl_3$) and EA washing afforded the compound (21) as light brown solid (2.8 g, 66.3%).

1H-NMR (300 MHz, CDCl3, δ): 8.31-8.30 (d, 1H), 8.07-8.04(d, 1H), 7.88-7.84(d, 1H), 7.80-7.74(d, 1H), 7.54-7.48(t, 1H), 7.28-7.21(t, 1H), 6.98(s, 1H)

1-(4-bromo-2-nitrophenyl)-2-(2-nitrophenyl)ethane-1,2-dione (22)

A 250 mL round-bottom flask, equipped with a magnetic stirrer bar was added the potassium permanganate (1.519 g, 9.611 mmol), Adogen 464 (catalytic amount), water (75 mL), methylene chloride (100mL), and acetic acid (3.75 mL). The mixture was stirred and evacuated and backfilled with Ar gas. The mixture was added the 4-bromo-2-nitro-1-((2-nitrophenyl)ethynyl)benzene (21) and then gently refluxed for 5 hours, cooled, and decolorized using $NaHSO_3$. The resulting two clear phases were separated, and the yellow organic phase was dried over $MgSO_4$ and filtered through a silica plug. The yellow filtrate was concentrated, and the resulting solid was washed with methanol to give compound (22) as yellow crystalline solid (0.87 g, 71%).

1H-NMR (300 MHz, CDCl3 δ): 8.31-8.28 (d, 1H), 8.04-8.01(d, 1H), 7.88-7.85(d, 1H), 7.80-7.77(d, 1H), 7.54-7.48(t, 1H), 7.28-7.21(t, 1H), 6.98(s, 1H)

2-bromo-5,10-dihydroindolo[3,2-b]indole (23)

A 250 mL round-bottom flask, equipped with a magnetic stirrer bar was

added the 1-(4-bromo-2-nitrophenyl)-2-(2-nitrophenyl)ethane-1,2-dione (22) (0.870 g, 2.2948mmol), and warm acetic acid (45 mL). With vigorous stirring, the reaction vessel was added the filtrate of stannous chloride (10.200 g, 55.075 mmol), acetic acid (30 mL), and 1 N HCl (25 mL) mixed solution. The vessel gently refluxed for 5 hours at 80°C. The resulting precipitate was filter, and washed with acetic acid, 1 N HCl, water, and ethanol. Flash column chromatography (ethyl acetate) and washing ($CHCl_3$) afford the compound (23) as gray solid (0.460 g, 70%).

1H-NMR (300 MHz, Acetone-d6, δ): 10.53(s.1H), 10.36(s, 1H), 7.85(d, 1H), 7.73-7.70(t, 2H), 7.55(d, 1H), 7.24-7.18(q 2H), 7.09-7.07(t, 1H)

2-bromo-5,10-bis(2-ethylhexyl)-5,10-dihydroindolo[3,2-b]indole (24)

A 100 mL round-bottom flask, equipped with a magnetic stirrer bar and reflux condenser was baked under reduced pressure and Ar backfilled (x3). The baked reaction vessel was added 2-bromo-5,10-dihydroindolo[3,2-b]indole (23) (0.250 g, 1.648 mmol), anhydrous THF (40 mL), NaH (0.126 g, 9.990 mmol). After 10 minutes at room temperature, 1.016g (9.990 mmol) of 7-(iodomethyl)pentadecane was added to the reaction mixture. After being stirring 10 minutes, the vessel gently refluxed 48 hours, the reaction mixture poured into brine (200 mL). The organic layer separated, washed (water, x 3), dried with $MgSO_4$, and concentrated. Resulting crude product was purified by flash column chromatography (ethyl acetate/n-hexane; 1:4, v/v) and recrystallization (ethyl acetate) to give compound (24) as white crystalline solid (0.320 g, 72%)

1H-NMR (300 MHz, THF, δ): 7.84-7.51(d, 1H) 7.75-7.72(d, 1H), 7.67(s,1H), 7.49-7.46(d, 1H), 7.24-7.18(t, 1H), 7.12-7.06(t, 1H), 4.41-

4.38(d, 4H), 3.49-3.44(m, 2H), 1.54-1.15(m, 16H), 0.98-0.74(m, 12H)

5,10-bis(2-ethylhexyl)-2-(4,4,5,5-tetramethyl-1,3,2-dioxaborolan-2-yl)-5,10-dihydroindolo[3,2-b]indole (25)

A 100 mL round-bottom flask, equipped with a magnetic stirrer bar and reflux condenser was baked under reduced pressure and Ar backfilled (x3). The baked reaction vessel was added 2-bromo-5,10-bis(2-ethylhexyl)-5,10-dihydroindolo[3,2-b]indole (24) (0.320g, 0.628 mmol) and Anhydrous THF (20mL) in dry ice and acetone bath. After 1 hour stirring, n-Butyllithium solution 1.6 M in hexane (0.101 g, 1.570 mmol) was gently injected. And after 1 hour stirring, 2-isopropoxy-4,4,5,5-tetramethyl-1,3,2-dioxaborolane (0.292g, 1.570 mmol) was injected. The solution was stirred at room temperature for 2 hours. After reaction finished, reaction mixture quenched with brine (300 mL), and extracted with methylene chloride. The combined organic phase was concentrated under reduced pressure. The crude product was purified by column chromatography (ethyl acetate/n-hexane; 1:100, v/v) to afforded 5,10-bis(2-ethylhexyl)-2-(4,4,5,5-tetramethyl-1,3,2-dioxaborolan-2-yl)-5,10-dihydroindolo[3,2-b]indole (25) as white oilish liquid (0.130g, 37%)

1H-NMR (300 MHz, DMSO, δ): .84-7.51(d, 1H) 7.75-7.72(d, 1H), 7.67(s,1H), 7.49-7.46(d, 1H), 7.24-7.18(t, 1H), 7.12-7.06(t, 1H), 4.41-4.38(d, 4H), 3.49-3.44(m, 2H), 1.98(s, 12H), 1.54-1.15(m, 16H), 0.98-0.74(m, 12H)

2,5-bis(2-hexyldecyl)-3,6-di(thiophen-2-yl)-2,5-dihydropyrrolo[3,4-c]pyrrole-1,4-dione (26)

A 250 mL round-bottom flask, equipped with a magnetic stirrer bar was added the 3,6-di(thiophen-2-yl)-2,5-dihydropyrrolo[3,4-c]pyrrole-1,4-dione(11) (5 g, 16.647 mmol), potassium carbonate (7.597 g, 54.936 mmol), DMF (150 mL). After being stirring 1 hour at 120℃, 7-(iodomethyl)pentadecane (17.596 g, 49.942 mmol), and 18-crown-6 (1 g, 3.783 mmol) were gently injected, and temperature went up to 150℃. After the vessel was gently refluxed for 24 hours, the reaction mixture was poured into water (400 mL). The crude solid precipitate was filtered with reduced pressure. Resulting crude product was purified by flash column chromatography (chloroform/ethyl acetate/n-hexane; 3:0.4:6.6, v/v) and then precipitated using methanol and methylene chloride to give compound (26) as purple solid. (2.10 g, 17%)

1H-NMR (300 MHz, $CDCl_3$, δ): 8.76 (s, 2H), 8.62-8.61 (d, 2H), 7.22 - 7.21 (d, 2H), 3.93-3.91(d, 4H), 1.88(m, 2H), 1.29-1.22(m, 48H), 0.88-0.82(m, 12H)

3,6-bis(5-bromothiophen-2-yl)-2,5-bis(2-hexyldecyl)-2,5-dihydropyrrolo[3,4-c]pyrrole-1,4-dione (27)

A 250 mL round-bottom flask, equipped with a magnetic stirrer bar was added the 2,5-bis(2-hexyldecyl)-3,6-di(thiophen-2-yl)-2,5-dihydropyrrolo[3,4-c]pyrrole-1,4-dione (26) (2.1 g, 2.001 mmol), chloroform (200 mL). After being stirring 1 hour at 0℃, NBS (1.048 g, 5.886 mmol) was gently injected, and temperature went up to room temperature. The solution was stirred for 2 hours in light shielded environment. The reaction mixture was poured into water (200 mL) and methylene chloride. The organic layer was separated, washed (water, x 3),

dried with MgSO4, and concentrated. Resulting crude product was purified by flash column chromatography (chloroform/ethyl acetate/n-hexane; 3:0.2:6.8, v/v) and then precipitated using methanol and methylene chloride to give compound (27) as dark red solid. (1.45 g, 57%)

1H-NMR (300 MHz, $CDCl_3$, δ): 8.60-8.58 (d, 2H), 7.20 -7.18 (d, 2H), 3.93-3.91(d, 4H), 1.74(m, 2H), 1.25-1.21(m, 48H), 0.86-0.80(m, 12H)

3,6-bis(5-(5,10-bis(2-ethylhexyl)-5,10-dihydroindolo[3,2-b]indol-2-yl)thiophen-2-yl)-2,5-bis(2-hexyldecyl)-2,5-dihydropyrrolo[3,4-c]pyrrole-1,4-dione (HD-DPP-EH-IDID)

A 100 mL round-bottom flask, equipped with a magnetic stirrer bar was added 3,6-bis(5-bromothiophen-2-yl)-2,5-bis(2-hexyldecyl)-2,5-dihydropyrrolo[3,4-c]pyrrole-1,4-dione (27) (0.048 g, 0.0.055mol), 5,10-bis(2-ethylhexyl)-2-(4,4,5,5-tetramethyl-1,3,2-dioxaborolan-2-yl)-5,10-dihydroindolo[3,2-b]indole (25) (0.064 g, 0.1147mmol), tetrakis(triphenylhosphine)palladium(0) (0.010g, 0.009 mmol), 2N K_2CO_3 aqueous solution (8 mL), and THF (16 mL). The vessel was than sealed with rubber septum, evacuated and backfilled with Ar gas and then gently refluxed for 48 hours at 70℃. After reaction finished, reaction mixture quenched with 1N HCl aqueous solution (300 mL), and extracted with methylene chloride. The combined organic phase was dried with $MgSO_4$ and concentrated under reduced pressure. The crude product was purified by flash column chromatography (chloroform/ethyl acetate/n-hexane; 4:0.007:5.993, v/v) and reprecipitated with methanol and methylene chloride to afforded 3,6-bis(5-(5,10-bis(2-ethylhexyl)-5,10-dihydroindolo[3,2-b]indol-2-yl)thiophen-2-yl)-2,5-bis(2-hexyldecyl)-2,5-

dihydropyrrolo[3,4-c]pyrrole-1,4-dione (HD-DPP-EH-IDID) as dark blue solid (0.50 g, 58%)

1H-NMR (300 MHz, THF, δ): 9.20(d, 2H), 7.92-7.86(q, 6H), 7.68-7.64(d, 2H), 7.56-7.49(q, 4H), 7.27-7.22(t, 2H), 7.13-7.08(t, 2H),4.53-4.42 (q, 8H), 4.18-4.16(d, 4H), 2.32-2.15(m, 6H), 1.46-1.26(m, 80H), 0.99-0.80(m, 36H).

3.2.3 Instruments and measurements

Chemical structures were identified with 1H NMR (Bruker, Avance-300) in $CDCl_3$, Acetone-d_6, DMSO-d_6, THF-d_6 solutions, GC-Mass(JEOL, JMS-700), and elemental analysis (EA1110, CE Instrument).

UV-vis absorption spectra were recorded on a Shimadzu UV-1650PC. HOMO levels were obtained from the cyclic voltammetry measurement using a 273 A (Princeton Applied Research) with a one-component electrolysis cell consisting of a platinum working electrode, a platinum wire counter-electrode, and a quati Ag+/Ag electrode as a reference. Measurements were performed in a 0.5 mM acetonitrile solution with tetrabutylammonium tetrafluoreborate as the supporting electrolyte, at a scan rate 100 mV/s. Each oxidation potential was calibrated using ferrocene as a reference. LUMO levels were obtained from the edge of the absorption spectra and HOMO levels were measured from cyclo-voltammetry measurement.

Optical microscopic observation of the crystals was carried out with a Leica Mikroskopie & System GmbH Wetzier.

The d-spacing of stacked molecules π-spacing between molecules in films on glass was measured through X-ray diffraction measurement with out of plane mode XRD and GIXD carried out with a New D8 Advance (Bruker), X'pert Pro (PANanalytical), respectively.

3.2.4 Fabrication and characterization of organic solar cells (OSCs)

The organic solar cells in this study were fabricated by following method. Patterned ITO glass substrates were cleaned in an ultrasonic bath with trichloroethylene, acetone, isopropyl alcohol, for 10 minute, respectively, and then blow dried with a N_2 stream followed by UV/O_3 treatment. A 40 nm of PEDOT:PSS (Clevios P VP.AI 4083, Heraeus) film was then spin-coated on to the substrate (5000 rpm / 30 s) using the PVDF 0.45 μm syringe filter. The film was dried at 150 °C for 20 min. Subsequently, the active layer films were spin coated (1500rpm / 40s for HD-IDID-EH-DPP and 2000rpm/40s for HD-DPP-EH-IDID) using HD-IDID-EH-DPP/HD-DPP-EH-IDID:$PC_{61}BM$ blended solution stirred over 12 hours at 30°C filtered by the PTFE 0.50 μm syringe filter to the thickness of around 80 nm in a N_2-fulled glovebox. Al electrodes were deposited via thermal evaporation in a vacuum chamer with thickness of 100 nm, followed by post-annealing at 110°C for HD-IDID-EH-DPP and at 90℃ for HD-DPP-EH-IDID for 3 min. The active area of these solar cells was 0.09 cm^2. All devices were encapsulated.

The current density-voltage (J-V) characteristics of the solar cells were measured with a Keithley 4200 source measurement unit. The solar cell performances were characterized under AM1.5G condition with an illumination intensity of 100 $mWcm^{-2}$ generated by an Oriel Sol 3 A solar simulator. Illumination intensity was set using NREL-certified silicon diode. J-V characteristics of the cells with illumination were measured with 0.1 cm^2 of effective active area defined by aperture. The intensity

dependent measurements have been performed with various neutral density filters. Characterization of device performance was carried out under ambient condition.

Incident photon to current conversion efficiency (IPCE) was measured using Oriel QE/IPCE measurement Kit which composed of 300 W Xenon Lamp, monochromator, the order sorting filter wheel, the Merlin lock-in amplifier and the chopper.

The active layer morphology was examined by atomic force microscope (AFM) technique in tapping mode (Jeol 5200, SPM instrument).

3.3 Results and discussion

3.3.1 Density functional theory (DFT) calculation

Theoretical molecular orbital calculation was carried out using Gaussian09 at B3LYP/6-31G* level to characterize optimized ground state geometry and electron density of HOMO and LUMO states.

In optimized ground state geometry, both A-D-A type and D-A-D type triad molecules (6 ethyl groups are substituted instead of hexyldecyl and ethyl hexyl groups) show planar IDID backbone. In A-D-A type structure, IDID-DPP derivative exhibits small torsion angle of 0.8° between thiophene and end-capped DPP, and torsion angle of 24.8° between thiophene and attached IDID core, while in D-A-D type structure, molecule exhibits torsion angle of 22.9° between thiophene and end-capped IDID, and 5.5° between thiophene and DPP core in calculated optimized ground-state geometry (as shown in Figure 3.2). The molecular size of A-D-A type derivative is 36.07Å in lateral direction, which is larger than that of D-A-D molecule (32.62Å). Calculated HOMO and LUMO energy density maps are shown in Figure 3.3. HOMO/LUMO levels of A-D-A type derivative are -4.66 eV and -2.56 eV, respectively, which are lower-lying than those of D-A-D type derivative with -4.44 eV/-2.31 eV of HOMO/LUMO level, as expected based on their chemical structures.

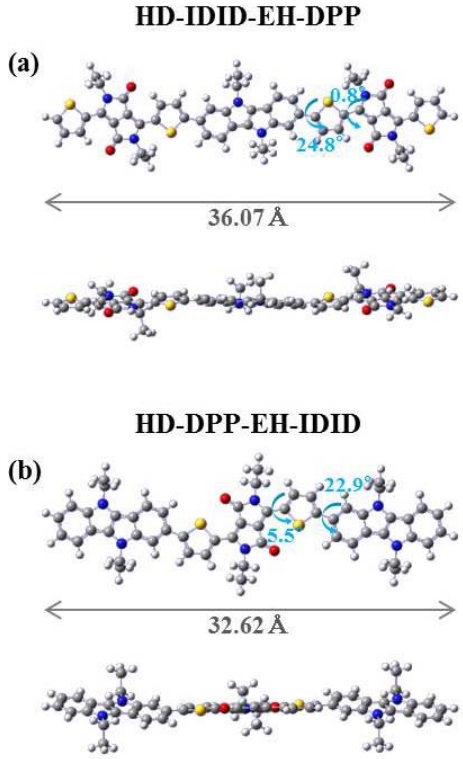

Figure 3.2. The calculated optimized ground state geometry of (a) HD-IDID-EH-DPP and (b) HD-DPP-EH-IDID (alkyl side groups are substituted with ethyl groups) using Gaussian 09 at the B3LYP/6-31G* level. (upper: front view, lower: top view).

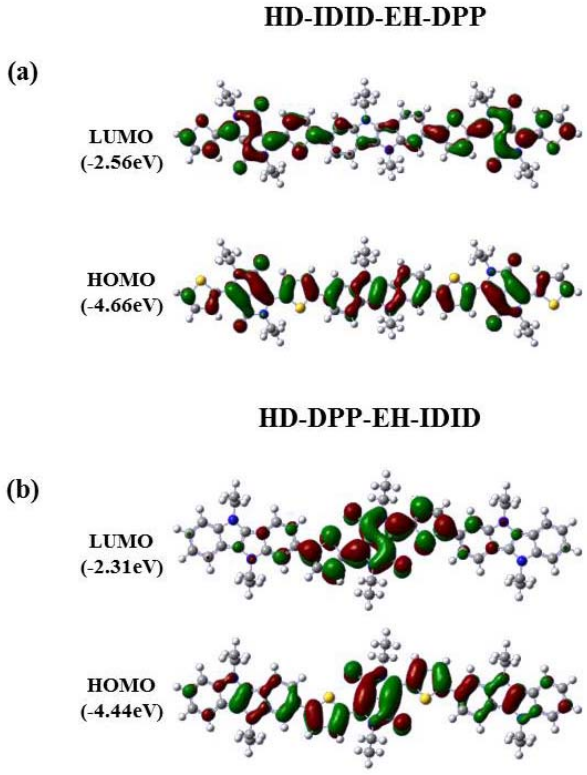

Figure 3.3. The calculated HOMO and LUMO energy density maps of (a) HD-IDID-EH-DPP and (b) HD-DPP-EH-IDID (alkyl side groups are substituted with ethyl groups) obtained using Gaussian 09 at B3LYP/6-31G* level.

3.3.2 Thermal properties

The thermal properties of both compounds were investigated by differential scanning calorimetry (DSC) and thermogravimetric analysis (TGA) under N_2 atmosphere. (see Figure 3.4 and Table 3.1).

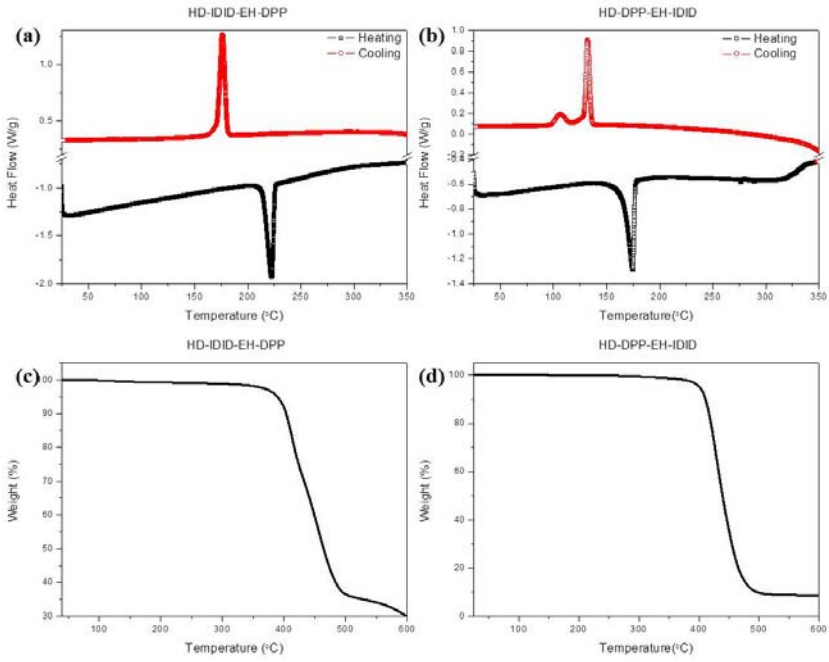

Figure 3.4. DSC result of (a) HD-IDID-EH-DPP and (b) HD-DPP-EH-IDID, and TSC traces of (c) HD-IDID-EH-DPP and (D) HD-DPP-EH-IDID.

Table 3.1. Thermal properties of HD-IDID-EH-DPP and HD-DPP-EH-IDID.

Compound	T_m(℃)	T_c(℃)	T_d(℃)[a)]
HD-IDID-EH-DPP	222.8	176.2	389.4
HD-DPP-EH-IDID	174.7	132.5	400.9

a) Decomposition temperature (5% weight loss)

3.3.3 Optical and electrochemical properties

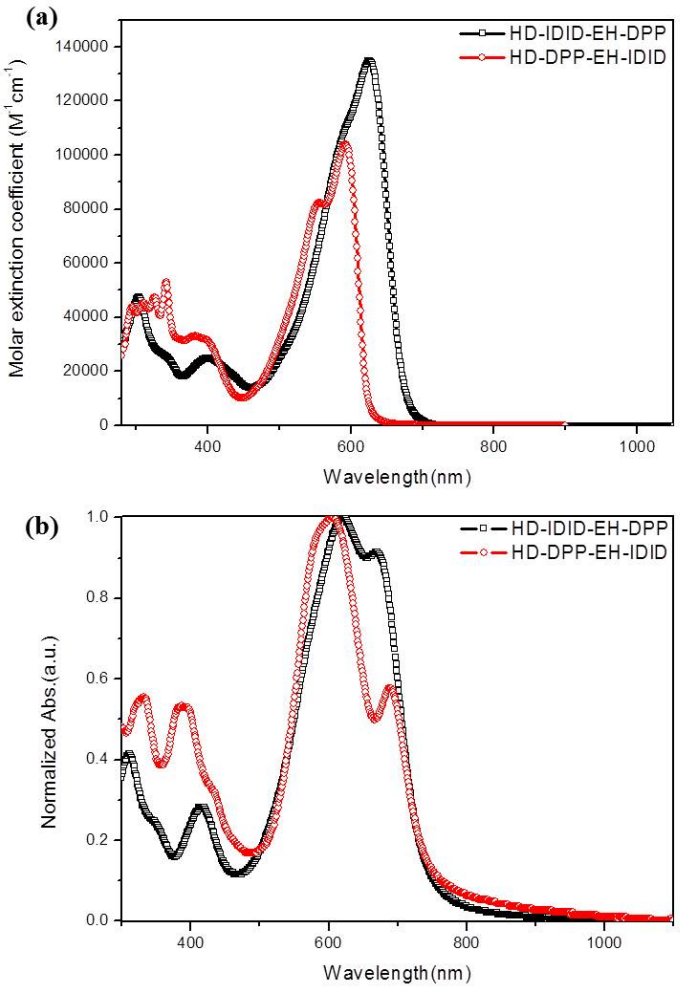

Figure 3.5. (a) Molar extinction coefficient of HD-IDID-EH-DPP (black) and HD-DPP-EH-IDID (red) in THF solution (b) Normalized UV/vis absorption spectra of HD-IDID-EH-DPP (black) and HD-DPP-EH-IDID (red) spin-coated film from chlorobenzene/chloroform solution.

Table 3.2. Optical properties of HD-IDID-EH-DPP and HD-DPP-EH-IDID in solution and film.

Compound	λ_{abs} (nm)	λ_{onset} (nm)	λ_g [c] (eV)
HD-IDID-EH-DPP(solution)[a]	304, 398, 626	672	1.85
HD-IDID-EH-DPP(film)[b]	311, 418, 620, 670	734	1.68
HD-DPP-EH-IDID(solution)[a]	296,311,326,342, 381,554,593	624	1.99
HD-DPP-EH-IDID(film)[b]	331, 387, 608, 690	742	1.67

a) Measured in THF solution of concentration of 10^{-5} M. b) Spin-coated 0.5 wt% using 1,2-dichloroethane solution.(1000rpm/30s) c) Optical band gap was obtained from absorption edge.

Figure 3.5 shows (a) molar extinction coefficient and (b) normalized UV-vis absorption spectra of A-D-A type derivative (HD-IDID-EH-DPP) and D-A-D type derivative (HD-DPP-EH-IDID) in THF solution and spin-coated film from chlorobenzene solution, respectively. HD-IDID-EH-DPP shows extremely high molar extinction coefficient, with maximum value of 134,900 $M^{-1}cm^{-1}$ at 625 nm. Due to strong intramolecular charge transfer (ICT) transition, the high degree of π-conjugation between electron donating moiety (IDID) and electron accepting moiety (DPP), as predicted by DFT calculation, is demonstrated in HD-IDID-EH-DPP solution, where the compound shows broad absorption with λ_{max}=626 nm, as mentioned in Table 3.2. However, HD-DPP-EH-IDID exhibits less and narrower light absorption than HD-IDID-EH-DPP as shown in Figure

3.5 (a). HD-DPP-EH-IDID possesses maximum molar extinction coefficient 104,000 $M^{-1}cm^{-1}$ at 593 nm. Furthermore, due to less number of dye DPP moieties, light absorbance of HD-DPP-EH-IDID is lower than that of HD-IDID-EH-DPP.

The film state absorption spectra of HD-IDID-EH-DPP and HD-DPP-EH-IDID show red-shifted absorption compared to their solution state absorption spectra due to aggregation and structural reorganization in solid state.[4(b)] Additionally, the film spectra of both molecules show relatively broad absorption spectrum extended to near IR region (~750 nm) with λ_{max} = 670 nm in HD-IDID-EH-DPP, and λ_{max} = 690 nm in HD-DPP-EH-IDID.

The absorption band edges of the compounds are shifted from 1.85 eV in solution to 1.68 eV in film state of HD-IDID-EH-DPP, and from 1.99 eV in solution to 1.67 eV in film state of HD-DPP-EH-IDID. Those significant changes are due to the coplanarization of the donor and acceptor moieties and intermolecular stacking in solid state.

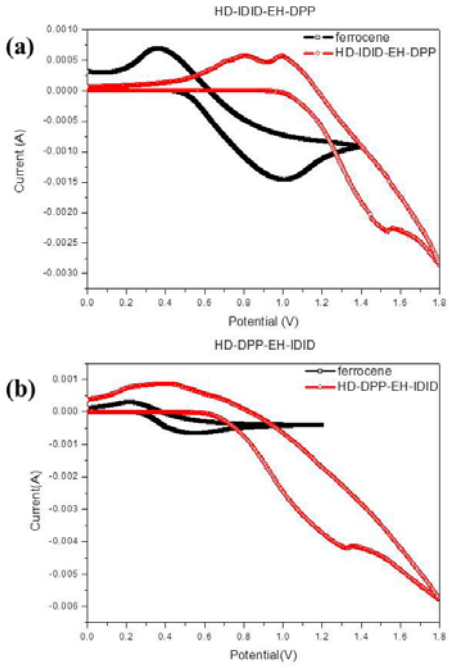

Figure 3.6. The cyclic voltammograms of (a) HD-IDID-EH-DPP (red) in film and ferrocene (black) and (b) HD-DPP-EH-IDID (red) in film and ferrocene (black) with TBATFB in acetonitrile as the supporting electrolyte.

Table 3.3. Electrochemical properties of HD-IDID-EH-DPP and HD-DPP-EH-IDID (film).

Compound	λ_g [a] (eV)	E_{HOMO} [b] (eV)	E_{LUMO} [c] (eV)
HD-IDID-EH-DPP (film)	1.68	-5.40	-3.72
HD-DPP-EH-IDID (film)	1.67	-5.28	-3.61

a) optical band gap was obtained from films absorption edge. b) Calculated by eqaution: $E_{HOMO} = \left[-\left(E_{onset} - E_{ferrocene}\right) - 4.8\right]$ c) LUMO level was calculated from optical band gap and HOMO level.

The electrochemical properties of HD-IDID-EH-DPP and HD-DPP-EH-IDID were measured by cyclic-voltammetry (LUMO levels were calculated from optical bandgap from UV/vis absorption spectrum, and electrochemically measured HOMO level, Table 3.3). The oxidation potential for HD-IDID-EH-DPP and HD-DPP-EH-IDID were measured relative to ferrocene (Fc/Fc^{+}=4.8eV) which is used as the internal reference. HOMO and LUMO levels were -5.40 eV and -3.72 eV for HD-IDID-EH-DPP, and -5.28 eV and -3.61 eV for HD-DPP-EH-IDID, respectively. Energy levels of both molecules exhibit similar tendency to energy levels from DFT calculation. As expected in their chemical structures, D-A-D type derivative HD-DPP-EH-IDID possesses stronger electron donating property than A-D-A type derivative HD-IDID-EH-DPP. Consequently, HD-DPP-EH-IDID exhibits higher-lying HOMO and LUMO levels than HD-IDID-EH-DPP. These values are appropriate electronic levels for BHJ solar cells using $PC_{61}BM$ as an electron acceptor in an organic layer. [1(c)]

3.3.4 Grazing incidence X-ray diffraction (GIXD)

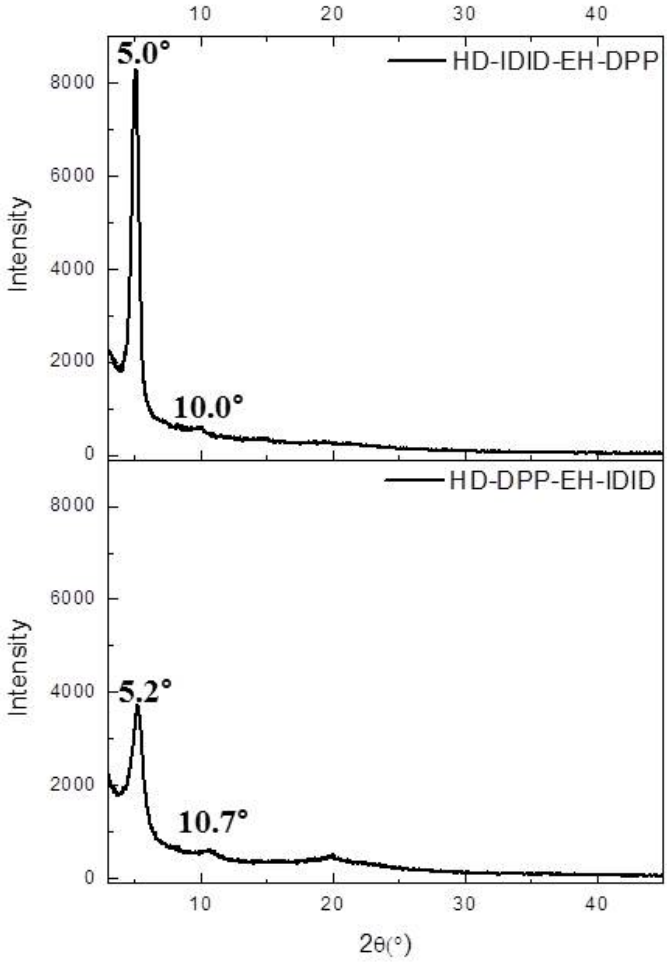

Figure 3.7. XRD diffraction data of HD-IDID-EH-DPP (upper) (30 mg/mL in chlorobenzene solution, spin-coated by 1500rpm for 40s, and annealed at 110℃ for 3min.) and HD-DPP-EH-IDID (lower) (30 mg/mL in chloroform solution, spin-coated by 1500rpm for 40s, and annealed at 90℃ for 3min.) in GI-mode.

To investigate molecular stacking of HD-IDID-EH-DPP and HD-DPP-EH-IDID, X-ray crystallography was carried out through x-ray diffraction method in GI (grazing incidence) mode. Figure 3.7 shows XRD patterns of HD-IDID-EH-DPP and HD-DPP-EH-IDID films spin-coated on Si/SiO_2 substrates, and annealed at same condition with device fabrication (110 ℃ for 3 minutes for HD-IDID-EH-DPP, 90℃ for 3 minutes for HD-DPP-EH-IDID). In the HD-IDID-EH-DPP film, the diffraction degree (2θ) of **a** direction is 5.0°, representing the lamellar stacking distance (d-spacing) of 17.6 Å, while in HD-DPP-EH-IDID film, 2θ is 5.2° with 17.0 Å of lamellar stacking distance. Theoretical calculations are based on the Bragg's law, as follows,

$$n\lambda = 2d\sin\theta$$

$$(Å) = \frac{1.54}{2sin\theta} \quad (\lambda=1.54Å \text{ for Cu K}\alpha \text{ radiation})$$

Furthermore, the intensity of the diffraction peak of HD-IDID-EH-DPP is 2 times larger than that of HD-DPP-EH-IDID, indicating HD-IDID-EH-DPP has more stacked supramolecular structure than HD-DPP-EH-IDID. However, diffraction peak along **b** direction in Figure 3.8 originating from π-π stacking was not shown in both HD-IDID-EH-DPP and HD-DPP-EH-IDID films through XRD measurement.

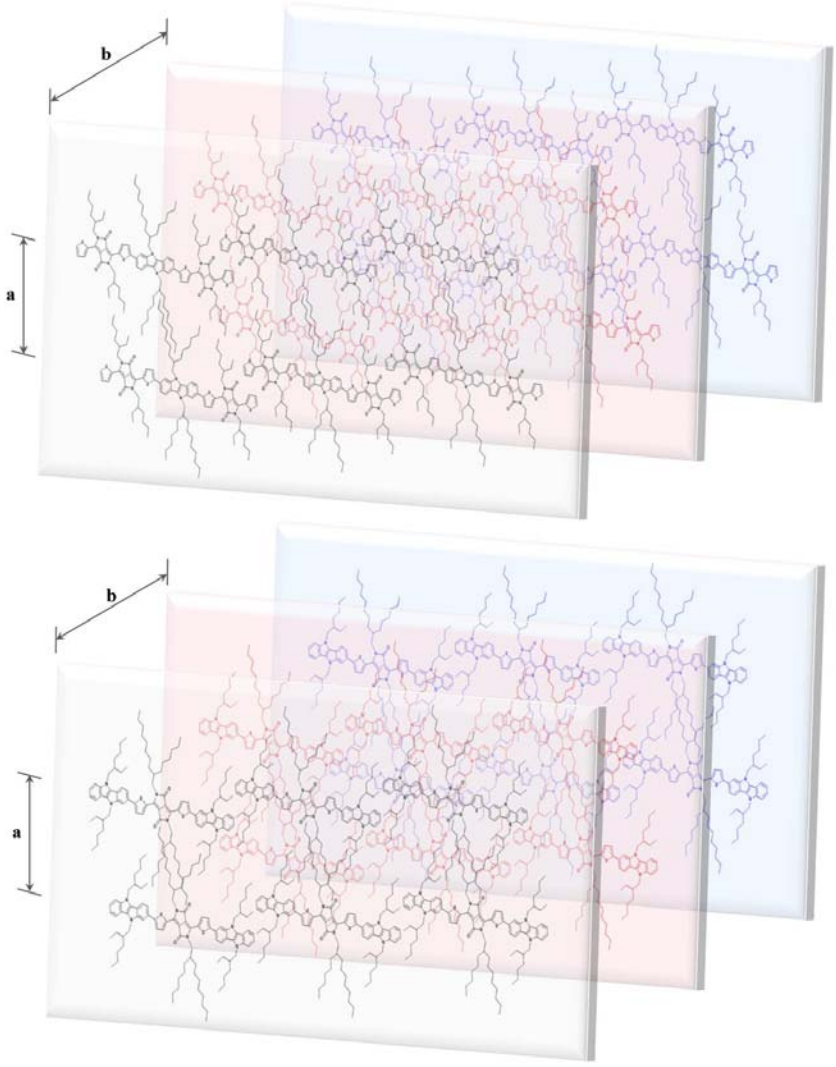

Figure 3.8. Schematic model of the HD-IDID-EH-DPP (upper) and HD-DPP-EH-IDID (lower) in solid state.

3.3.5 Photovolatic properties

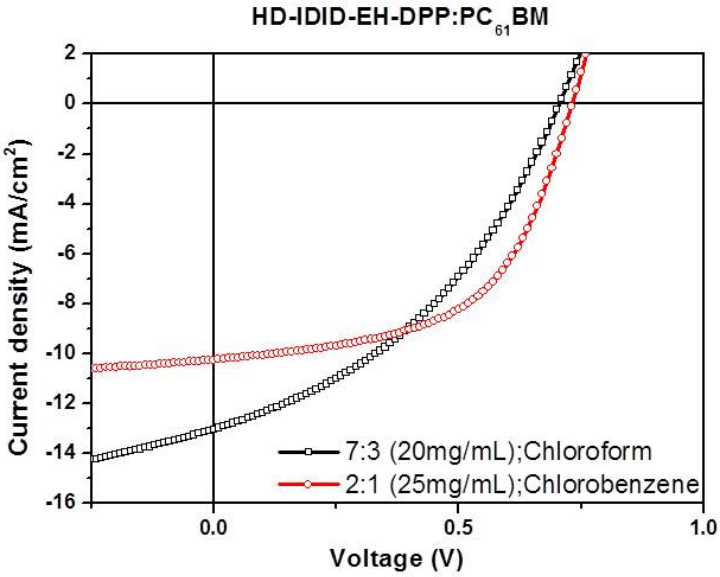

Figure 3.9. Characteristic J-V curves of solar cells fabricated from HD-IDID-EH-DPP:$PC_{61}BM$ in chloroform (black) and chlorobenzene (red) illuminated under AM 1.5G, 100 mW/cm^2.

Table 3.4. Photovoltaic properties of OPV cells using HD-IDID-EH-DPP blended with $PC_{61}BM$. (spin-coated by 1500rpm/40s).

Blend ratio, concentration, solvent	J_{sc} (mA/cm^2)	V_{OC} (V)	FF (%)	PCE (%)
7:3, 20mg/mL, Chloroform	13.02	0.71	39.1	3.61
2:1, 25mg/mL, Chlorobenzene	10.24	0.73	55.6	4.15

To demonstrate the potential of HD-IDID-EH-DPP and HD-DPP-EH-IDID as an electron donor in organic layer of solution-processed OPVs, devices were fabricated with the conventional architecture of ITO / PEDOT:PSS (40nm) / HD-IDID-EH-DPP (or HD-DPP-EH-IDID) :$PC_{61}BM$ blend / Al (100nm). The effect of different HD-IDID-EH-DPP:$PC_{61}BM$ active layer compositions and concentration of solution using chloroform and chlorobenzene was investigated, respectively. And significant change of device performance from different spin rate was also investigated. Optimal devices were obtained when concentration of 25 mg/mL in chlorobenzene solution was used with HD-IDID-EH-DPP:$PC_{61}BM$ blending ratio of 2:1 by weight, and spin-coated with 1500rpm for 40s. Optimized devices were annealed at 110℃ for 3 minutes after Al deposition. HD-DPP-EH-IDID exhibits poorer device performances than HD-IDID-EH-DPP. For device fabrication, HD-DPP-EH-IDID:$PC_{61}BM$ solution, blended by ratio of 2:1 (w/w) with concentration of 15 mg/mL in chloroform solution, was spin-coated with 2000rpm for 40s. Fabricated device exhibits PCE of 1.94%, with J_{SC} of 4.90 mA/$cm^{2,}$ V_{OC} of 0.65 V and FF of 61.0%.

Current density-voltage (J-V) characteristics under one sun and device performance parameters using HD-IDID-EH-DPP:$PC_{61}BM$ blended in chloroform and chlorobenzene solution are shown in Figure 3.9 and Table 3.4 In both devices using different solvent, device performance were slightly different. Device spin-coated using chloroform solution, device performance shows extremely high J_{SC} up to 13.02 mA/cm^2 with V_{OC} of 0.71 V, FF of 39.1%, and PCE of 3.61%. On the other hand, chlorobenzene solution spin-coated device exhibits high fill factor up to

55.6% with J_{SC} of 10.24 mA/cm^2, V_{OC} of 0.73 V, and PCE of 4.15%. Consequently, both devices spin-coated using different solvent exhibited great device performance with different tendency of device parameters. Devices using HD-IDID-EH-DPP as a donor in active layer show greatly high J_{SC} compared to other reported small molecule bulk-heteronjunction OSCs, which is oriented from strong intramolecular charge transfer (ICT) transition between IDID and DPP. Due to combination of strong electron donating property of IDID moiety and strong electron accepting property of DPP moiety, compound shows low bandgap, high extinction coefficient, relatively broad absorption extended to near IR region in solid state, and efficient charge transport property with supramolecular structure originating from coplanar structure, resulting in high J_{SC}.

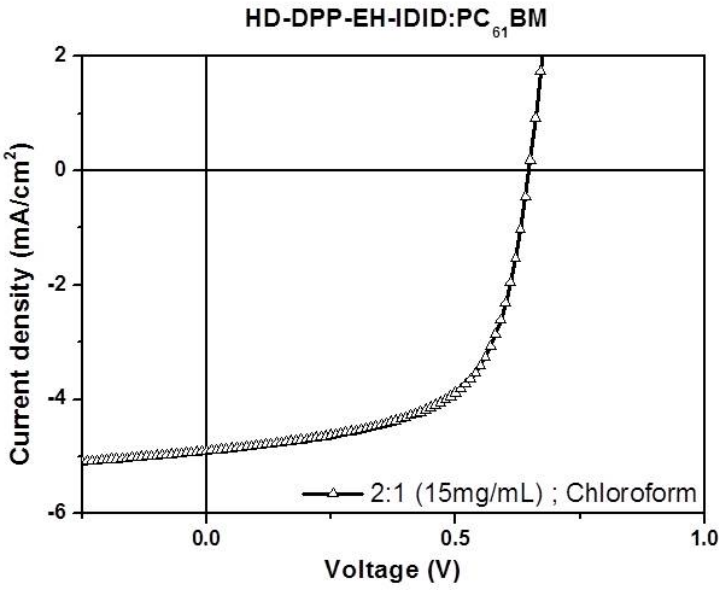

Figure 3.10. Characteristic J-V curves of solar cells fabricated from HD-DPP-EH-IDID:$PC_{61}BM$ in chloroform illuminated under AM 1.5G, 100 mW/cm^2.

Table 3.5. Photovoltaic properties of OPV cells using HD-DPP-EH-IDID blended with $PC_{61}BM$ in chloroform (spin-coated by 2000rpm/40s).

Blend ratio, concentration, solvent	J_{sc} (mA/cm^2)	V_{OC} (V)	FF (%)	PCE (%)
2:1, 15mg/mL, Chloroform	4.90	0.65	61.0	1.94

J-V characteristics and device performance parameters using HD-DPP-EH-IDID as a donor in organic layer are shown in Figure 3.10 and Table 3.5. Poorer device performances are shown in HD-DPP-EH-IDID OPV device than HD-IDID-EH-DPP. Because of lower molar extinction coefficient of HD-DPP-EH-IDID, J_{SC} was considerably low compared to that of HD-IDID-EH-DPP. Furthermore, as the HOMO level of HD-DPP-EH-IDID was higher-lying than that of HD-IDID-EH-DPP, V_{OC} was smaller in HD-DPP-EH-IDID than that of HD-IDID-EH-DPP. From those values, PCE of device using HD-DPP-EH-IDID as a donor was smaller than HD-IDID-EH-DPP, indicating A-D-A type HD-IDID-EH-DPP is superior donor material compared to D-A-D type HD-DPP-EH-IDID.

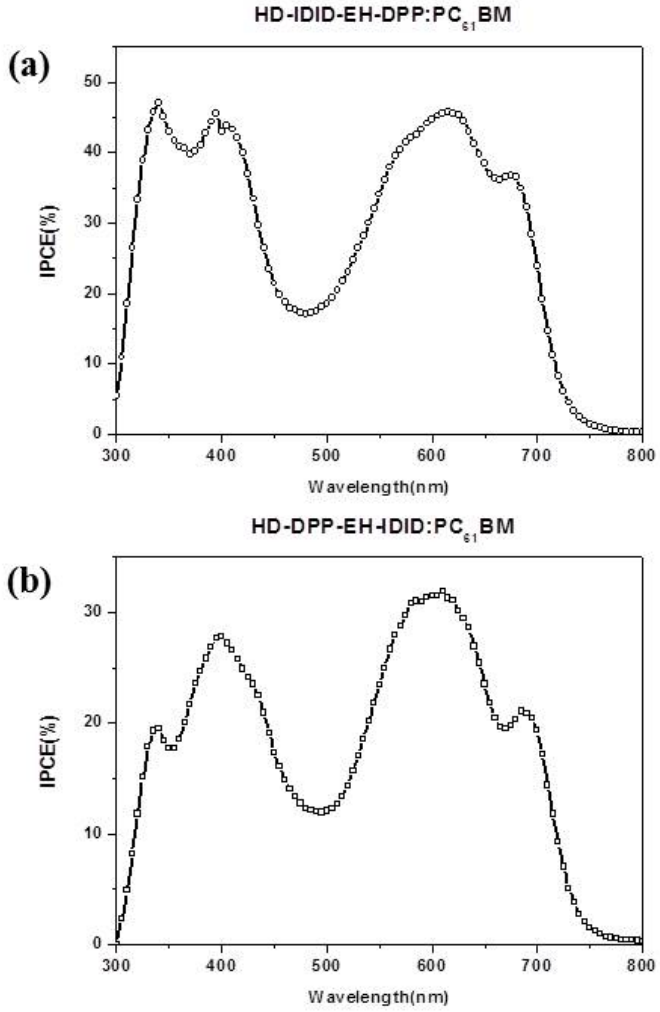

Figure 3.11. IPCE spectrum of (a) HD-IDID-EH-DPP:$PC_{61}BM$ (25 mg/mL in chlorobenzene by 2:1 w/w blended and annealed at 110℃ for 3 min.), and (b) HD-DPP-EH-IDID:PC61BM (15mg/mL in chloroform by 2:1 w/w blended and annealed at 90℃ for 3 min).

The incident photon to current efficiency (IPCE) spectra for the optimized devices using HD-IDID-EH-DPP and HD-DPP-EH-IDID are shown in Figure 3.11, respectively. HD-IDID-EH-DPP blended with $PC_{61}BM$ device shows a peak IPCE of 47.04% at 340nm and a broad IPCE response from 300nm to 800nm; while HD-DPP-EH-IDID blended with $PC_{61}BM$ device shows a peak IPCE of 31.87% at 610nm and a broad IPCE response from 300nm to 800nm

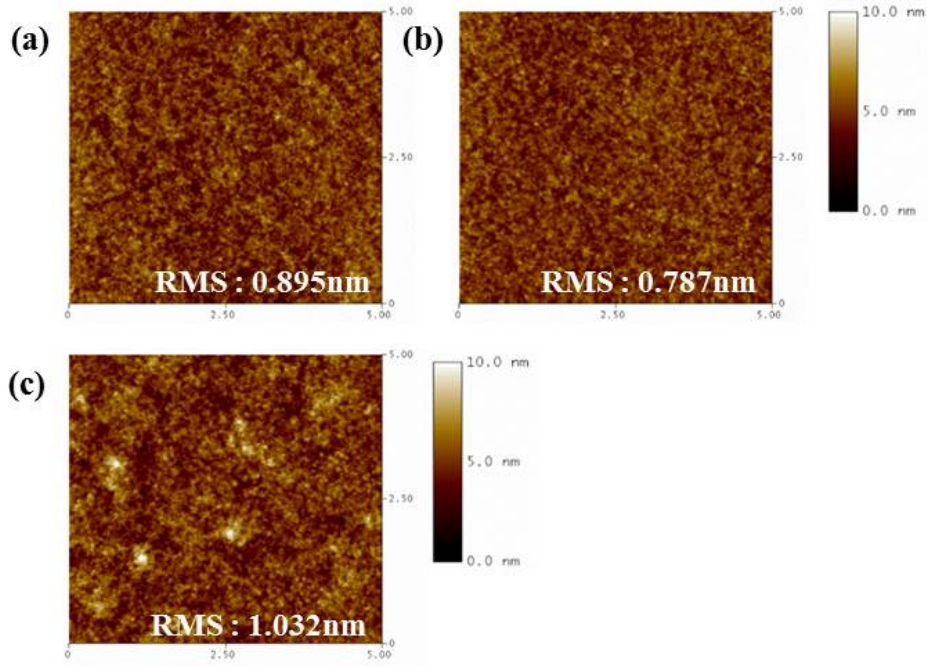

Figure 3.12. Tapping mode AFM topography of HD-IDID-EH-DPP:$PC_{61}BM$ devices fabricated using (a) chloroform solution (7:3 w/w, 20mg/mL, 1500rpm), and (b) chlorobenzene solution (2:1 w/w, 25mg/mL, 1500rpm) and (c) HD-DPP-EH-IDID:$PC_{61}BM$ devices fabricated using chloroform solution (2:1 w/w, 15mg/mL, 2000rpm).

It is known that the film morphology of the active layer in BHJ solar cells significantly affects the device performance. For the high performance of OPVs, nanoscale phase separation of active layer is required. [4(b),7] AFM topographical images of the active layer between Al electrodes are shown in Figure 3.12. Both HD-IDID-EH-DPP:$PC_{61}BM$ blended devices using chloroform solution and chlorobenzene solution show smooth surface with a root-mean-square (RMS) roughness of 0.895nm, and 0.787nm, respectively, indicating HD-IDID-EH-DPP and $PC_{61}BM$ blended mixture could effectively form interpenetrating pathway for charge transport to electrodes. However, HD-DPP-EH-IDID:$PC_{61}BM$ devices exhibit increased surface roughness with 1.032nm of RMS, indicating film morphology and phase separation is not suitable for effective charge transport, which is correlated with poor device performance and low J_{SC} of HD-DPP-EH-IDID device.

3.4 Conclusion

In conclusion, to explore strong electron donating property of IDID, novel A-D-A and D-A-D type triad small molecules (HD-IDID-EH-DPP and HD-DPP-EH-IDID), using IDID as a donor and DPP as an acceptor, were designed and synthesized. Their optical, electrochemical, and photovoltaic properties were measured, and ground state geometry and stacking structure were expected through DFT calculation and X-ray diffraction. Both molecules have planar backbone units, extended π-conjugation, good solubility, and low crystallinity in solid state.

Due to the strong intramolecular charge-transfer transition, both A-D-A and D-A-D type molecules exhibit significantly enhanced and broad light absorption with low bandgap energy. Based on the light absorption property, solution-processed OSCs using HD-IDID-EH-DPP as a donor and $PC_{61}BM$ as an acceptor exhibited high PCE of 4.15% with extremely high J_{SC}. On the other hand, HD-DPP-EH-IDID has considerably low light absorbance compared to HD-IDID-EH-DPP. Furthermore, due to stronger electron donating property, HD-DPP-EH-IDID has high-lying HOMO level. From those disadvantages of HD-DPP-EH-IDID exhibits significantly poorer device performances with low J_{SC} and V_{OC}, compared to those of HD-IDID-EH-DPP.

Through this work, comparison of A-D-A and D-A-D type IDID-DPP derivatives is clearly demonstrated with optical, electrochemical properties of molecules and device performance. As a result, A-D-A type HD-IDID-EH-DPP, is considerably confirmed as a suitable donor molecule more than D-A-D type HD-DPP-EH-IDID in OSCs, due to

appropriate energy level and extremely high light absorption property based on strong ICT between donor and acceptor moieties in HD-IDID-EH-DPP.

3.5 Bibliography

1. (a) M. C. Sharber, D. Mühlbacher, M. Koppe, P. Denk, C. Waldauf, A. J. Heeger, and C. J. Brabec, *Adv. Mater.*, **2006**, 18, 789 (b) G. Li, R. Zhu, Y. Yang, *nature photonics*, **2012**, 6, 153 (c) B. C. Thompson, and J. M. J. Fréchet, *Angew. Chem. Int. Ed*., **2008**, 47, 58

2. (a) J. Zhou, X. Wan, Y. Liu, Y. Zuo, Z. Li, G. He, G. Long, W. Ni, C. Li, X. Su, and Y. Chen, *JACS*, **2012**, 134, 16345. (b) Y. Liu, X. Wan, F. Wang, J. Zhou, G. Long, J. Tian, J.You, Y. Yang, and Y. Chen, *Adv. Energy Mater.*, **2011,** 1, 771. (c) Y. Sun, G. C. Welch, W. L. Leong, C. J. Takacs, G. C. Bazan, and A. J. Heeger, *Nature materials*, **2012**, 11, 44. (d) T. S. van der Poll, J. A. Love, J. –Q. Nguyen, and G. C. Bazan, *Adv. Mater*., **2011**, 24,3646.

3. (a) H. Shang, H. Fan, Y. Liu, X. Zhan, *Adv. Mater*, **2011**, 23, 1554. (b) J. Zhang, D. Deng, C. He, Y. He, M. Zhang, Z. G. Zhang, Z. Zhang, and Y. Li, *Chem. Mater*., **2010**, 23, 817.

4. (a) J.-W. Mun, I. Cho, D. Lee, W. S. Yoon, O. K. Kwon, C. Lee, and S. Y. Park, *Organic Electronics*, **2013**, 14, 2341. (b) J. Huang, C. Zhan, X. Zhang, Y. Zhao, Z. Ju, J. Jia, B. Jiang, J. Ye, S. Zhang, A. Tang, Y. Liu, Q. Pei, and J. Yao, *Appl. Mater. Interfaces*, **2013**, 5, 2033, (c) Y. S. Choi, W. H. Jo, *Organic Electronics*, **2013**, 14, 1621. (d) B. Walker, A. B. Tamayo, X. –D. Dang, P. Zalar, J. H. Seo, A. Garcia, M. Tantiwiwat, and T. –Q. Nguyen, *Adv. Funct. Mater*., **2009**, 19, 3063. (e) O. P. Lee, A. T. Yiu, P. M. Beaujuge, C. H. Woo, T. W. Holcombe, J. E. Millstone, J. D. Douglas, M. S. Chen, and J. M. J. Fréchet, *Adv. Mater*., **2011**, 23, 5359. (f) S. Loser, C. J. Bruns, H. Miyauchi, R. P.

Ortiz, A. Facchetti, S. I. Stupp, and T. J. Marks., *JACS*, **2011**, 133, 8142.

5. J. Mei, K. R. Graham, R. Stalder, and J. R. Reynolds, *Org. Lett*. **2010,** 12, 660.

6. Z. Li, G. He, X. Wan, Y. Liu, J. Zhou, G. Long, Y. Zuo, M. Zhang, and Y. Chen, *Adv. Energy Mater*., **2012**, 2, 74.

7. (c) Y . Lin, L. Ma, Y. Li, Y. Liu, D. Zhu, and X. Zhan, *Adv. Energy Mater.*, **2013**, 3, 9, 1166.

Abstract in Korean

초 록

인돌로인돌을 기반으로 한 새로운 전자주개 공액 유기 물질: 합성, 특성 분석, 그리고 광전자소자로의 응용에 대한 연구

정 혜 연

공과대학 재료공학부

서울대학교 대학원

헤테로아센을 포함하는 방향족 유기 물질들은 독특한 광학적, 전기적 특징을 가지고 있어서 물질의 특성에 대한 기초적인 연구와 유기 반도체소자로의 응용에 대한 연구가 활발하게 진행되어 왔으며, 높은 전하 이동도, 주변 환경에 대한 높은 안정성 등의 여러 장점으로 유망한 유기 반도체 물질군으로 높은 관심을 받고 있다. 인돌로인돌(IDID) 유도체는 이러한 헤테로아센 구조체 중 하나로, 평평한 화학적 구조, 용해도의

조절 용이성 그리고, 헤테로아센 중심 구조체에 치환된 질소 원자로 인한 강한 전자주개 성질, 치환의 용이성 등의 특징을 가져 광전자소자의 유기 반도체 물질로 사용하기 매우 적합하다.

본 연구에서는, 인돌로인돌 유도체의 광학적, 전기화학적 특징을 통해 에너지레벨이 크게 조절될 수 있는 것을 확인함과 동시에, 인돌로인돌 유도체의 전자 주개 성질을 연구하기 위하여, 전자 받개 물질인 TCNQ와 혼합하여 전하이동착물 (CT complex)을 형성하여 광화학적인 특징을 확인하였다. 인돌로인돌 유도체인 IDIDp와 TCNQ의 공결정을 이용한 단결정 유기전계효과 트랜지스터를 제작하여 그 특성을 살펴본 결과, p형 IDIDp 단독 광소자에서 보이던 정공 이동도 $2.29\text{x}10^{-2}$ $cm^2V^{-1}s^{-1}$가 아닌 전자와 정공이 모두 이동하는 형태의 양극성 전하 이동의 모습을 보였다 (정공 이동도 $1.27\text{x}10^{-3}$ $cm^2V^{-1}s^{-1}$, 전자 이동도 $3.40\text{x}10^{-2}$ $cm^2V^{-1}s^{-1}$).

또한, 강한 전자주개형 물질인 인돌로인돌과 강한 전자받개형 물질인 디피피(DPP)를 공유결합한 단분자 유기 물질(HD-IDID-EH-DPP)을 설계하고 합성한 결과, 강한 분자내 전하이동 특성으로 인하여 낮은 밴드갭을 가지며, 고효율의 벌크이종접합 태양전지를 구현할 수 있었다. A-D-A 타입과 D-A-D 타입의 두 물질 (HD-IDID-EH-DPP, HD-DPP-EH-IDID)을 각각 PC61BM을 혼합하여 용액 공정을 통한 유기태양 전지를 제작한 결과, A-D-A 타입 물질은 0.73 V의 V_{OC}, 10.24 $mAcm^{-2}$의 J_{SC}, 55.6%의 FF를 가지는 4.15%의

높은 효율을 보였으며, D-A-D 타입의 물질은 0.65 V의 V_{OC}, 4.90 $mAcm^{-2}$의 J_{SC}, 61.0%의 FF를 가지는 1.94%의 효율을 보였다. 이러한 두 물질의 소자 특성과 물질의 기본적인 화학 구조와 광학적, 전기화학적 특성을 비교한 결과, A-D-A 타입 인돌로인돌-디피피 유도체가 고효율의 태양전지를 구현하기에 더 적합한 물질임을 확인하였다.

주요어 : 인돌로인돌, 헤테오아센-방향족 유기물질, 전하이동착물, 단결정 유기전계효과 트랜지스터, 유기 태양전지

학 번 : 2012-20635

List of Presentation

H. Y. Chung, I. Cho, and S.Y. Park, “Charge transfer complexes of novel electron donating indolo[3,2-b]indoles and various electron accepting molecules”, **KOREA-FRANCE Joint Symposium 2013**, January 31, 2013, Seoul, Korea.

Hae Yeon Chung, Illhun Cho, Sang Kyu Park, and Soo Young Park, “Charge transfer complexes of novel electron donating indolo[3,2-b]indole derivatives with various electron accepting molecules and its organic electronics application”, **The 9th Korea-Japan Symposium on Frontier Photoscience-2013**, November 24-27, 2013, Seoul, Korea.